LEVEL II

AFGL-TR-77-0252

REMOTE SOUNDING OF CLOUD COMPOSITIONS FROM NOAA IV AND NIMBUS VI INFRARED SOUNDERS

by

Kuo-Nan Liou, Robert G. Feddes, Thomas L. Stoffel
Grant C. AufderHaar

Department of Meteorology

University of Utah

Salt Lake City, Utah 84112

F19628-75-C-0107

31 October 1977

Final Report

15 December 1974 - 15 September 1977

Approved for public release; distribution unlimited

627A, 6698

00, 04

DDC
RECEIVED
JUL 31 1978
E

AD A056852

AD No.

DDC FILE COPY

78 07 24 024

401 103

REPORT DOCUMENTATION PAGE	READ INSTRUCTIONS BEFORE COMPLETING FORM

1. REPORT NUMBER AFGL-TR-77-0252	2. GOVT ACCESSION NO.	3. RECIPIENT'S CATALOG NUMBER

4. TITLE (and Subtitle) REMOTE SOUNDING OF CLOUD COMPOSITIONS FROM NOAA IV AND NIMBUS VI INFRARED SOUNDERS	5. TYPE OF REPORT & PERIOD COVERED Final Report 12/15/1974 - 9/15/1977
	6. PERFORMING ORG. REPORT NUMBER

7. AUTHOR(s) Kuo-Nan Liou, Robert G. Feddes, Thomas L. Stoffel, Grant C. AufderHaar	8. CONTRACT OR GRANT NUMBER(s) F19628-75-C-0107

9. PERFORMING ORGANIZATION NAME AND ADDRESS Department of Meteorology University of Utah Salt Lake City, Utah 84112	10. PROGRAM ELEMENT, PROJECT, TASK AREA & WORK UNIT NUMBERS 63311F 62101F 627A0003 66980401

11. CONTROLLING OFFICE NAME AND ADDRESS Air Force Geophysics Laboratory Hanscom AFB, Massachusetts 01731 Contract Monitor: James T. Bunting/LYU	12. REPORT DATE 31 October 1977
	13. NUMBER OF PAGES 102

14. MONITORING AGENCY NAME & ADDRESS(if different from Controlling Office)	15. SECURITY CLASS. (of this report) Unclassified
	15a. DECLASSIFICATION/DOWNGRADING SCHEDULE

16. DISTRIBUTION STATEMENT (of this Report)

Approved for public release; distribution unlimited.

17. DISTRIBUTION STATEMENT (of the abstract entered in Block 20, if different from Report)

18. SUPPLEMENTARY NOTES

19. KEY WORDS (Continue on reverse side if necessary and identify by block number)

Remote Sensing	Infrared Sounder	Radiative Transfer
Clouds	HIRS	Satellite Meteorology
Nimbus VI Satellite	VTPR	Cirrus Clouds
NOAA IV Satellite	Infrared Radiation	Cloud Radiation

20. ABSTRACT (Continue on reverse side if necessary and identify by block number)

A spectral infrared radiative transfer model based on the discrete-ordinate method has been developed for atmospheres containing clouds and absorbing gases above, below and within the cloud. The transfer model takes into consideration the inhomogeneity of the cloudy atmosphere, the gaseous absorption in scattering cloud layers and the wavenumber dependence of radiative transfer. In addition, the cloud layer is further divided into a number of sub-layers to account for the non-isothermal and inhomogeneous cloud characteristics.

The spectral infrared transfer program is applied to VTPR channels of the ⟶ CONT.

DD FORM 1473 EDITION OF 1 NOV 65 IS OBSOLETE
1 JAN 73

78 07 24

20. (cont.)

NOAA 4 satellite to simulate upward radiances in cirrus cloud conditions. Single-scattering properties for ice crystals are calculated assuming ice cylinders 200 and 60 μm in length and width, respectively, randomly oriented in a horizontal plane. Comparisons between satellite observed and theoretically simulated upward radiances are carried out for selected cirrus cloud cases. Incorporating atmospheric profiles obtained from radiosonde and the observed cloud information into the spectral transfer program, we show a systematic agreement between observed and computed upward radiances. Systematic reduction patterns of the upward radiance caused by the increase of the cloud ice content are demonstrated for VTPR channels employing tropical and midlatitude atmospheric profiles. Having the quantitative relationships between upward radiance and ice contents, procedures are described for the inference of the cloud ice content and cloud amount. The proposed method has been successfully applied to the three cirrus cloud cases.

Moreover, radiative transfer model of spectral infrared radiation in cloudy atmospheres is applied to the most complete set of radiance observations currently available from the Nimbus VI HIRS instrument. We show that the effect of the atmospheric temperature profile is minimized by dividing the clear column radiance to the cloudy radiance. A method for the estimate of cloud compositions from multispectral HIRS radiances, including both short-wave and long-wave CO_2 channels, is developed. Theoretical calculations of the upwelling radiance at satellite altitude for a number of thicknesses involving middle level and cirrus clouds are carried out. The resulting theoretical radiances are then parameterized and an empirical method to determine cloud type and ice and water content of the clouds is described. Satellite passes from five days over the western United States are employed to test the empirical parameterizations of the theoretical results. Comparisons of the cloud type determinations with NOAA 4 Mosaic are shown to agree reasonably well. Cloud ice and water content derived from the parameterizations of the HIRS data is compared with that obtained from the Air Force Three Dimensional Nephanalysis (3DNEPH) program. Examples of the application of this technique to global mapping of ice and water content are displayed.

In the appendix, a retrieval technique is presented for the determination of the surface temperature, the thickness and transmissivity of cirrus clouds, and the fraction of the cirrus cloudiness by means of four observed upwelling radiances in the 10 μm window region. On the basis of radiative transfer calculations for mean wavenumbers of 900, 950, 1100 and 1150 cm^{-1}, assumptions are made in the theoretical retrieval analyses that water vapor effects above cirrus clouds are negligible and that ratios of the transmissivities are linear functions of the cloud thickness. Error analyses employing climatological data reveal that independent random errors in temperature and humidity profiles introduce insignificant errors in the four resulting parameters. The resulting errors caused by random errors in the expected upwelling radiances, however, depend upon their standard deviations. Once the thickness and the transmissivity at a given wavenumber of a cirrus cloud have been determined, we illustrate that the vertical ice content may be estimated assuming that ice particles are randomly oriented in a horizontal plane.

TABLE OF CONTENTS

iii

ACKNOWLEDGEMENTS

SECTION I

INTRODUCTORY REMARKS

The structure and composition of clouds obtained from passive remote sensing from satellites on a routine basis have been extremely limited. Many of the methods utilized are based strictly on the statistical analysis of the observed data. This may be due to the complexity of cloud interaction with the radiation field of the atmosphere. This is especially evident for the globally distributed high, semi-transparent cirrus clouds. The objectives of the satellite sensing and radiative transfer project initiated in the Department of Meteorology, University of Utah and sponsored by the Air Force Geophysics Laboratory are to develop (1) a computer program to simulate the transfer of infrared radiation through cirrus cloudy atmospheres, (2) a passive satellite retrieval technique to estimate the vertical ice content profile of cirrus and (3) a possible three-dimensional cloud scene method from a combination of available satellite sounding instruments such as those on board Nimbus VI and NOAA IV.

In this final report we present some of the highlights of results obtained during the past three years. Section 2 consists of discussions on the theoretical foundation for the calculations of the transfer of spectral infrared radiation in cloudy atmospheres. The infrared transfer model allows the inhomogeneity of cloudy atmospheres to be treated approximately and it takes into account the gaseous absorption in scattering cloud layers and the wavenumber dependence of radiative transfer. Application of

1

the infrared transfer model to VTPR (Vertical Temperature Profile Radiometer) channels of the NOAA IV satellite is described in Section 3. Radiative properties of cirrus clouds are investigated and possible cirrus cloud scenes are explored. In Section 4, we apply the infrared transfer program to HIRS(High Resolution Infrared Sounder) channels of the Nimbus VI satellite with several combinations of middle and cirrus clouds. The theoretical results are parameterized and are then used to infer cloud characteristics from actual HIRS data. In the appendix, we attach a paper (Liou, 1977) in conjunction with the development of a retrieval technique for the inference of cirrus cloud characteristics based on a set of synthetic radiance calculations in the window region.

2

SECTION 2

SPECTRAL INFRARED RADIATION PROGRAM FOR
CLOUDY ATMOSPHERES

2.1   Basic Equations and Approximations

The infrared radiation program begins with solving the transfer
equation for a plane-parallel cloud layer consisting of absorbing gases
in local thermodynamic equilibrium. The basic equation describing the
monochromatic infrared radiation field is given by

$$\mu \frac{dI_\nu(\tau,\mu)}{d\tau} = I_\nu(\tau,\mu) - \frac{\tilde{\omega}_\nu}{2} \int_{-1}^{+1} P_\nu(\mu,\mu') I_\nu(\tau,\mu') d\mu'$$

$$- (1-\tilde{\omega}_\nu) B_\nu[T(\tau)], \tag{2.1}$$

where

$$\tilde{\omega}_\nu = \beta_{s,\nu}/(\beta_{s,\nu}+\beta_{a,\nu}+nk_\nu), \tag{2.2}$$

$$B_\nu(T) = 2hc^2\nu^3/(e^{hc\nu/KT}-1), \tag{2.3}$$

and I_ν represents the monochromatic radiance of wavenumber ν, μ the cosine
of the emergent angle with respect to the zenith, τ the optical depth, P_ν
the normalized axially symmetrical phase function, T the cloud temperature
which is a function of height or optical depth, $\tilde{\omega}_\nu$ the single scattering
albedo, $B_\nu(T)$ the Planck function, h and K the Planck's and Boltzmann's
constants, respectively, c the velocity of light, $\beta_{s,\nu}$ and $\beta_{a,\nu}$ the volume

3

scattering and absorption cross sections for cloud particles of wavenumber ν, n the number density of the absorbing gases within the cloud layer, and k_ν the absorption coefficient of the gases.

The normalized phase function may be expanded into Legendre polynomials consisting of a finite number of terms. Upon replacing the integration in Eq. (2.1) by summation according to the Gauss' quadrature formula, a set of first-order inhomogeneous differential equations are derived. By seeking the homogeneous and particular solutions of the differential equations as described by Chandrasekhar (1950), the complete solutions of the scattered radiance for a given discrete-stream j assuming an isothermal cloud temperature T_c may be written (Liou, 1973;1974)

$$I_\nu(\tau,\mu_i) = \Sigma_m L_m \phi_m(\mu_i) e^{-k_m \tau} + B_\nu(T_c), \qquad (2.4)$$

where Σ_m denotes summation over the 2n discrete streams employed, ϕ_m and k_m are the eigenfunction and eigenvalue of the differential equations whose values depend upon the phase function and single-scattering albedo, and L_m are a set of constants of proportionality to be determined from the radiation boundary conditions above and below the cloud layer.

The upward and downward radiances arising from the molecular absorption and emission reaching the cloud bottom and top, respectively, can be obtained by solving the transfer equation for a non-scattering atmosphere in local thermodynamic equilibrium. They are given by

$$I_\nu^{\;+}(z_t,-\mu_i) = \int_{z_t}^{\infty} B_\nu[T(z)] d\, T_\nu(z,z_t;-\mu_i), \qquad (2.5)$$

4

$$I_\nu^\uparrow(z_b,\mu_i) = B_\nu(T_s)T_\nu(z_b,0;\mu_i)$$

$$+ \int_0^{z_b} B_\nu[T(z)]d\,T_\nu(z_b,z;\mu_i), \tag{2.6}$$

where T_s is the surface temperature, and z_t and z_b are cloud top and base heights, respectively, and the monochromatic transmittance is

$$T_\nu(z_2,z_1;\mu_i) = \exp\left[-\frac{1}{\mu_i}\int_{z_1}^{z_2} k_\nu(z)n(z)dz\right]. \tag{2.7}$$

Assume that the variation of the Planck function with respect to the wavenumber is much smaller than that of the transmission function T_ν. Thus, upon multiplying Eqs. (2.5) and (2.6) by the instrumental slit function $\phi(\nu)$ and performing the wavenumber integration over the spectral interval (ν_1,ν_2), we have

$$I_{\Delta\nu}^\downarrow(z_t,-\mu_i) = \int_{\nu_1}^{\nu_2} I_\nu^\downarrow(z_t,-\mu_i)\phi(\nu)\frac{d\nu}{\Delta\nu}$$

$$= \int_{z_t}^{\infty} B_{\Delta\nu}[T(z)]d\,T_{\Delta\nu}(z,z_t;-\mu_i), \tag{2.8}$$

$$I_{\Delta\nu}^\uparrow(z_b,\mu_i) = \int_{\nu_1}^{\nu_2} I_\nu^\uparrow(z_b,\mu_i)\phi(\nu)\frac{d\nu}{\Delta\nu}$$

$$= B_{\Delta\nu}(T_s)T_{\Delta\nu}(z_b,0;\mu_i)$$

$$+ \int_0^{z_b} B_{\Delta\nu}[T(z)]d\,T_{\Delta\nu}(z_b,z;\mu_i), \tag{2.9}$$

where the spectral transmittance is defined by

5

$$T_{\Delta\nu}(z_2, z_1; \mu_i) = \int_{\nu_1}^{\nu_2} \exp\left[-\frac{1}{\mu_i}\int_{z_1}^{z_2} k_\nu(z)n(z)dz\right]\phi(\nu)\frac{d\nu}{\Delta\nu}. \qquad (2.10)$$

We first examine the transmission function (or transmittance). For a given height z, the transmittances are normally available in the form

$$T_{\Delta\nu}(z) = T_{\Delta\nu}(z,\infty;1) = \int_{\nu_1}^{\nu_2} \exp\left[-\int_{\infty}^{z} k_\nu(z)n(z)dz\right]\phi(\nu)\frac{d\nu}{\Delta\nu}. \qquad (2.11)$$

In reference to Eqs. (2.1) and (2.2), we notice that the gaseous absorption coefficient k_ν is needed to carry out the transfer of infrared radiation in cloud layers composed of absorbing gases. However, k_ν is known only through the absorption line parameters of gases and its values vary greatly with wavenumber in a small spectral interval. It is very difficult, if not impossible, to carry out line-by-line calculations including scattering contributions of cloud particles. Thus, a simpler approach for the gaseous absorption in a scattering layer would be to make use of the known transmittances which have been obtained to a good accuracy by means of line-by-line calculations for inhomogeneous atmospheres in conjunction with satellite sensing. Recognizing the definition of the vertical transmittance in Eq. (2.11), we may approximate it by

$$T_{\Delta\nu}(u) \simeq \int_{\nu_1}^{\nu_2} e^{-\overline{k}_\nu u}\frac{d\nu}{\Delta\nu} \simeq \sum_{j=1}^{M} w_j e^{-k_j u}, \qquad (2.12)$$

where the vertical path length

6

$$u = \int_{\infty}^{z} \rho_v(z')dz',$$

k_j may be thought of as an equivalent absorption coefficient, w_j is the weight and M denotes the total number of finite terms in the fitting of the transmittances. Once k_j and w_j have been determined, we may consider the transfer of spectral infrared radiation as monochromatic in the sub-spectral interval j and carry out transfer calculations in a cloud layer M times with a new single scattering albedo $\tilde{\omega}_v^{\ j}$. Here, we assume that the phase function and the absorption and scattering cross sections of ice crystals are independent of the wavenumber within a spectral interval. These assumptions are justified in view of the relatively slow varying refractive indices of ice in the infrared regions as evident in the next section.

Without postulating any assumptions and approximations, the upward radiance at the satellite point of view in completely cloudy conditions may be expressed by

$$I_{\Delta v}^C(\infty,\mu_i) = \int_{v_1}^{v_2} I_v^{\uparrow}(z_t,\mu_i) T_v(\infty,z_t;\mu_i) \, \phi(v)\frac{dv}{\Delta v}$$

$$+ \int_{z_t}^{\infty} B_{\Delta v}[T(z)]dT_{\Delta v}(\infty,z;\mu_i), \tag{2.13}$$

where T_v denotes the monochromatic transmittance associated with the up-ward radiance $I_v^{\uparrow}$ at the cloud top. The second term on the right-hand side is for the clear atmosphere above the cloud layer and it is an exact expression. However, the first term requires approximations in order to

7

take the scattering of cloud particles into account.

On the basis of the exponential fit to the transmission function described in Eq. (2.12), let $I_j^\uparrow$ ($j=1,2,...,M$) be the resulting radiances calculated from the transfer program involving cloud layers. Eq. (2.13) can be approximated by

$$I_{\Delta\nu}^C(\infty,\mu) \cong \sum_{j=1}^M I_j^\uparrow(z_t,\mu_i) \, w_j \, T_j(\infty,z_t;\mu_i)$$

$$+ \int_{z_t}^\infty B_{\Delta\nu}[T(z)] \, dT_{\Delta\nu}(\infty,z;\mu_i), \tag{2.14}$$

where $I_j^\uparrow$ at the cloud top is to be evaluated from the upward and downward radiances arising from the molecular absorption and emission reaching the cloud bottom and top using the equivalent absorption coefficients and weights derived from the exponential fit noted in Eq. (2.12), and T_j is associated with the exponential function given by Eq. (2.12). The success of carrying out such a semi-monochromatic infrared transfer calculation depends solely on the reliability of fitting the satellite transmission functions for the entire atmosphere.

Since the variation of the radiative property of clouds over a small spectral interval is much smaller than that of the transmittance and since the spectral transmittances for satellite channels, $T_{\Delta\nu}$, are available from the top of the cloud to the top of the atmosphere, we postulate from Eq. (2.13) that

$$I_{\Delta\nu}^C(\infty,\mu_i) \cong I_{\Delta\nu}^\uparrow(z_t,\mu_i) \, T_{\Delta\nu}(\infty,z_t;\mu_i)$$

$$+ \int_{z_t}^\infty B_{\Delta\nu}[T(z)] \, dT_{\Delta\nu}(\infty,z;\mu_i). \tag{2.15}$$

8

where

$$I_{\Delta\nu}^{\uparrow}(z_t,\mu_i) = \sum_{j=1}^{M} I_j^{\uparrow}(z_t,\mu_i), \tag{2.16}$$

and semi-monochromatic upward radiances $I_j^{\uparrow}$ are to be evaluated from the procedures described below. The approach described here makes use of the known spectral transmission functions above and below the cloud and utilizes the exponential fitting program for the cloud layer. If the cloud layer is a black body, then Eq. (2.15) is an exact expression where $I_{\Delta\nu}^{\uparrow}$ will be given by the Planck function of the cloud top temperature. For moderately thick and thick clouds, we would think that the approximation is a good one since cloud particles, not the gases within the cloud, dominate the transfer processes.

The upward radiance at the satellite point of view in clear conditions is simply

$$I_{\Delta\nu}^{NC}(\infty,\mu_i) = B_{\Delta\nu}(T_s)\, T_{\Delta\nu}(\infty,o;\mu_i)$$

$$+ \int_o^{\infty} B_{\Delta\nu}[T(z)]\, dT_{\Delta\nu}(\infty,z;\mu_i). \tag{2.17}$$

Thus, if within the field-of-view of the satellite radiometer there is η portion of cloudiness, the upward radiance at the top of a partly cloudy atmosphere is then given by

$$I_{\Delta\nu}^{PC}(\infty,\mu_i) = \eta I_{\Delta\nu}^{C}(\infty,\mu_i) + (1-\eta)I_{\Delta\nu}^{NC}(\infty,\mu_i). \tag{2.18}$$

2.2   Radiative Transfer in Non-Isothermal and Inhomogeneous Cloud
       Layers

The solution of the infrared radiative transfer equation given by Eq. (2.4) is applicable only to isothermal and homogeneous cloud layers.

9

The question of inhomogeneity of cirrus cloud compositions is a difficult one. In the first place, there have not been many observations available. For the purpose of radiative transfer calculations, it seems that averaged properties of cloud compositions may be appropriate. However, the effect of the non-isothermal structure of clouds on their radiative properties is more critical. Physically, a cold cloud top would reduce the transmitted radiances. It is conceivable, therefore, that an overestimation of upward radiances is likely to take place. Although our main concern is the non-isothermal structure, the transfer program described below may be utilized to investigate, if desirable, the inhomogeneous properties of clouds as well.

In reference to Figure 2.1, the cirrus cloud layer is divided into a number of sub-layers each of which is considered to be isothermal and homogeneous. The optical depth is evaluated from the cloud top to the bottom of the sub-layer. The index ℓ is used to denote the number of sub-layer. We now apply the solution of the radiative transfer equation given by Eq. (2.4) to each sub-layer and sub-spectral interval j to obtain ($\sum_m$ denotes summation over discrete-streams, $(-n,n)$)

$$I_j^{\ell}(\tau,\mu_i) = \sum_m L_m^{\ell} \phi_m(\mu_i) e^{-k_m^{\ell}\tau} + B_j(T_c^{\ell}). \qquad (2.19)$$

In order to determine the unknown coefficients L_m^{ℓ}, the radiation continuity relationships are needed in addition to two radiation boundary conditions specified in Eqs. (2.8) and (2.9). At the cloud top the downward radiance has to be equal to that from the molecular atmosphere above, so that

10
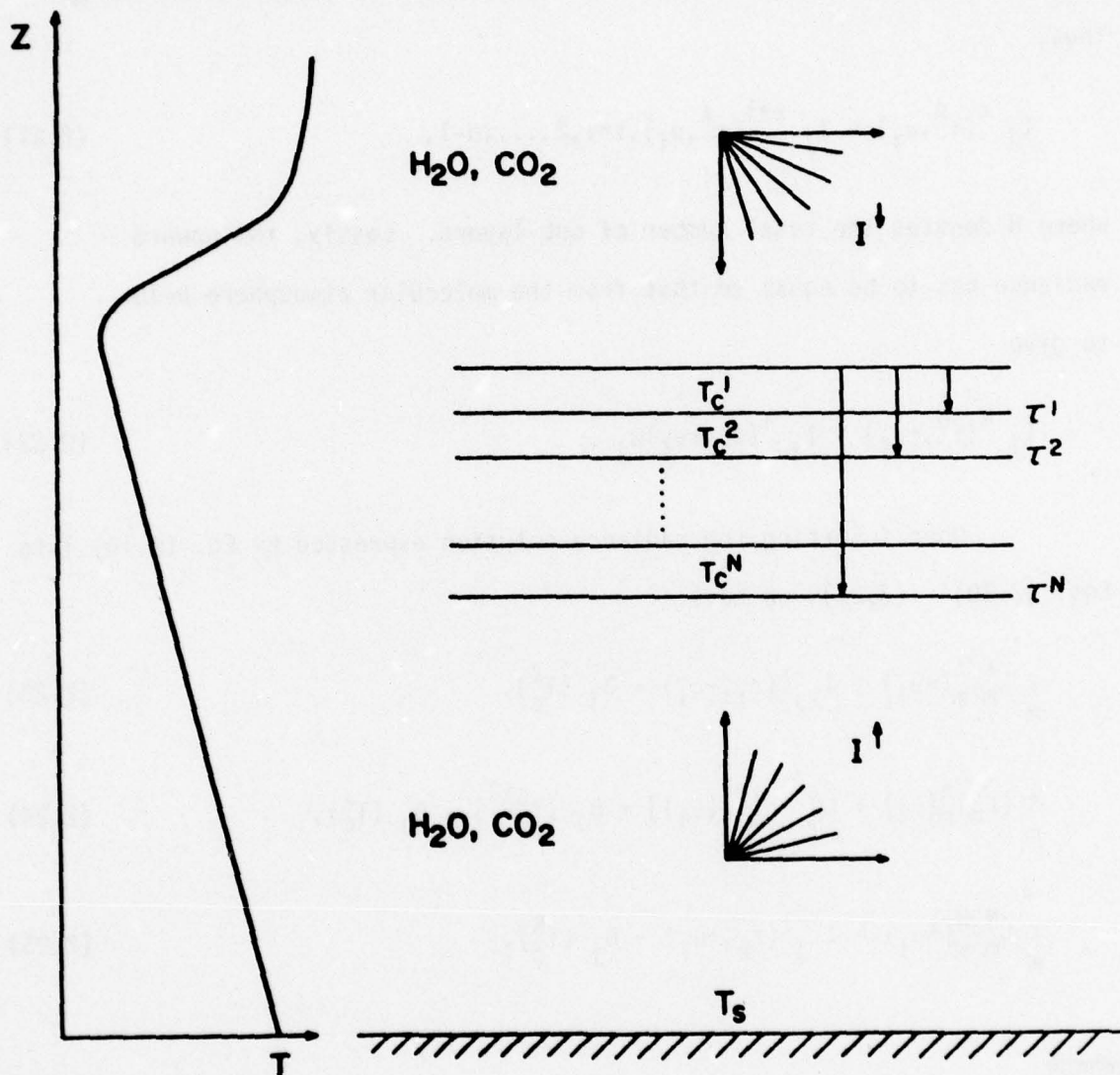
Figure 2.1. Radiative transfer model for an inhomogeneous cirrus cloudy atmosphere. The cirrus cloud layer is divided into several sub-layers each of which is considered to be isothermal and homogeneous.

11

$$I_j^{\ 1}(0,-\mu_i) = I_{\Delta\nu}^{\ \downarrow}(z_t,-\mu_i)w_j \ . \tag{2.20}$$

Between the layers, the radiances from all directions must be continuous.
Thus,

$$I_j^{\ \ell}(\tau^\ell,\mu_i) = I_j^{\ \ell+1}(\tau^\ell,\mu_i), \ell=1,2,\ldots;N-1, \tag{2.21}$$

where N denotes the total number of sub-layers. Lastly, the upward
radiance has to be equal to that from the molecular atmosphere below
to give

$$I_j^{\ N}(\tau^N,+\mu_i) = I_{\Delta\nu}^{\ \uparrow}(z_b,+\mu_i)w_j \ . \tag{2.22}$$

Upon inserting the radiance solution expressed by Eq. (2.19) into
Eqs. (2.20) - (2.22), we have

$$\sum_m L_m^\ell \phi_m^\ell(-\mu_i) = I_j^{\ \downarrow}(z_t,-\mu_i) - B_j(T_c^\ell), \tag{2.23}$$

$$\sum_m [L_m^\ell \gamma_m^\ell(\mu_i) + L_m^{\ell+1}\delta_m^{\ell+1}(\mu_i)] = B_j(T_c^{\ell+1}) - B_j(T_c^\ell), \tag{2.24}$$

$$\sum_m L_m^N \gamma_m^N(+\mu_i) = I_j^{\ \uparrow}(z_b,+\mu_i) - B_j(T_c^N), \tag{2.25}$$

where

$$\gamma_m^\ell(\mu_i) = \phi_m^\ell(\mu_i)e^{-k_m^\ell \tau^\ell}, \tag{2.26}$$

$$\delta_m^{\ell+1}(\mu_i) = -\phi_m^\ell(\mu_i)e^{-k_m^{\ell+1}\tau^\ell}, \tag{2.27}$$

Eqs. (2.23) - (2.25) represent a system of 2n x N linear equations from which the L_m^ℓ coefficients may be determined using a matrix inversion technique. We may rewrite Eqs. (2.23) - (2.25) in a compact matrix form

$$\phi\; \underset{\sim}{L} \;=\; \underset{\sim}{B}, \tag{2.28}$$

where the unknown coefficients of proportionality

$$\underset{\sim}{L} = \begin{bmatrix} L_{-n}^1 \\ \vdots \\ L_n^1 \\ L_{-n}^2 \\ \vdots \\ L_n^2 \\ \vdots \\ L_{-n}^N \\ \vdots \\ L_n^N \end{bmatrix}. \tag{2.29}$$

The matrix denoting the contribution due to cloud emission and upward and downward radiances reaching the cloud base and top, respectively, is

$$B = \begin{bmatrix} I_j{}^{\downarrow}(z_t, -\mu_n) - B_j(T_c^1) \\ \vdots \\ I_j{}^{\downarrow}(z_t, -\mu_i) - B_j(T_c^1) \\ B_j(T_c^2) - B_j(T_c^1) \\ \vdots \\ B_j(T_c^2) - B_j(T_c^1) \\ I_j{}^{\uparrow}(z_b, +\mu_1) - B_j(T_c^N) \\ \vdots \\ I_j{}^{\uparrow}(z_b, +\mu_n) - B_j(T_c^N) \end{bmatrix}, \tag{2.30}$$

13

and the $2n \times N$ by $2n \times N$ matrix

$$\Phi = \begin{bmatrix} \phi_{-n}^{1}(-\mu_n) & \cdots & \phi_{n}^{1}(-\mu_n) & & & & & & \\ \vdots & & \vdots & & & & & & \\ \phi_{-n}^{1}(-\mu_1) & \cdots & \phi_{n}^{1}(-\mu_1) & & & & & & \\ \gamma_{-n}^{1}(-\mu_n) & \cdots & \gamma_{n}^{1}(-\mu_n)\delta_{-n}^{2}(-\mu_n) & \cdots & \delta_{n}^{2}(-\mu_n) & & & & \\ \vdots & & \vdots & \vdots & \vdots & & & & \\ \gamma_{-n}^{1}(\mu_n) & \cdots & \gamma_{n}^{1}(\mu_n)\delta_{-n}^{2}(\mu_n) & \cdots & \delta_{n}^{2}(\mu_n) & & & & \\ & & \vdots & \vdots & \vdots & \vdots & & & \\ & & & & & \gamma_{-n}^{N}(\mu_1) & \cdots & \gamma_{n}^{N}(\mu_1) & \\ & & & & & \vdots & & \vdots & \\ & & & & & \gamma_{-n}^{N}(\mu_n) & \cdots & \gamma_{n}^{N}(\mu_n) \end{bmatrix} \qquad (2.31)$$

In Eq. (2.31), the blank spaces denote zero elements. A similar procedure has been employed by Liou (1975) for the transfer of solar radiation in inhomogeneous atmospheres. Once L_m^{ℓ} have been determined, they can be inserted in Eq. (2.19) to obtain the sub-spectral radiance distribution within each sub-layer.

2.3   Discussions on Numerical Procedures

Calculations for single scattering parameters were first carried out for ice cylinders randomly oriented in a horizontal plane according to a previous theoretical model for ice crystal clouds (Liou, 1972). Based on observations of Weickmann (1949) and experimental results from Heymsfield and Knollenberg (1972), a mean length of 200 μm, a mean radius of 30 μm and a mean concentration of 0.05 cm^{-3} along with the corresponding refractive indices for ice (Schaaf and Williams, 1973) were assumed in the scattering calculations. The single scattering parameters for the water cloud utilized a

14

drop size distribution developed by Feddes and Smith (1974). This distribution is an exponential fitting of the best published measurements taken from cloud physics literature. Although this fitting was done for ten cloud types, only the altostratus cloud distribution is used. In the calculation of the single scattering parameters for altostratus clouds, a liquid water content of 0.15 gm m^{-3} was used. The real and imaginary parts of the refractive index for water were taken from Hale and Querry (1973). Single-scattering computations were carried out for the central wavenumber of each channel.

The phase functions are expanded in a series of Legendre polynomials in the form

$$P_\nu(\mu,\mu') \simeq \sum_{\ell=0}^{N} \tilde{\omega}_\ell P_\ell(\mu)P_\ell(\mu'), \qquad (2.32)$$

where $\tilde{\omega}_\ell$ are obtained from the orthogonal properties of the Legendre polynomials. The expanded form is to be used in the transfer calculations.

To derive a set of equivalent absorption coefficients for use in cloud scattering calculations, an exponential fit of the form denoted in Eq. (2.12) was applied to transmission curves of the CO_2 and H_2O channels. Note that the transmission curves take into account absorption by H_2O, CO_2 and O_3 simultaneously, with each gas distributed differently, and the instrumental slit function. These curves cover the entire atmosphere from 0.01 mb to the surface, which introduces a significant pressure variation.

A simplified fitting routine was developed which guaranteed the required restriction on w_j and k_j (both have to be positive). The numerical

15

scheme is based on the following iterative process. An initial $T_{\Delta\nu}(u_1)$ and w_1 are chosen (initially $w_1 = 1$) and k_1 is generated from (see Eq. (2.12))

$$k_1 = \frac{1}{u_1} \ln \frac{w_1}{T_{\Delta\nu}(u_1)} .$$

(2.33)

The curve $T'_{\Delta\nu}(u) = w_1 e^{-k_1 u}$ is then generated point by point; as each new point is generated it is compared with the true value $T_{\Delta\nu}(u)$, which is the known transmittance.to make sure it meets the following conditions:

$$\left. \begin{array}{l} T'_{\Delta\nu}(u) < T_{\Delta\nu}(u) \\[2ex] \dfrac{dT'_{\Delta\nu}(u)}{du} < \dfrac{dT_{\Delta\nu}(u)}{du} \end{array} \right\} .$$

(2.34)

The second condition requires only a rough approximation for the derivative. If either of these are not met, a new w_1 is generated, (i.e., $w_1 = w_1 \times$ constant) so that the new w_1 is slightly less than the old one, and the above is repeated. If no w_1 can be found, a new u_1 is selected (larger than the old point). When a good w_1 and k_1 are found, the above process is then repeated to produce a w_2 and k_2 using values of $T_{\Delta\nu}(u) - T'_{\Delta\nu}(u)$ instead of $T_{\Delta\nu}(u)$. The number of points needed to fit the curve then depends only on the size of the error tolerance used and on the range of u over which $T_{\Delta\nu}(u)$ is to be fitted. *The exponential fitting approximation is restricted in the scattering cloud layer, so that the gaseous absorption within the cloud layer may be included.* Note here that spectral transmittances are available both above and below the cloud.

Once the scattering and absorption properties of ice crystals and the spectral absorption characteristics of gases have been determined,

16

we may evaluate the volume single-scattering properties for a mixture of ice crystals and gases within the clouds. According to Eq. (2.2) and the exponential fitting program described above, the single-scattering albedo, including gaseous contribution for a spectral interval whose central wavenumber is ν, may be written

$$\tilde{\omega}_\nu^j = \beta_s \ /(\beta_e + nk_j), \ j = 1, \ldots, N. \tag{2.35}$$

where β_e represents the volume extinction cross section. The total optical depth for a cloud with a thickness of Δz is given by

$$\Delta\tau_\nu^j = \beta_e\Delta z + uk_j, \ j = 1, \ldots, N, \tag{2.36}$$

where we omit the subscript ν in the right-hand side of these two equations. Note that u is the gaseous pathlength. The amount of H_2O within clouds is estimated by using a mean temperature and assuming saturated conditions. CO_2 concentration is assumed uniformly distributed in the atmosphere. Thus, the pathlength of gases within the cloud may be obtained. Finally, it is also assumed that the spectral phase function is

$$P_\nu^j(\mu,\mu') = P_\nu(\mu,\mu'), \tag{2.37}$$

as described previously. The single-scattering albedo, the total optical depth for a given thickness Δz and the phase function in the form of Legendre polynomials are the basic parameters for carrying out the spectral radiative transfer calculations.

The monochromatic transfer program first generates the required eigenvalues for a set of homogeneous differential equations from the single-scattering albedo and the expanded phase function. Liou (1973)

17

pointed out the mathematical and numerical ambiguities involving Chandrasekhar's (1950) method for searching the eigenvalues corresponding to the 2n associated homogeneous differential equations, and developed a matrix method directly from the associated homogeneous differential equations for the eigenvalue problem. Recognizing the symmetric relationships between the matrix elements, Asano (1975) further developed the analytic procedures for the reduction of the rank of the matrix. These developments thus allow the accuracies of eigenvalues to be improved and the computer time involved greatly reduced. Computations presented in this paper follow the numerical procedures outlined by Liou (1973) and Asano (1975) for eigenvalue problems in the discrete-ordinate method for radiative transfer.

Secondly, the program calculates the clear column angular upward and downward radiances arising from the absorption and emission of gases (in forms of transmittances) above and below the cloud as well as the surface contribution. Each model atmospheric profile is divided into 101 levels from the surface to 100 km by means of linear interpolation between the available data on pressure, temperature and humidity. The non-isothermal cloud temperatures are assumed the same as those of the surroundings.

The program then solves the unknown coefficients of proportionality of radiance solutions for an inhomogeneous system of equations described in Section 2.2. After proper summation over the sub-spectral weight derived from the exponential fit, the transmitted and reflected spectral radiances at the cloud top and bottom, respectively, can be obtained. Since the infrared computer program employs 16 discrete streams in the calculations, interpolations of the 16 radiance values are finally

needed to obtain 0°, 180° and limb (90°) directions. Note that 0° and
180° directions are used to define the transmissivity and reflectivity
of clouds.

SECTION 3

APPLICATION TO NOAA IV VTPR CHANNELS

3.1   Characteristics of VTPR Channels

In this section we investigate effects of cirrus clouds on
NOAA IV VTPR (Vertical Temperature Profile Radiometer) channels and explore
cirrus cloud scenes utilizing upwelling radiance observations from these
channels.

The NOAA 4 VTPR instruments consist of six channels in the 15 μm
band of CO_2, one channel in the window region at 12 μm and one channel in
the rotational band of water vapor. Table 3.1 shows the nominal character-
istics of the eight filters in the VTPR instruments. The center wavenumbers
are employed to calculate the single scattering properties

Table 3.1. Nominal spectral intervals for VTPR channels.
after McMillin et al. (1973).

Channel	Center wavelength		Half-width
	(μm)	(cm^{-1})	(cm^{-1})
1	14.96	668.5	3.5
2	14.77	677.5	10
3	14.38	695.0	10
4	14.12	708.0	10
5	13.79	725.0	10
6	13.38	747.0	10
7	18.69	535.0	18
8	11.97	833.0	10

20

of ice crystals which are presumably valid for the entire spectral region.
Atmospheric transmittances for the eight spectral intervals are available
for the zenith angles of 0° and 23°47' (McMillin et al., 1973). Accord-
ing to their report, transmittances for CO_2 are based upon calculations
made by Drayson (1971) employing the point-by-point method for a number
of temperature profiles. From these transmittances, transmittances for a
given temperature profile may be obtained by means of interpolation. Ozone
transmittances, which are a minor correction, are calculated from a line-by-
line technique for the lower atmosphere using climatological ozone profiles
(McClatchey et al., 1971). As for water vapor, a procedure proposed by Weinreb
and Neuendorffer (1973) is utilized to obtain the transmittances of selec-
tive absorption in inhomogeneous atmospheres. The effect of the water
vapor continuum is also included based on laboratory measurements (Bignell,
1970). Thus, the transmittance of a VTPR channel for a given height z is
given by

$$T_{\Delta\nu}(z) = T_{\Delta\nu}^{CO_2}(z) T_{\Delta\nu}^{H_2O}(z) T_{\Delta\nu}^{O_3}(z) . \qquad (3.1)$$

Figure 3.1 depicts the weighting functions of the VTPR channels.
Since clouds are normally tropospheric in origin and are located below about
200 mb or so, we would anticipate that their effects on upward radiances ob-
served in channels 1, 2 and 3 of the CO_2 band are relatively insignificant.

There are only two sets of transmittances being generated for
VTPR instruments corresponding to 0° (nadir) and 23°47' zenith angles.
However, spectral radiative transfer for cirrus clouds require the clear
column angular upward and downward radiances reaching the cloud base and
top, respectively. To evaluate these radiances, the angular dependent

21
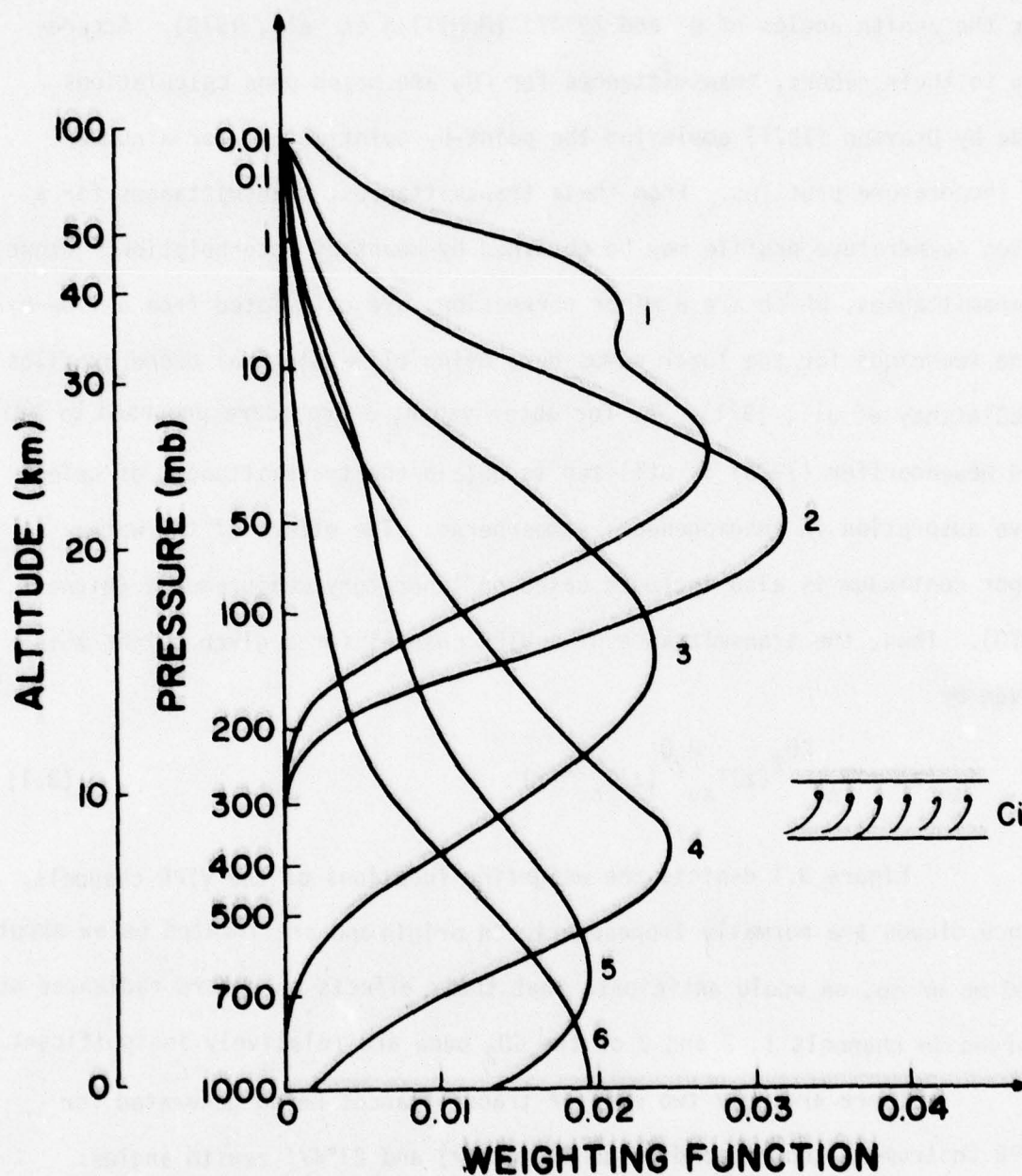
Figure 3.1. Weighting functions of the VTPR CO_2 channels (after McMillin et al., 1973).

22

transmittances from 0° to 90° zenith angles are needed. The maximum VTPR scan angle is about 40° zenith angle. Thus, angular transmittances other than 0° and 23°47' are also needed for the interpretation of the observed upward radiances. According to McMillian (1976, personal communication), the angular transmittances for the 15 μm CO_2 channels are approximately given by

$$T_{\Delta\nu}(z,\mu) = [T_{\Delta\nu}(z)]^{f_1}, \tag{3.2}$$

where

$$f_1 = [\sec(\cos^{-1}\mu)]^{0.1 \ f_2}. \tag{3.3}$$

The empirical coefficient f_2 was derived from a four term polynomial fitting. It is related to the pressure and temperature for a given level and certain empirically determined constants. For water vapor channels 7 and 8, however, angular dependent transmittances are approximated by

$$T_{\Delta\nu}(z,\mu) = [T_{\Delta\nu}(z)]^{\sec(0.77 \ \cos^{-1}\mu)}. \tag{3.4}$$

Verification of the empirical angular transmittances was done by comparing the calculated and observed radiances for various scan angles. It appears that up to about 40°, they are reasonably reliable. Since no additional information is available, we have used these empirical equations to evaluate the angular transmittances from 0° to 90° zenith angles for the eight VTPR channels. It is anticipated that errors may be produced for large zenith angles close to the limb. But we also note that contributions of radiances close to the limb are insignificant owing to the very long

23

gaseous path length.

Table 3.2 lists optical properties for randomly oriented ice cylinders based on a scattering program developed by Liou (1972). The real and imaginary parts of the refractive indices are taken from the recent measurements by Schaaf and Williams (1973). We see that imaginary parts decrease from the shorter wavelength to the longer wavelength in this part of the infrared spectrum with the window wavelength having the largest value. However, the window wavelength is also associated with the smallest value of the real part of the refractive index. The ice cylinders appear to have the largest extinction cross-section and largest single scattering albedo in the rotational band wavelength owing to the smallest imaginary part. The fact that the extinction and single-scattering albedo vary insignificantly in these wavenumbers is probably because of the large particle size considered in this study.

Table 3.2 Optical properties of ice cylinders (length 200 μm, width 60 μm) for the central wavenumbers of VTPR channels.

Channel	$\nu(cm^{-1})$	n_r	n_i	$\tilde{\omega}_0$	$\sigma_{ext}(10^{-4}cm^2)$
1	668.5	1.573	0.178	0.527	2.94
2	677.5	1.581	0.194	0.528	2.94
3	695.0	1.583	0.232	0.530	2.94
4	708.0	1.577	0.262	0.532	2.92
5	725.0	1.556	0.305	0.533	2.92
6	747.0	1.522	0.349	0.534	2.92
7	535.0	1.503	0.074	0.554	3.12
8	833.0	1.259	0.409	0.531	2.86

3.2   Comparison Between Satellite Observations and Theoretical
        Simulations for Selected Cirrus Cloud Cases

Three cirrus cloud cases under the NOAA satellite pass were

selected for comparison between the present theoretical calculations

and satellite observations. Figures 3.3a, 3.3b, and 3.3c represent

the case studies to which the cloud model was applied. Each case study

is described to include the atmospheric profile, the synoptic situation,

and the cloud composition determination. These cases were selected

from a group of cases developed by the AFGL during 1974 and 1975. These

three case studies were used to test the cloud model program under three

conditions and include cirrus with low clouds (Jan. 11, 1974), thin

cirrus with no low clouds (Feb. 1, 1974), and thick cirrus with no low

clouds (Jan. 22, 1975).

Each figure depicts the profile of temperature, pressure, and

water vapor versus height. Each parameter was interpolated to 101 levels

used in the clear column radiance calculations. Input into each profile

was the actual temperature and water vapor profiles of the nearest radio-

sonde station to the point of interest in time and space linearly inter-

polated to the required pressure heights. Above the level of the radiosonde

the temperature, water vapor, height and pressure profiles compiled by

McClatchey et al. (1971) for a midlatitude winter atmosphere were used for

each case study.

The position and ice content of the cloud for each case were

estimated from airborne instrumentation equipped with a Knollenberg

probe (Knollenberg, 1970) used by AFGL during the cloud physics experi-

ment. These estimates were obtained by an aircraft spiralling downward

from 10 km at the approximate time of the satellite pass. Objective

25
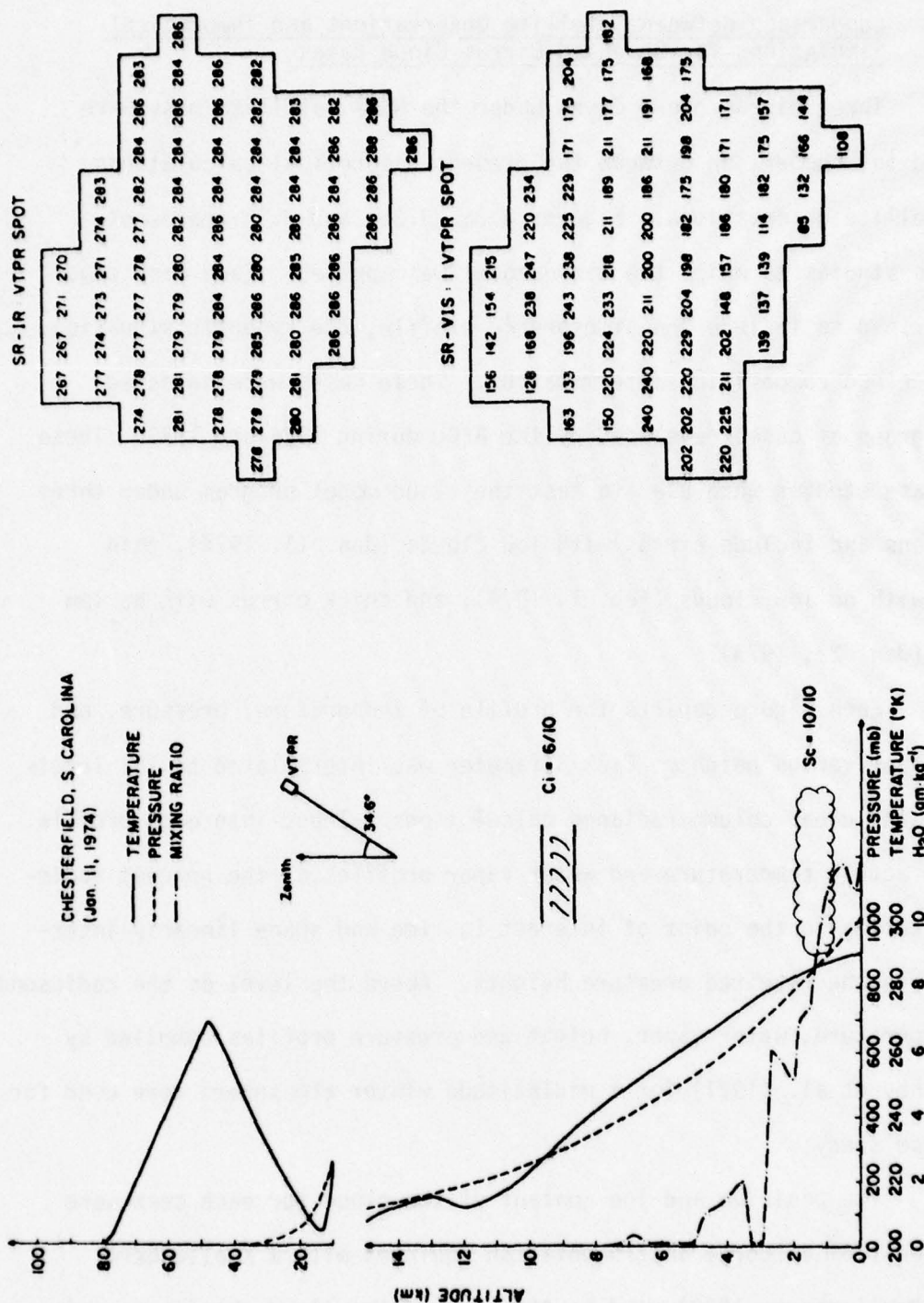
Figure 3.3(a). The first cirrus cloud case consisting of a high cirrus with a stratocumulus below. The left-hand side of each figure depicts the profile of temperature, pressure and mixing ratio as functions of height and the scan angle of the VTPR instrument. The right-hand side of each figure represents the scanning radiometer data for the area sensed at one scan position of the VTPR sensor. The upper and lower presentations are for IR (equivalent temperature) and visible (foot-Lambert), respectively.

SR-IR · I VTPR SPOT

241
239 245 258 255 255 259 262 259 259 251
247 250 249 262 258 243 247 246 250
251 262 258 251 245 245 245 246 256
251 259 253 250 243 250 243 252 256
240 252 251 246 248 240 240 244 241
235 234 243 246 243 244 241
246
251 240

SR-VIS · I VTPR SPOT

164
186 177 125 94 64
155 119 128 103 106 174 145
152 88 106 128 174 174 143
143 76 131 149 152 145
119 106 140 140 161 124 101
128 149 131 128 110 110
149 149 177 143 153
186 177 143 100
152 100 136

RICHMOND, INDIANA
(Jan. 22, 1975)

—— TEMPERATURE
–– – PRESSURE
–·– MIXING RATIO

Zenith □ VTPR
10.2°

Ci = 5/10
Cs = 10/10
Ci = 10/10

PRESSURE (mb)   200 220 240 260 280 300 320
TEMPERATURE (°K) 200   400   600   800   1000   1200
H₂O (gm kg⁻¹)   0   2   4   6   8   10   12

100
80
60
40
20

14
12
10
8
6
4
2
0

Figure 3.3(b). As in Figure 3.3(a) except for a cirrus cloud case consisting of a high cirrus with a stratocumulus below.

27

SR-IR I VTPR SPOT

```
          265 263 267
          266 263 261 239
      261 263 258 255 259 249 244 246
      263 260 265 258 259 265 262 254
      268 265 262 269 265 264 269 265 266
          263 270 272 273 273 269 269 264
              273 273 274 272 272 269 269
                  270 272 269 265
                      266 266
```

SR-VIS I VTPR SPOT

```
          55 51 95
          55 41 114 133
      77 77 80 87 60 65 60 97 97
      46 32 46 60 39 68 82 65 72
      51 49 44 39 49 46 37 53 31 60
          37 35 32 46 56 44 79
              28 70 67 46 35
                  74 36
```

RICHMOND, INDIANA
(Feb 1, 1974)

——— TEMPERATURE
- - - PRESSURE
— · — MIXING RATIO

Zenith VTPR
   17.0°

Ci = 7/10

Figure 3.3(c). As in Figure 3.3(a) except for a cirrus cloud case consisting of multi-layered cirrus clouds.

28

analyses of ice contents were also made. The ice content analyses involve best estimates derived from detailed aircraft observations consisting of visual observations, snow intensity, particle size replica, visibility, temperature and photography (Conover, 1976, personal communication). From all these pieces of information as functions of the altitude, Conover (with the consultation of AFGL cloud physists headed by R. Cunningham) derived the total vertical ice contents used in this investigation.

To use the observed cloud information in the theoretical transfer calculations, the vertical ice content for the ice cloud model employed in this study has to be defined. For randomly oriented ice cylinders in a horizontal plane, it is given by

$$IC = \pi r^2 \ell \, \rho_I \, N \, \Delta z, \tag{3.5}$$

where r and ℓ are the radius and the length of the cylinder, respectively, ρ_I the density of ice, N the number density and Δz the thickness of the cloud. As described earlier, the vertical ice content and the cloud thickness are available from aircraft observations. Since the radius and the length of the ice cylinder have been specified to obtain the single-scattering parameters, it follows that the "equivalent" particle number density can be derived. Once the number density has been obtained, the optical depth of ice within the cirrus cloud under consideration is simply equal to $\sigma_{ext} \, N \, \Delta z$. Together with the optical depth of the gases within the cloud, the total optical depth represents one of the fundamental parameters in transfer calculations. Having the atmospheric temperature and water vapor profiles from radiosonde, and the cloud structure and composition specified, transfer calculations may now be carried out for

these cases.

The satellite data depicted on each figure is the scanning radiometer (SR) data representing the area sensed at one scan position of the VTPR sensor, where the zenith angle is that angle that the center of the VTPR scan position makes with the earth's local zenith. The upper presentation is the temperature reading obtained from the scanning radiometer, while the lower presentation is the visible channel of the scanning radiometer. Brief descriptions on each case are in order.

January 11, 1974

The area of the United States east of the Rocky Mountains was under the influence of a weak low, which at 500 mb had its center in north central Canada. The trough axis was very flat extending through North Dakota southwestward into western Texas. A weak surface low was centered in western Pennsylvania with a weak cold front extending southwestward to New Orleans. A weak warm front extended due eastward. Precipitation was spread along the frontal system from Alabama to the east coast. Chesterfield, South Carolina 34.65 N - 80.20 W was located under the cirrus shield of the frontal system. The location had an observation of overcast stratocumulus with the top at 2 km and a 6/10 cirrus layer from 8.8 to 9.8 km. The temperature, pressure and water vapor profiles were obtained from the 1200Z Athens, Georgia sounding. The time of the observation and the satellite pass time was 1521Z. The cirrus cloud ice content was estimated to be 11 gm m^{-2} in the VTPR field of view. The SR field of view of the VTPR spot had a mean brightness of 181 and a mean temperature of 281.3°K. These readings suggest that the cirrus is semi-transparent in both channels. Most of the observed brightness was probably contributed by the stratocumulus since the cirrus was semi-transparent to

30

the aircraft observer.

February 1, 1974

The area of the United States east of the Rocky Mountains was under the influence of zonal flow at 500 mb with a surface high pressure centered near the Minnesota-Canadian border. A weak frontal system was oriented east-west across central Alabama to a low pressure in western Oklahoma. A major area of precipitation was apparent over Michigan westward to North Dakota. Richmond, Indiana 39.75 N - 84.83 W was located under cirrus clouds south of the main precipitation area. The location had an observation of a thin 7/10 cirrus cover from 9-9.8 km. The temperature, pressure and water vapor profiles were obtained from the 1200Z Dayton, Ohio sounding. The time of the observation and satellite pass time was 1526Z. The cirrus cloud ice content was estimated to be 2 gm m^{-2} in the VTPR field of view. In this case, the SR means are 58 in the visible channel and 263.9°K in the IR channel. The cirrus is again transparent in both channels since the mean readings are very close to the surface conditions. Note that during the above two days, the cloud physics observations were under the NOAA 2 satellite. Inspection of the VTPR transmittances of NOAA 2 and NOAA 4 indicates insignificant differences. Thus, we have consistently used the NOAA 4 VTPR transmittances in the present study.

January 22, 1975

The area of the United States east of the Rocky Mountains was dominated by zonal flow with a cutoff low over New Mexico at 500 mb. The surface had high pressure centers over western Virginia and central Iowa divided by a weak frontal system. Richmond, Virginia 37.53 N - 77.27 W

31

was located in a general area of scattered fog and overcast cirrus. The location had an observation of 10/10 cirrus from 4.4 - 5.7 km and 10/10 cirrostratus from 6.7 - 8.7 km and 5/10 cirrus from 8.7 - 10.7 km. The temperature, pressure and water vapor profiles were obtained from the Richmond 1200Z sounding. The cirrus cloud ice content was 6.4 gm m^{-2} for the top layer, 67.8 gm m^{-2} for the middle layer and 104.2 gm m^{-2} for the lower layer in the VTPR field of view. The time of the observation and satellite pass time was 1417Z. The SR averages were 248.4°K and 134.5 for the IR and visible channels, respectively. The temperature reading is the same temperature as located at 6.5 km in the sounding.

Figure 3.4 illustrates comparisons between the observed and computed upward radiances for the three cirrus cloud cases described previously. Note that the VTPR scan angles are denoted in Figure 3.3. For the case when thick, layered cirrus clouds are present, the top layer consists of only 50% cloud cover. Thus, calculations were made by averaging the resulting values for a three- and a two-layer cloud system. The calculated radiances for channels 4-8 are consistently lower than those observed from the NOAA 4 satellite. Possible explanations are that the observed value of the ice content was overestimated, or the particle size used in calculations was too small, or the cloud temperature was improperly assumed. Comparisons between the observed and computed radiances for the single cirrus cloud case reveal systematically higher values based on theoretical simulations. Again it is perhaps caused by one of several possibilities such as an underestimation of the vertical ice content within the field of view of the VTPR instrument. In our judgement, the systematic behavior of the calculated and observed radiance values for those two cases indicates to certain extents the reliability of the theoretical model for the transfer of spectral
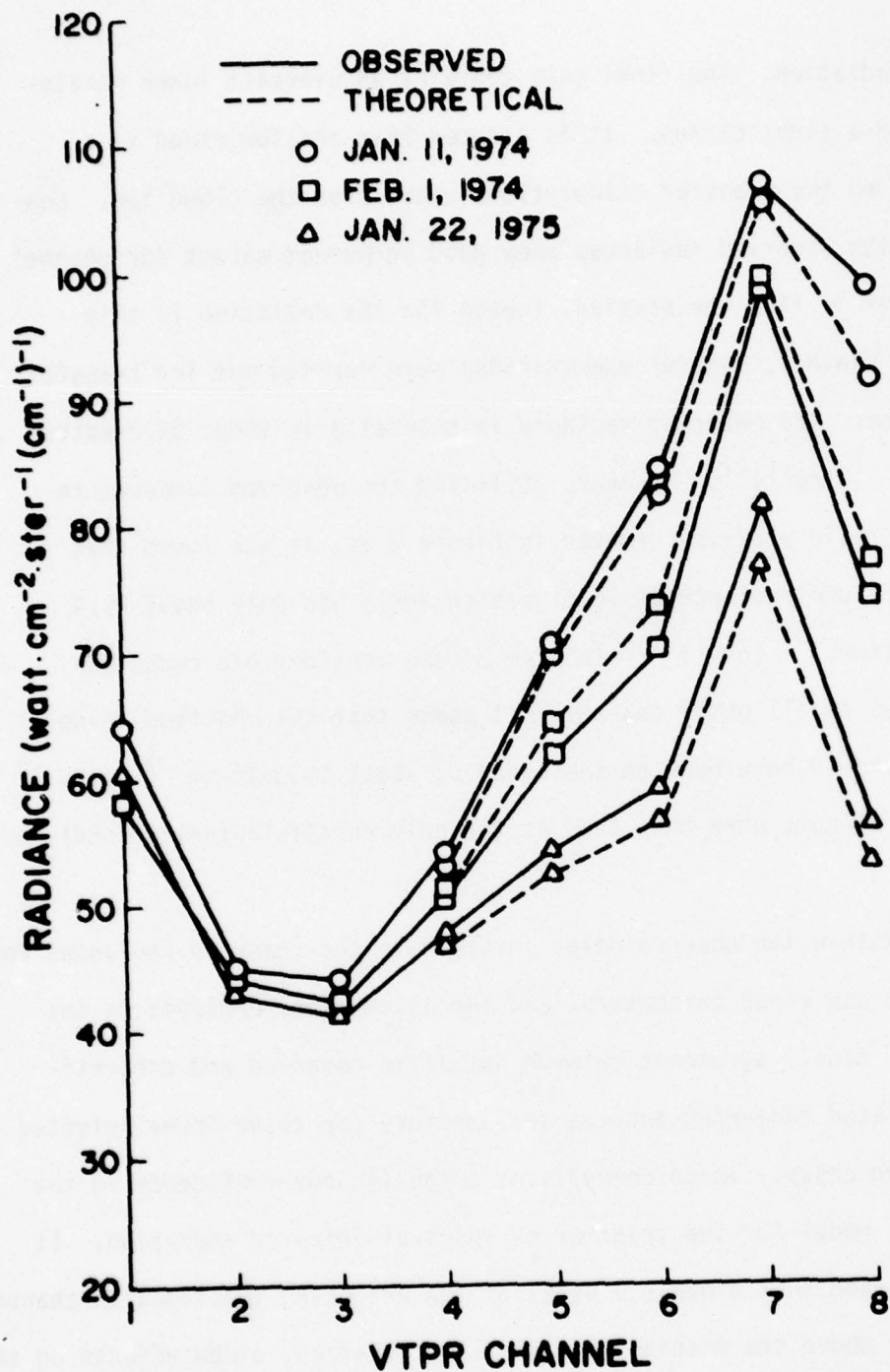
32

Figure 3.4. Comparisons between satellite observed and theoretically simulated upward radiances for the three cirrus cloud cases described in Figure 3.3.

33

infrared radiation. The final case contains an overcast lower strato-
cumulus and a light cirrus. It is assumed that the low cloud is a
black body so the transfer calculations start from the cloud top. Com-
parisons with observed radiances show good agreement except for channel
8. In order to find the physical reason for the deviation in this
particular channel, careful examinations were carried out for transfer
calculations. The observed radiance in channel 8 is about 98.3 watts
cm^{-2} ster. $^{-1}$ $(cm^{-1})^{-1}$. However, utilizing the observed temperature
and mixing ratio profiles denoted in Figure 3.3a, it was found that
the clear column radiance at 34.6° zenith angle was only about 99.4
watt cm^{-2} ster. $^{-1}$ $(cm^{-1})^{-1}$. In view of the considerable reduction
of radiances in all other channels, it seems that the observed value in
channel 8 should have been on the order of about 90 watt cm^{-2} ster. $^{-1}$
$(cm^{-1})^{-1}$. We note here that this is the only unsatisfactory channel com-
parison.

Within the uncertainties involved in the measured radiances and
atmospheric and cloud parameters, and the assumptions employed in the
theoretical model, agreement between satellite observed and theoreti-
cally simulated radiances appears satisfactory for these three selected
cirrus cloud cases. These comparisons establish our confidence in the
theoretical model for the transfer of spectral infrared radiation. It
should be noted that since the peaks of the weighting functions in channels
1-3 are all above the possible cirrus cloud location, cloud effects on the
upward radiances in these channels can be ignored.

3.3   Theoretical Results and Cloud Scene Discussions

3.3.1   Spectral transmission and reflection of cirrus. In this section

34

we present some results of the radiative properties of cirrus clouds and cirrus cloudy atmospheres. It is convenient to define the spectral transmission $T_{\Delta\nu}^C$ and reflection $R_{\Delta\nu}^C$ of a cloud layer as follows (see Eqs. (2.5) and (2.6)):

$$
\left.
\begin{aligned}
T_{\Delta\nu}^C &= I_{\Delta\nu}^{\uparrow}(z_t,1) \,/\, I_{\Delta\nu}^{\uparrow}(z_b,1) \\[2mm]
R_{\Delta\nu}^C &= I_{\Delta\nu}^{\downarrow}(z_b,-1)/I_{\Delta\nu}^{\uparrow}(z_b,\,1)
\end{aligned}
\right\} .
\tag{3.6}
$$

Physically, the transmission defined above represents the actual percentage attenuation of upwelling radiances reaching the cloud base, and it may be employed for the parameterization of cloud radiative properties from a satellite point of view. Note that both transmission and reflection include contributions of cloud emission, which is automatically generated in transfer calculations.

Figure 3.5 illustrates the spectral reflection of cirrus as a function of the thickness and the vertical ice content for VTPR channels. The left and right-hand graphs are for a tropical (wet) and a midlatitude winter (dry) atmosphere, respectively (McClatchey et al., 1971). The vertical scale applies to the lower-most curves. The scales for other curves are to be obtained by subtracting consecutively a factor of 0.2 such that the horizontal bar on each curve is zero. Cloud infrared reflection appears independent of the atmospheric profile. Its value increases asymptotically with increasing cloud thickness. Cloud reflection arises primarily from scattering of cloud particles. The single-scattering albedos are about the same for channels 4, 5, 6, and 8 resulting in similar reflection patterns. For channel 7, however, a higher single-scattering
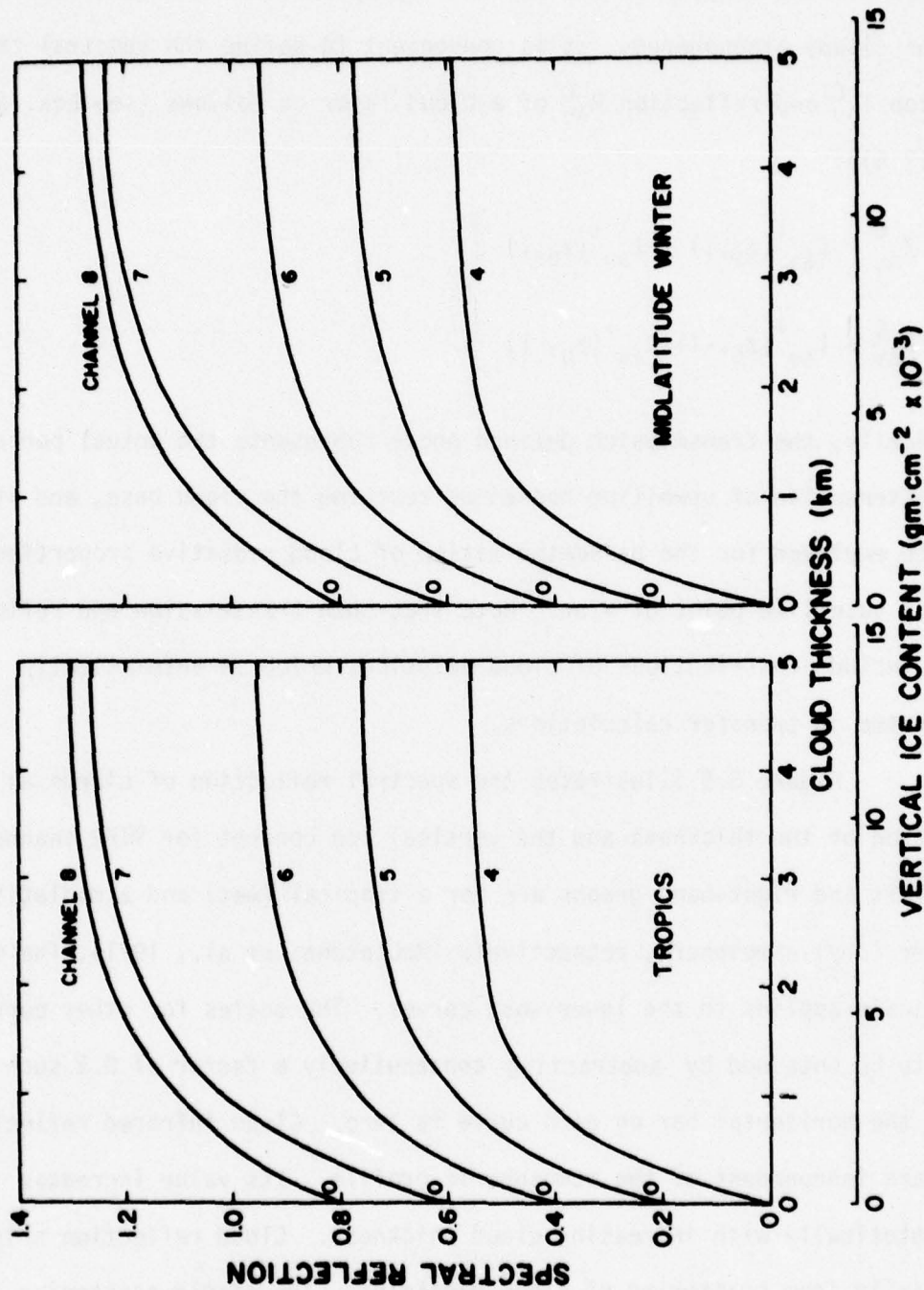
35

Figure 3.5. Spectral reflection of cirrus (see text for definition) as a function of the cloud thickness for a tropical and a mid-latitude atmosphere. The lower abscissa denotes the ice content scale corresponding to the cloud thickness using a particle number density of 0.05 cm⁻³.

albedo is derived (see Table 3.2). This results in larger reflection values as evident in Figure 3.5. Note that reflection defined earlier includes emission contribution from clouds, primarily the warmer cloud base. For a 1 km thick cirrus, we see that the reflection value already reaches about 0.4.

Figure 3.6 shows the spectral transmission of cirrus. As in Figure 3.5, the vertical scale applies to the lower-most curves. The scales for other curves are to be obtained by subtracting successfully a factor of 0.2 such that the horizontal bar on each curve is 1. Cloud infrared transmission decreases with increasing thickness and reaches a value of about 0.3 for a cloud thickness of 5 km for channels 4-6 and 8. As for channel 7, a cloud whose thickness is 5 km transmits about 43% of the incident upwelling radiance owing to a larger single-scattering albedo at a wavenumber of 535 cm^{-1}. Inspection of the transmission curves indicates a similar behavior for the CO_2 and window channels. In particular, variations of the spectral transmission of CO_2 channels for all the thicknesses presented here are less than about 3%. Even the transmission value of the window channel does not vary by more than 10% with respect to those of the CO_2 channels. Larger deviations are seen to take place for larger thicknesses. Since cirrus clouds are not normally thick, we may, to a good approximation, assume that the cloud transmission values are constants for the CO_2 and window channels.

In view of the spectral transmission defined in Eq. (3.6), we may parameterize radiative transfer processes in cloud layers and express the upwelling radiance at the top of the atmosphere in the form
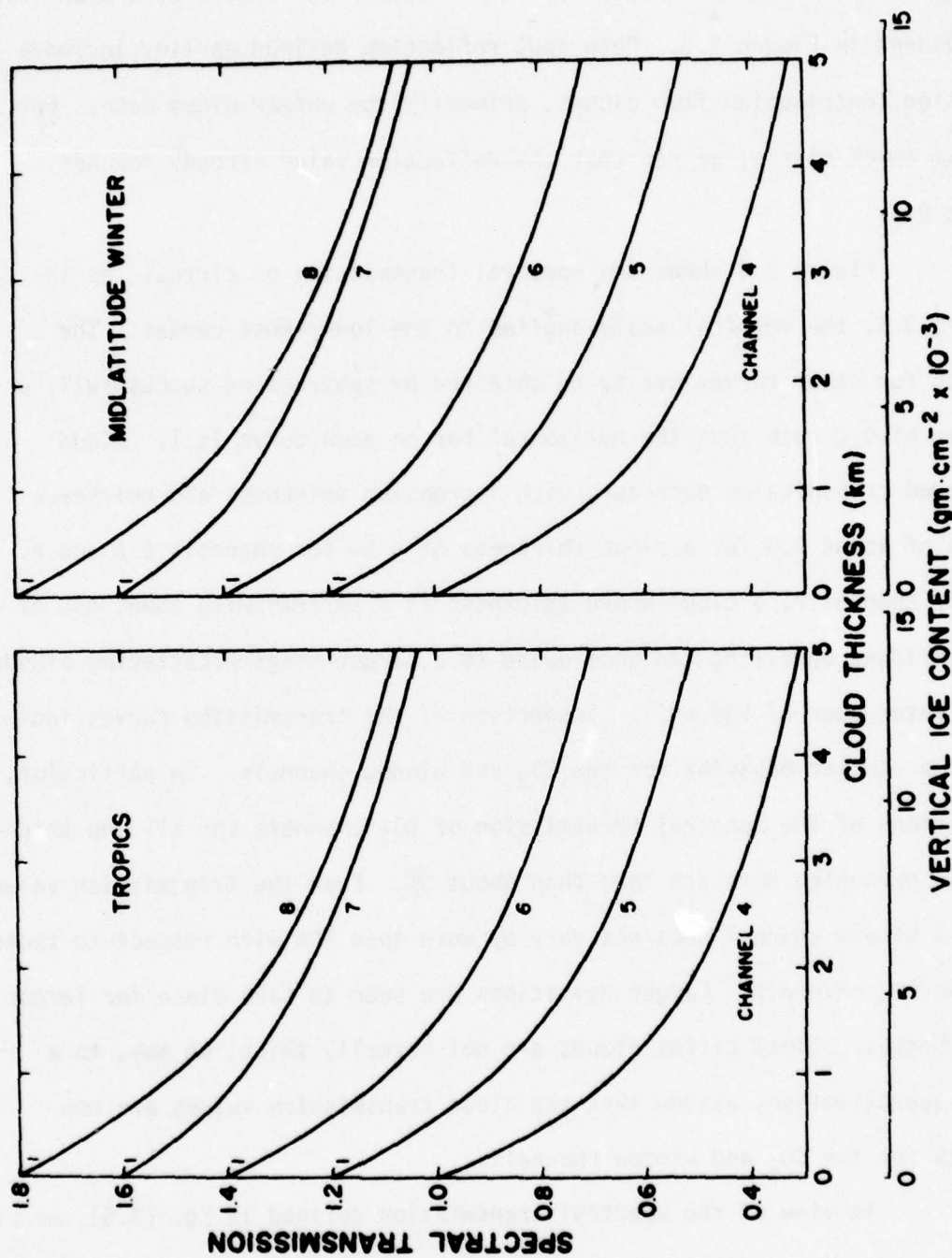
Figure 3.6. Spectral transmission of cirrus (see text for definition) as a function of the cloud thickness for a tropical and a mid-latitude atmosphere. The lower abscissa denotes the ice content scale corresponding to the cloud thickness employing a particle number density of 0.05 cm^{-3}.

$$I_i = \{B_i(T_s)T_i(z_b,0) + \int_0^{z_b} B_i[T(z)]d\,T_i(z_b,z)\}$$

$$\times\, T_i^C(z_t,z_b)T_i(\infty,z_t) + \int_{z_t}^{\infty} B_i[T(z)]d\,T_i(\infty,z). \qquad (3.7)$$

Here the subscript $\Delta\nu$ is replaced by i, z_b and z_t denote the cloud base and top heights, respectively, and T_s is the surface temperature. The first term represents the upwelling radiance reaching the cloud base and it is attenuated by the cloud and gases above the cloud subsequently, while the second term denotes the absorption and emission contributions from gases above the cloud. According to spectral transmission calculations reported previously, T_i^C ($i = 4,5,6$ and 8) may be considered as one unknown parameter which is composed of the cloud ice content (or optical depth) information. Thus, for overcast cirrus cloud cases, it seems feasible to construct numerical procedures for recovering the cloud transmission (in terms of ice content, for example) and, perhaps, temperature profile simultaneously utilizing CO_2 and window channels.

3.3.2   Upward radiances and possible ice content determination.   The most important quantity associated with satellite sensing of the atmosphere is the upward radiance at the top of the atmosphere. Upward radiances are the only information for the inference of the structure and composition of the atmosphere.

Figure 3.7 shows graphs of upward radiances in VTPR channels as functions of the zenith angle for various cloud ice contents in a tropical atmosphere. For a given ice content value, it is clear that upward radiances increase from channel 4 to channel 8 (note that upward radiances in channel
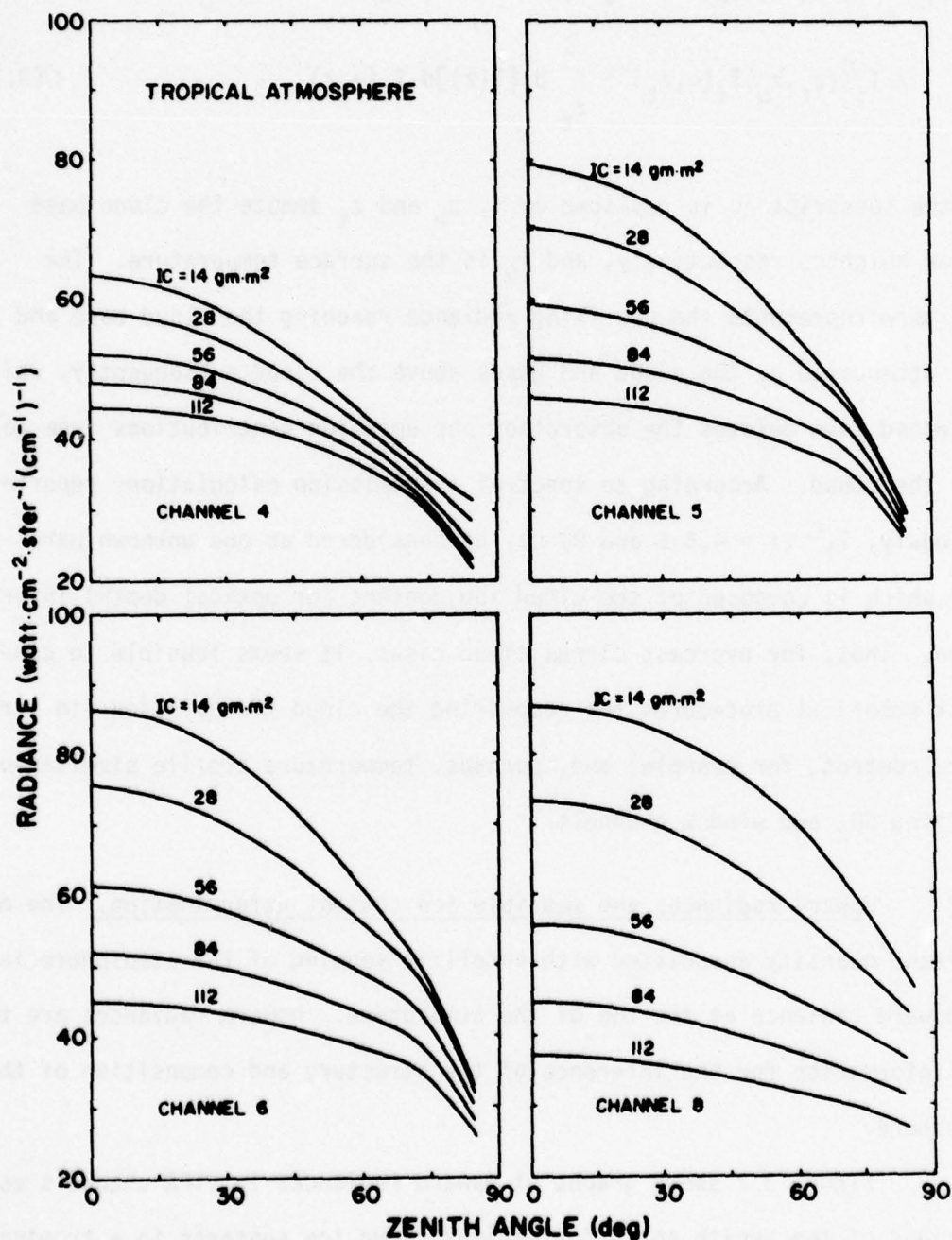
39

Figure 3.7. Upward radiances at the top of the atmosphere in VTPR CO_2 and window channels as functions of the zenith angle for various cloud ice contents ranging from 14 to 112 gm m^{-2}. The model atmosphere used in calculations is a tropical profile.

7 is not shown). This is probably due to decreasing absorption strength from the CO_2 band center to the wing. For an ice content of 112 gm m^{-2}, we see that upward radiances in channels 4-6 are about the same with patterns close to isotropic radiation except in the limb. Upward radiances in these channels show strong limb darkening effect for zenith angles greater than about 30° or so. From 0° (nadir) to about 30° zenith angles, upward radiances do not vary appreciably. With respect to each channel, increasing the ice content of cirrus leads to a reduction of upward radiances. This is particularly evident for channel 8. Physically, this means that clouds affect more significantly radiance measurements in the window channel as compared with the CO_2 channels. Spectral transfer calculations were also carried out for other climatological profiles tabulated by McClatchey et al. (1971). These calculations reveal that relationships between upward radiances and ice contents depend somewhat on the atmospheric temperature profile, except for very large values of ice contents which dominate transfer processes.

In Figure 3.8, we present the upwelling (nadir) radiance of VTPR channels for two model cirrus cloudy atmospheres representing wet (tropics) and dry (midlatitude winter) conditions, respectively. The solid curves in this figure denote upwelling radiances for clear columns. For the tropical atmosphere, systematic reductions of the upwelling radiance due to the increase of the ice content are illustrated. In reference to Figure 3.1, it is seen that the peak of the weighting function for channel 4 is located at about the position of cirrus clouds. Consequently, even a thin cirrus produces a significant signature of radiance reduction. In the water vapor rotational band (smaller wavenumber) larger upwelling
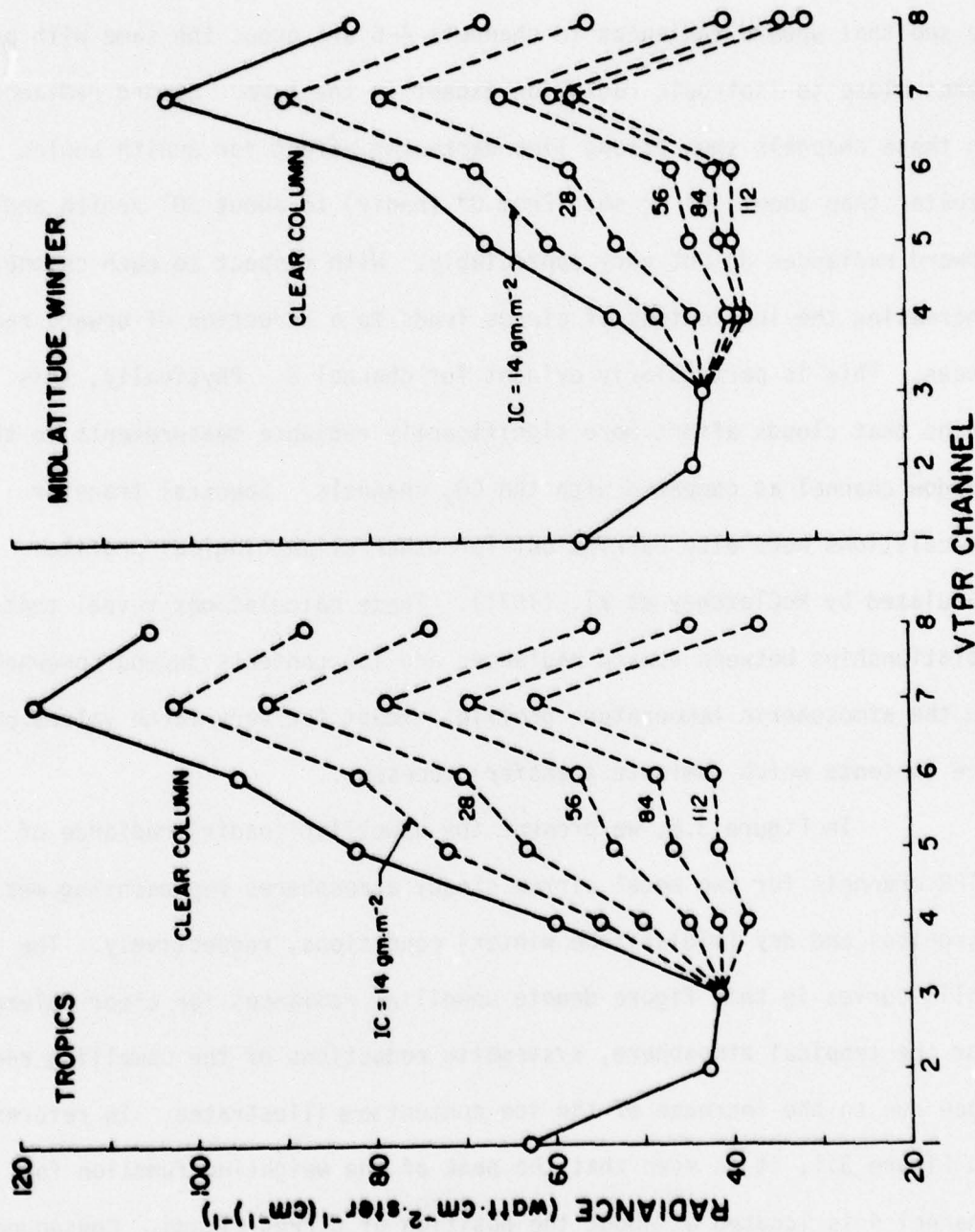
41

Figure 3.8. Upwelling (nadir) radiances of VTPR channels for a tropical (left-hand side) and a mid-latitude (right-hand side) atmosphere. The solid curves denote upwelling radiances for clear columns. Systematic reductions caused by the increase of the cirrus ice content is shown by dashed curves.

radiances arise from the behavior of the Planck function and the emission
from water vapor. The systematic reduction caused by the increase of ice
content is so distinct that the observed radiances obtained from VTPR
channels in a completely cloudy atmosphere may be utilized to evaluate
the amount of ice within the field-of-view. This, of course, would rely
upon a first estimation of clear column radiances from available atmospheric
profiles. Upwelling radiances in a midlatitude winter atmosphere exhibit
similar reduction patterns, but their values are lower owing to the lower
temperatures in the troposphere. Reduction values in cases when ice con-
tents are 84 and 112 gm m^{-2} are very close, revealing that the cloud is
reaching a black-body thermodynamic state.

Having the upward radiance calculated for a series of cirrus ice
content values in various model atmospheric profiles, the following proce-
dures seem feasible for the ice content determination. Assume that within
the field-of-view of VTPR channels there is η portion of cirrus cloudiness,
the upward radiance in a partly cloudy atmosphere is given by Eq. (2.18)
in the form $(\Delta\nu \to i)$.

$$I_i^{PC} = \eta \, I_i^{C} + (1-\eta)I_i^{NC}. \tag{3.8}$$

It can be shown that for any two cloud-contaminated radiances at distinct
wavenumbers that

$$\frac{I_i^{PC} - I_i^{NC}}{I_{i+1}^{PC} - I_{i+1}^{NC}} \bigg/ \frac{I_i^{C} - I_i^{NC}}{I_{i+1}^{C} - I_{i+1}^{NC}} = 1, \tag{3.9}$$

43

where

$$I_i^C < I_i^{PC} < I_i^{NC}, \quad i = 4, 5, 6, 7, 8.$$

As mentioned previously, clear column radiances are to be estimated. Estimation may be accomplished by employing available atmospheric profile analyses such as those provided by NMC or from climatology. Although Eq. (3.9) now contains two unknown parameters I_i^C and I_{i+1}^C, these two variables are both functions of the ice content. Based on transfer calculations, for a given ice content in a specified atmosphere, both values may be derived. Upon inserting a series of ice content values, we may obtain a best estimate such that Eq. (3.9) holds. This procedure can be carried out for pairs of adjacent channels in which the optical property of ice varies insignificantly. Consequently, each pair gives an ice content estimation. By further inspection of these estimations, a final value for ice content which satisfies all the channel observations could be determined. This could be accomplished by examining the mean and standard deviation with respect to 1 according to Eq. (3.9) for all available channel observations. Once an ice content value has been chosen, I_i^C is known and from Eq. (3.8), the cloud cover information can be calculated. An averaged value of η may be subsequently obtained such that it satisfies all the channel observations.

The above procedures were followed for the three cirrus cloud cases described in section 3.2. The best ice content estimates that we obtained were 10, 8, and 112 gm m^{-2} for 11 January, 1974, 1 February, 1974 and 22 January, 1975, respectively, whereas the in-situ aircraft observations gave 11, 2 and 176 gm m^{-2}, respectively. Since these are the only three available cirrus cloud cases, it is not possible to perform significant

44

statistical error analyses.

It should be emphasized that the semi-empirical method for ice content estimation makes use of the results from transfer calculations and assumes a prior knowledge of the clear column radiance. The latter assumption relies upon reliable atmospheric profiles which are unknown in cloudy conditions. Hence, the best estimation for the profile, which is needed, may lead to the uncertainty in the ice content determination. Nevertheless, the procedure described here, at least, represents an objective and workable means for recovering cloud information from satellite sensing.

3.4   Conclusions

The infrared transfer model described in Section 2 was applied to VTPR channels of the NOAA 4 satellite to simulate upward radiance at the top of the atmosphere in cirrus cloud conditions. Available transmittances for each channel were employed and modified to incorporate them into the spectral infrared transfer program. Comparisons between satellite observed and theoretically simulated radiances reveal systematic agreement for selected cirrus cloud cases involving thin and thick cirrus, and thin cirrus with stratocumulus below. Theoretical calculations employ observed atmospheric profiles from radiosondes, and the best estimated cloud parameters from aircraft observations under the satellite pass. These comparisons give confidence in the theoretical model for the spectral infrared transfer in cloudy atmospheres.

Utilizing the spectral infrared transfer model, radiative properties of cirrus cloudy atmospheres in VTPR channels were investigated for two model atmospheric profiles. The spectral transmission and reflection, defined as the ratios of the upwelling radiance at the cloud

45

bottom to that at the cloud top and to the downwelling radiance at the cloud bottom, respectively, were calculated. We show that effect of the atmospheric profile on cloud transmission and reflection is insignificant and that close resemblance of these two parameters is found for VTPR channels 4-6 and 8. We further demonstrate that using the concept of cloud transmission it appears possible to parameterize complicated radiative transfer processes through clouds.

Calculations of upward radiances were made for several model cirrus cloudy atmospheres by varying the value of cloud ice content. For a given atmosphere, it is shown that the decrease of upward radiances is closely related to the ice content of cirrus clouds. Systematic reduction patterns of the upwelling radiance caused by the increase of the ice content are clearly illustrated for VTPR channels employing tropical and midlatitude atmospheric profiles. Finally, procedures are outlined for estimating the cirrus ice content in partly covered conditions. Employing three cirrus cloud cases in which satellite observed radiances are available, we demonstrate that the ice content and the amount of cloud cover may be estimated objectively.

46

SECTION 4

APPLICATION TO NIMBUS VI HIRS CHANNELS

4.1   Characteristics of HIRS Channels and Model Atmosphere

This section presents a method for cloud type and cloud mass determination utilizing the High Resolution Infrared Sounder (HIRS) data based upon parameterization of calculations from the spectral infrared model described in Section 2. The Nimbus VI HIRS instrument is a third generation infrared radiation sounder and is similar to the Infrared Temperature Profile Radiometer (ITPR) on the Nimbus V Satellite. The instrument scans perpendicular to the satellite subtrack. There are 42 scan spots per scan line with a resolution of 23 km near nadir and 31 km at the extremes of the scan. The Nimbus VI satellite was successfully launched in June 1975. The HIRS instrument had short periods during which all channels were operating successfully. We have obtained a sample of good data from Smith (private communication). The data correspond to a period of 20-30 August, 1975 and cover a geographical area from 80°-150°W and 20°-50°N. The HIRS instrument senses infrared radiation in 17 channels which include 7 channels in the 15 μm CO_2 band, 5 channels in the 4.3 μm CO_2 band, water vapor channels at 6.8 μm, and 3 channels in windows at 11 μm, 3.68 μm and 0.69 μm.

The data we received were not corrected for solar radiation contamination in the short wave channels. Reflected sunlight has a pronounced affect on channel 16, the short wave window, which, however, was not used in the present analysis.

47

The information compiled in Table 4.1 and Figure 4.1 are taken from Smith, et al. (1975). Figure 4.1 depicts weighting functions for the channels in Table 4.1. The peak in this figure indicates the approximate location in the troposphere from which its energy is derived. Only those channels whose weighting functions peak below 100 mb would be substantially affected by clouds.

Table 4.1. HIRS channel characteristics.

| Channel	$\nu(cm^{-1})$	λ (μm)	Principal Absorbers	Level of Maximum (weighting function (mb))
1	668	15.0	CO_2	30
2	679	14.7	CO_2	60
3	690	14.4	CO_2	100
4	702	14.2	CO_2	250
5	716	14.0	CO_2	500
6	733	13.6	CO_2/H_2O	750
7	749	13.4	CO_2/H_2O	900
8	900	11.0	Window	Surface
9	1224	8.2	H_2O	900
10	1496	6.7	H_2O	400
11	2190	4.57	N_2O	950
12	2212	4.52	N_2O	850
13	2242	4.46	CO_2/N_2O	700
14	2275	4.40	CO_2/N_2O	600
15	2357	4.24	CO_2	5
16	2692	3.71	Window	Surface
17	14.443	0.69	Window	Surface

48
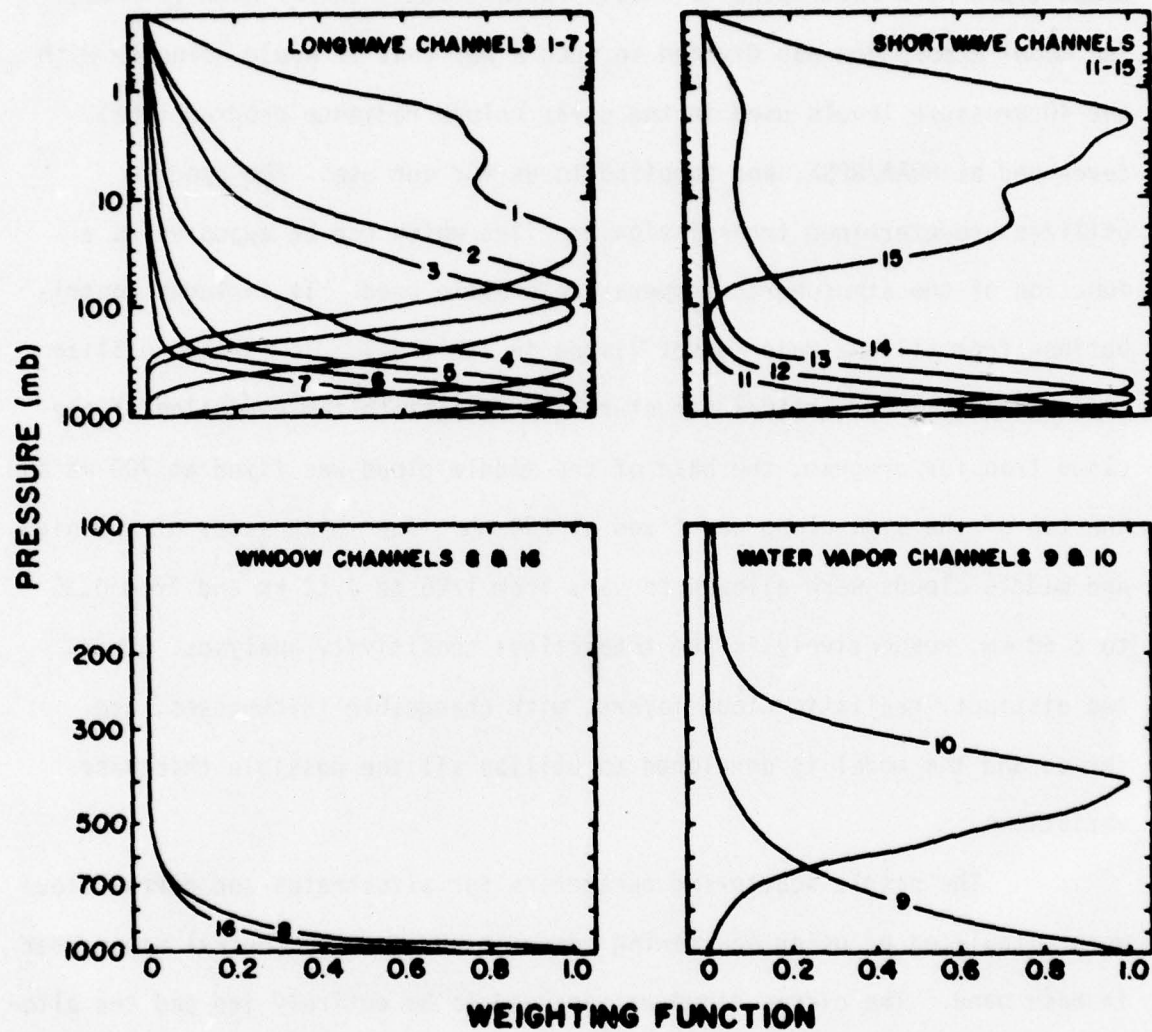
Figure 4.1 The weighting functions of the HIRS channels.

The model atmosphere used in the theoretical analysis was the
mid-latitude summer atmosphere described by McClatchey et al., (1972).
Cloud types were restricted to middle (altostratus) and/or high (cirrus).
The model atmosphere was divided in such a way that it would coincide with
the 40 pressure levels used in the clear column radiance program (CCR)
developed at NOAA/NESS, and supplied to us for our use. The program
utilizes predetermined transmission profiles which can be adjusted as a
function of the atmospheric temperature profile used. It includes contri-
butions from all the major gases listed in Table 4.1. To further utilize
this predetermined vertical structure and facilitate the execution of the
cloud transfer program, the base of the middle cloud was fixed at 700 mb and
the top of the high cloud was fixed at 250 mb. The thicknesses of the high
and middle clouds were allowed to vary from 1.26 to 4.12 km and from 0.35
to 2.68 km, respectively in the theoretical sensitivity analyses. Thus,
two distinct, realistic cloud layers, with changeable thicknesses, are
formed and the model is developed to utilize all the possible thickness
variations.

The single scattering parameters for altostratus and cirrus cloud
were calculated by using scattering computations for the central wavenumber
in each band. The cirrus cloud was assumed to be entirely ice and the alto-
stratus cloud was assumed to be all water. Table 4.2 lists the optical pro-
perties of the ice cylinders. The real and imaginary parts of the index of
refraction are taken from the recent measurement by Schaaf and Williams (1973).
From Table 4.2 it is apparent that the real part of the index of refraction
increases with decreasing wavenumber and the imaginary part decreases with
increasing wavenumber. The single scattering albedo is largest in the

50

window channels (channels 16 and 8) and the extinction cross section is greatest in the 15 μm band (channel 4-7). Table 4.2 also contains the optical properties of the water droplets. The real and imaginary parts of the index of refraction for each band were taken from Hale and Querry (1973). From Table 4.2 it can be seen that the real part of the index of refraction generally increases with increasing wavenumber and the imaginary part decreases. The single scattering albedo is the largest at the largest wavenumber and the extinction cross section is the greatest in the water vapor bands (channels 9 and 10). Only one calculation was made for each of the CO_2 bands since the real and imaginary parts of the index of refraction vary slightly.

Table 4.2. Optical properties of cirrus and altostratus clouds.

Channel	ν (cm^{-1})	ICE				WATER			
		n_r	n_i	$\tilde{\omega}_o$	β_{ext} (km^{-1})	n_r	n_i	$\tilde{\omega}_o$	β_{ext} (km^{-1})
4	701.91								
5	716.83								
6	732.55	1.556	.305	.533	1.464	1.193	.356	.442	13.05
7	749.18								
14	2274.63								
13	2244.21								
12	2211.97	1.299	.0218	.527	1.391	1.333	.0128	.719	13.82
11	2191.02								
16	2691.20	1.392	.007	.625	1.360	1.372	.00356	.867	13.58
8	899.99	1.101	.280	.698	1.33	1.147	.105	.487	11.77
10	1508.29	1.316	.057	.51	1.326	1.332	.035	.619	14.69
9	1223.22	1.307	.04	.698	1.33	1.287	.035	.677	15.72

4.2   <u>Ratioing of Upwelling Radiances: A Case Study on the Cloud</u>
       <u>Thickness Estimation</u>

For each channel, the theoretical model calculated upwelling
clear column and cloudy radiances at the different scan angles of the HIRS
instrument, given an atmosphere, cloud temperature and cloud composition
for each cloud type. In addition, for computational purposes the cloud
top height for the cirrus and the cloud base for the middle cloud were
held constant. In the real atmosphere, the temperature profile is always
changing, the cloud composition is variable, and the location of the clouds
in the vertical is never constant. A method that will minimize the effects
of the model assumptions when parameterizing the real atmosphere is desir-
able. To minimize the computer requirements and redundancy in analysis
all the subsequent relationships were derived for a scan angle of 0°.
These same relationships could be developed for any scan angle or range
of scan anges.

To minimize the model assumptions and to normalize the real data
for the model, the clear column radiances were divided into the cloudy ra-
diances for each channel. This ratio represents the relative reduction of
upwelling radiances due to the cloud effects in the atmosphere and the
quantity is dimensionless. There are several advantages in working with
these ratios. Physically, the ratio will reduce the effect of the change
in atmospheric profile on the cloudy radiances. In addition, the degrada-
tion of the ratio coupled with the peaking of the weighting function gives
an immediate indication of clouds at that level or above. Another advant-
age of the ratio technique is that in addition to normalization between
different atmospheres, the effects of clouds on the ratio of each channel

52

can be compared with other channels. In the subsequent analysis, channels 4-7 of 15 μm CO_2 band, 11-14 of the 4.3 μm CO_2 band, 8 at 11.11 μm in the window, 9 in the 8.2 μm water vapor band and 10 in the 6.3 μm water vapor band were utilized.

The theoretical model was executed for cirrus thicknesses of 1, 2, 3, and 4 km for the case study described below. These ratios are plotted in Figure 4.2 (solid lines). Examination of Figure 4.2 shows that cirrus is transparent in the infrared spectrum. There is a successive decrease of upwelling radiances in all channels as cloud thicknesses increase. The successive decrease of the ratios continues all the way to 4 km. Between 3 and 4 km the decrease in ratio in each channel is only slight indicating that near 4 km the cirrus cloud used in the model is becoming opaque to the infrared radiation.

Comparison of the channels in Figure 4.2 gives a good indication of the effects of clouds on upwelling radiances in different wavenumber regions of the infrared spectrum relative to the peak of the channel's weighting function. The physical factors that influence the ratio for a given cloud type, cloud thickness and channel could be determined from ratios presented in Figure 4.2. In the present model, the cloud top is constant at 250 mb. Using a 2 km cirrus as an example, the interaction of these two physical factors (the weighting function and the channel wavenumber) are examined. The channels that are in the 15 μm CO_2 band show a decreasing ratio as the weighting functions peak deeper in the atmosphere. The same decrease is noted in 4.3 μm CO_2 channels but to a greater degree. This fact would indicate a greater impact of clouds on shorter wavelengths. For example, channel 7 (peak at 900 mb) has a ratio nearly double that of channel 12 (peak at 850 mb).
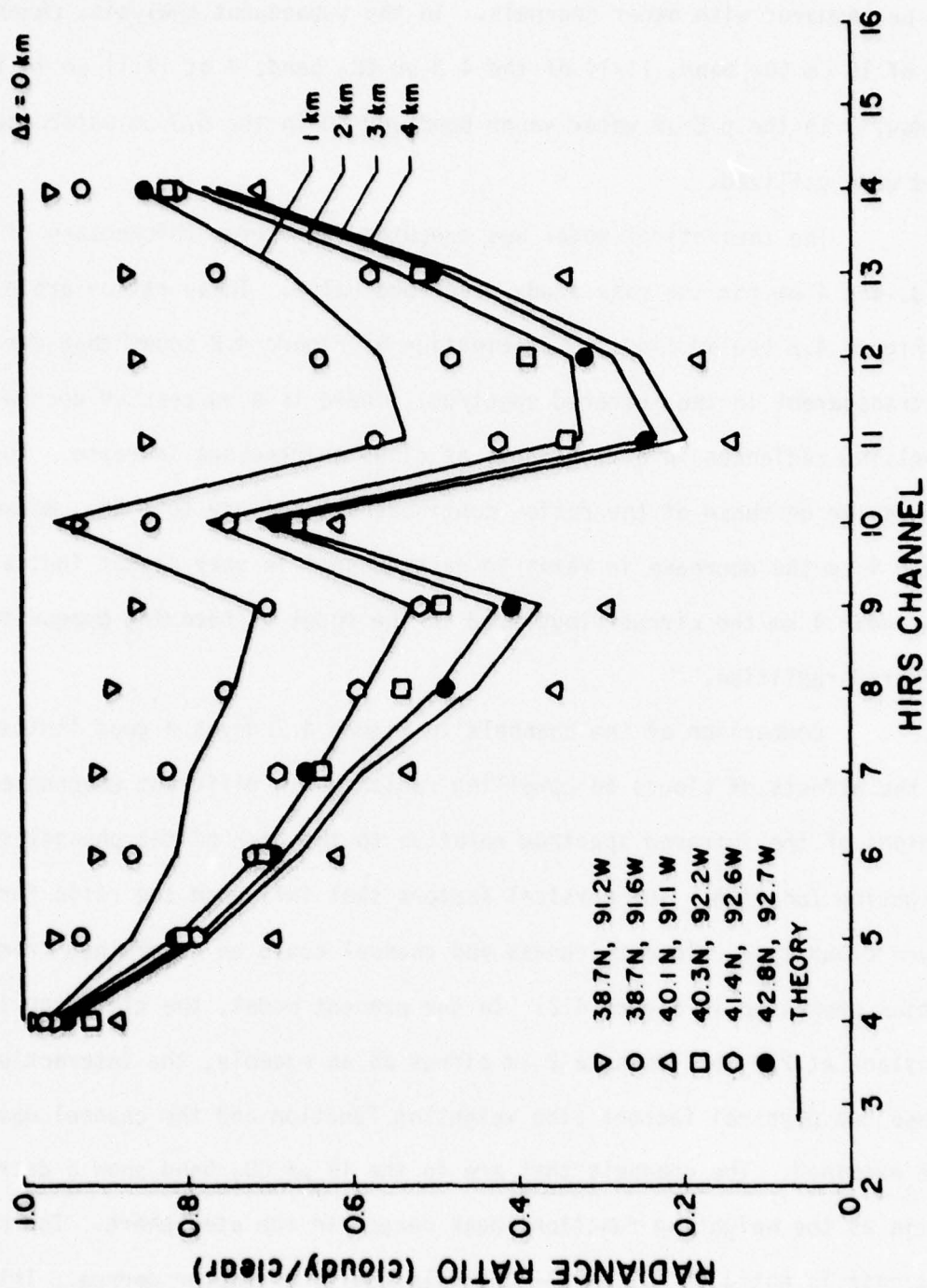
53

Figure 4.2. Comparison of theoretical results (solid curves) and satellite HIRS data ($\triangledown$, $\bullet$, $\triangle$, $\square$, $\bigcirc$, $\bullet$) for the 11 HIRS channels in terms of the cloudy to clear column radiance ratios.

54

There were 26 passes available in the 20-30 August, 1975, HIRS data set. Inspection of NOAA 4 mapped, normalized, and gridded mosaics from the Very High Resolution Radiometer (VHRR) for this time period reveals one pass of particular interest. On 25 August a cirrus shield was associated with a squall line near 40°N in the central U.S. The corresponding HIRS pass was analyzed for cloud information at scan angles closest to nadir. Figure 4.3 shows both the broad band visible channel (0.5-0.7 μm) and the broad band window channel (10.5-12.5 μm).

To apply the theoretical results to the real HIRS data a method had to be developed to reduce the cloudy radiances to ratios. The theoretical and the real data are assumed compatable since both atmospheres are mid-latitude summer. To obtain a clear column radiance that is representative of a localized area, the HIRS data was examined in conjunction with the satellite pictures. The point chosen for the clear column radiance (at about 38°N, 91°W) was then used to obtain the cloudy ratios for that day. The point chosen has the same scan angle as the cloudy radiances.

In reference to Figure 4.3, we have selected a number of locations at about 40°N and 90°W along the satellite track for the inference of cloud thickness based on the theoretical sensitivity analyses described previously. Examinations of these cloud photographs as well as of synoptic surface and 500 mb maps show that the cloud is cirrus with no low cloud present below. Six scan radiance ratios are depicted in Figure 4.2. The scan points at 38.7N/91.2W($\triangledown$) and 38.7N/91.6W(0) represent areas that are close to the cirrus edge. Based on the comparisons with the theoretical
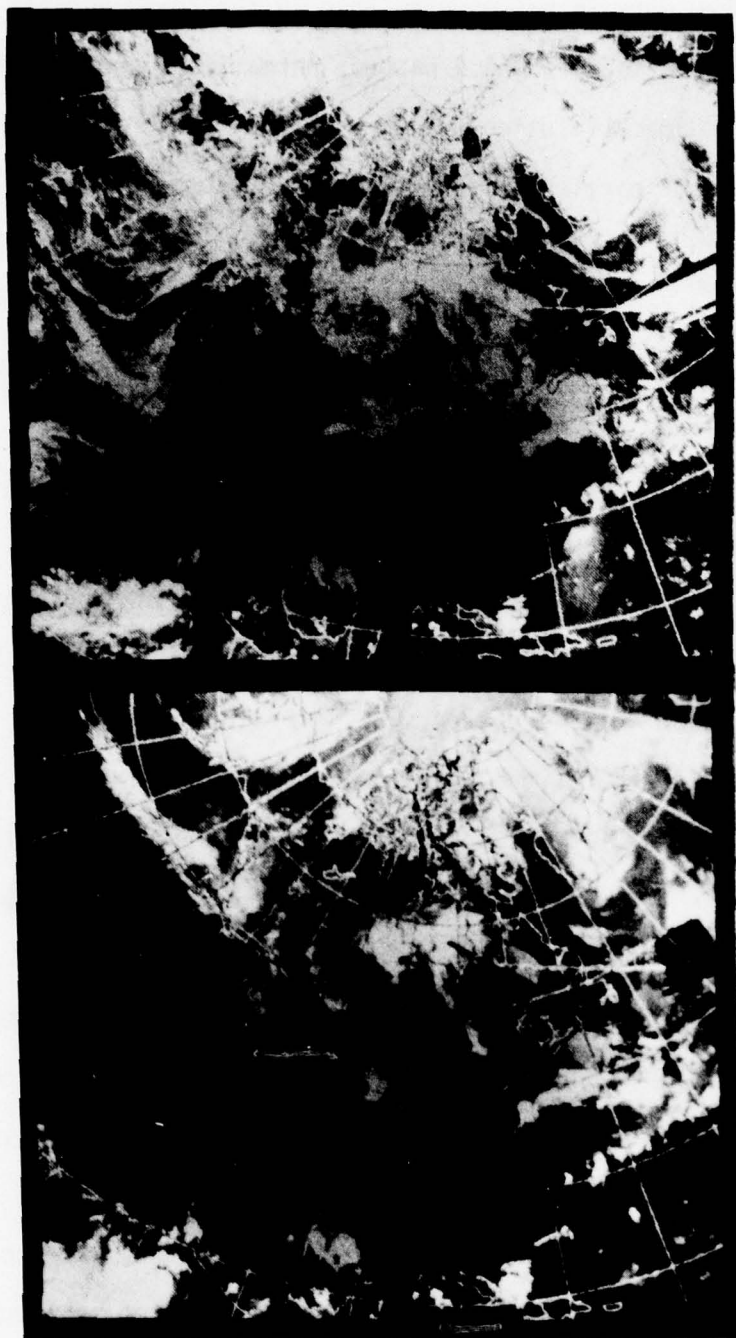
55

Figure 4.3 NOAA 4 mosaic for August 25, 1975 with the visible channel on the top and the infrared channel on the bottom.

curves, thicknesses of 0.4 and 1 km were estimated. As the satellite scan goes deeper into the cloud center, a thickness of greater than 4 km $(40.1N/92.1W, \triangle)$ is obtained. Other scans further north under investigation indicate cirrus thicknesses on the order of 2 to 3 km as illustrated by square, hexagon and black dot. Note that the resolution of HIRS instruments is approximately 23 km at nadir. From this case study it appears that the HIRS radiance ratios resemble reasonably well those calculated from the theoretical analyses. The 4.3 and 15 μm CO_2 channel behave especially well. However, the water vapor channels show some non-systematic variation, perhaps owing to the use of the observed clear column radiance which arises from an atmosphere differing from cloudy cases.

4.3   Parameterization of Radiance Calculations from Cloudy Atmospheres

4.3.1   Cloud type determination. To utilize the theoretical results in a real atmosphere, we first need to determine the vertical location of the cloud in the atmosphere. This, in effect, will give a measure of the cloud type. The theoretical calculations were carried out for cirrus thicknesses of 1, 2, 3, and 4 km and middle cloud thicknesses of 0.3, 0.5, 0.7, 1.0, 2.0, and 3.0 km. Examination of the upwelling ratios shows that the transparent quality of cirrus is evident in the infrared spectrum. There is a successive decrease of upwelling radiances in all channels as the cloud thicknesses increase. The successive decrease of the ratios continues all the way to 4 km. Between 3 and 4 km the decrease in ratio in each channel is only slight indicating that near 4 km the cirrus cloud used in the model is becoming opaque to the infrared radiation, and the

57

cloud temperature now becomes important in the transfer process. At cirrus thicknesses greater than 4 km, the upwelling radiance is representative to the Planckian temperature of the cloud top. Analysis of middle cloud thickness indicates the cloud mass becomes opaque between 2 and 3 km. This may be attributed to greater particle concentrations found in middle clouds compared to cirrus clouds.

For the purpose of determining the cloud type from the theoretical data, the channels were rearranged in order of decreasing ratios for a moderately thick cirrus. The rearrangement of the channels is shown in Figure 4.4. Analysis of this figure shows the effects of wavenumber and weighting function peak. The long wave channels 4-7 all have greater ratios than the short wave channels 11-14, even though they have similar weighting function peaks, which would indicate that the cloud mass has more impact on shorter wavelengths. The location of channel 14 between channels 5 and 6 would indicate that there is an overlap between the two CO_2 bands depending on the weighting function peak. The locations of channels 10 and 9 are according to weighting function peaks, with channel 10 having a higher ratio and a higher weighting function peak than channel 9. The location of their ratios within the CO_2 channel ratios in the figure is due to the model atmosphere humidity profile. By increasing the water vapor amount, there would be an increase in attenuation and thus a lower ratio. Conversely, a decrease in the water vapor would decrease the attenuation and increase the ratio.

The radiance ratios and channel numbers shown in Figure 4.4 were fitted with a linear equation by means of regression analysis.
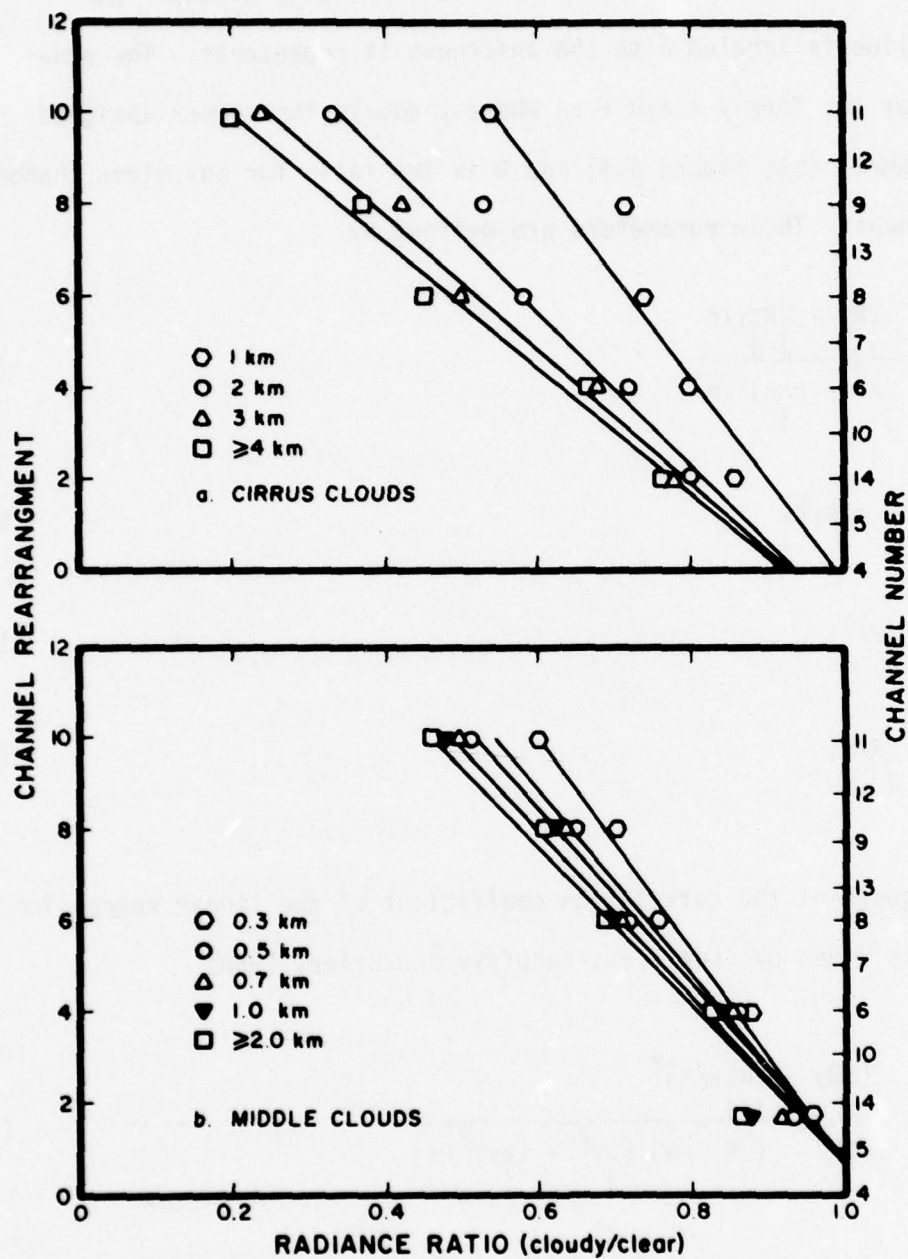
58

Figure 4.4   The best straight line fit for four cirrus cloud
thicknesses (Part a) and for six middle cloud
thicknesses (Part b).

59

Part a is for cirrus clouds and Part b is for middle clouds. Each straight line is labeled with the thickness it represents. The equation is for the form $y = a_1 R + a_0$ where y equals the number assigned to the channel (see Figure 4.4) and R is the ratio for any given channel and thickness. These parameters are defined by

$$a_1 = \frac{\sum_j Ry - \sum_j R \sum_j y/n}{\sum_j R^2 - (\sum_j R)^2/n} \quad , \tag{4.1}$$

$$a_0 = \overline{y} - a_1 \overline{R}, \tag{4.2}$$

$$\overline{y} = \sum_j y/n, \tag{4.3}$$

$$\overline{R} = \sum_j R/n, \tag{4.4}$$

and the square of the correlation coefficient of the linear regression analysis is given by (see e.g., Panofsky and Brier, 1968)

$$r^2 = \frac{[\sum_j Ry - \sum_j R \sum_j y/n]^2}{[\sum_j R^2 - (\sum_j R)^2/n] \, [\sum_j y^2 - (\sum_j y)^2/n]} \quad . \tag{4.5}$$

In the equations the summations are for all 11 channels.

Table 4.3 contains the slope, y-intercept, and r^2 for each thickness of cirrus and middle clouds. Analysis of the table shows that the correlation (r^2) is much better in the cirrus case (0.96) when compared to the

60

middle cloud case (0.90). The decrease in correlation in the middle clouds
and the 1 km cirrus cases can be explained by the placement of the ratio of
channel 10. The original arrangement was done for a thick cirrus case
where the effects of the cirrus cloud mass on channel 10 were present. In
the middle cloud and 1 km cirrus cases there is no effect of the cloud mass
on channel 10. Therefore, the location of channel 10 in the fitting process
decreases the correlation for the 1 km cirrus and the middle cloud cases.
The linear fit developed here will be used when parameterizing actual HIRS
data in the next section. Another important thing to note in this analysis
is that the magnitude of the slope is greater than the magnitude of the y-
intercept for all cirrus thicknesses and the reverse is true for middle
clouds. This fact will be used in subsequent analysis to distinguish be-
tween middle and cirrus clouds.

Table 4.3. Slope, y-intercept, and correlation coefficient
squared for several cloud thickness for cirrus
(part a) and middle (part b) clouds.

Part a (cirrus clouds)

| | Thickness (km) | | | |
	1	2	3	4
slope	-21.75	-16.82	-14.79	-13.94
y-intercept	21.69	15.70	13.68	12.84
r^2	.872	.968	.977	.977

Part b (middle clouds)

| | Thickness (km) | | | | | |
	.3	.5	.7	1.	2.	3.
slope	-22.78	-19.80	-18.80	-18.10	-17.50	-17.50
y-intercept	23.56	20.70	19.70	18.80	18.10	18.10
r^2	.904	.925	.925	.913	.906	.906

4.3.2   Ice and water content determination. A measure of liquid water
and ice content distribution over the planet is important to many areas of
meteorology. These include the initialization of numerical models to in-
crease long term forecast accuracy and the study of global circulation and
climatic change models. From the theoretical calculations, each cloud
thickness is representative of a cloud mass since only one drop size dis-
tribution was used for water clouds and only one particle concentration
was used for ice clouds. For water clouds a liquid water content of
0.15 gm m^{-3} was assumed, and for ice clouds an ice content of 0.0283 gm m^{-3}
was used.

The recovery of liquid water and ice content from the fitted
ratios is possible by knowing within certain limits the theoretical mass
of the cloud for which the ratios are being calculated. In the cirrus cloud
case, it was found that for a cloud mass of less than 28.3 gm m^{-2} the cor-
relation coefficient decreased significantly below 95 percent and the
ratios could no longer be fit with a straight line. This was also true
for middle clouds with a mass of less than 45 gm m^{-2}. Thick middle clouds
(greater than 390 gm m^{-2}) had the same ratios as the 300 gm m^{-2} (2 km
thickness) cloud. This would indicate that the cloud mass is a black
body and all the energy from below is absorbed by the cloud layer and
reradiated. The 113.2 gm m^{-2} (4 km thick) cirrus still seems to be
somewhat transparent, but this cloud mass was near the maximum that could
be handled by the theoretical model.

To recover ice or water content from the parameterizations of
the theoretical radiance ratios, the slopes and y-intercepts for the two
cloud types could be fit by a least square logarithmic function that is
given for the slope by

62

$$a_1 = c_1 + c_2 \ln \Delta z \qquad\qquad (4.6)$$

and for the y-intercept by

$$a_0 = c_3 + c_4 \ln \Delta z, \qquad\qquad (4.7)$$

where Δz is the thickness of the ice or water cloud, and c_1, c_2, c_3, and c_4 are constants to be determined for each set of slopes and y-intercepts. For the slope a_1, we have

$$c_1 = \frac{\sum\limits_i (a_1 \ln \Delta z) - \sum\limits_i \ln \Delta z \sum\limits_i a_1 / n}{\sum\limits_i (\ln \Delta z)^2 - (\sum\limits_i \ln \Delta z)^2 / n}, \qquad\qquad (4.8)$$

$$c_2 = \frac{1}{n} (\sum\limits_i a_1 - c_1 \sum\limits_i \ln \Delta z). \qquad\qquad (4.9)$$

These equations are derived by substitution of the natural logarithm of the thickness for R, and a_1 for y in Eqs. (4.1) and (4.2). The square of the correlation coefficient is given by

$$r^2 = \frac{[\sum\limits_i a_1 \ln \Delta z - \sum\limits_i \ln \Delta z \sum\limits_i a_1 / n]^2}{[\sum\limits_i (\ln \Delta z)^2 - (\sum\limits_i \ln \Delta z)^2 / n][\sum\limits_i a_1^2 - (\sum\limits_i a_1)^2 / n]}, \qquad\qquad (4.10)$$

which is again a direct substitution into Eq. (4.6). The y-intercept, c_3, c_4 and r^2 can be calculated by substituting a_0 for a_1 in Eqs. (4.8) - (4.10). The summation is over six cloud thicknesses for middle clouds and over four cloud thicknesses for cirrus.

Using the data from Table 4.3, the slopes and y-intercepts were fitted for each cloud type. The resulting fits are shown in Figure 4.5
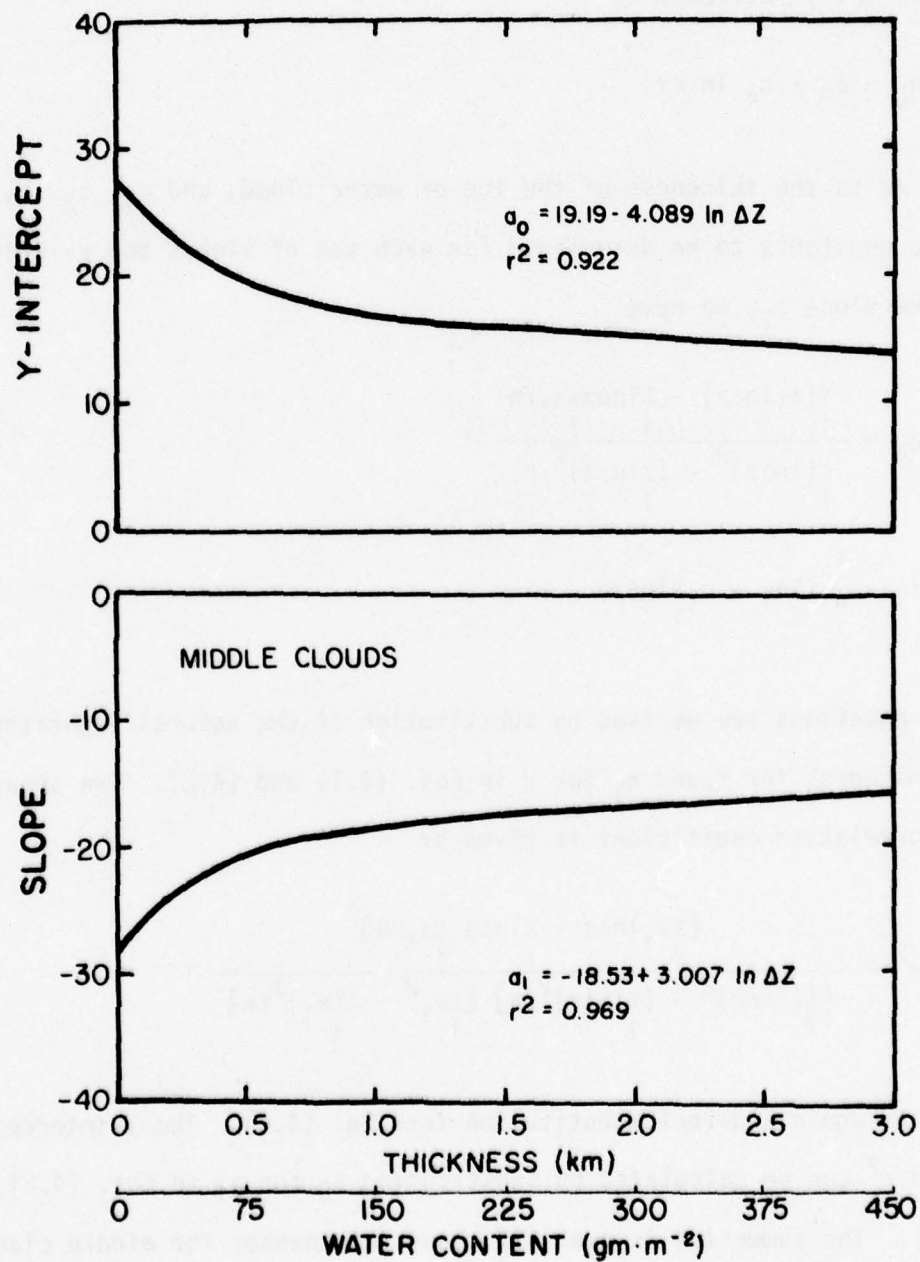
Figure 4.5 Best fit of y-intercept (top) and slope (bottom)
for six middle cloud thicknesses.

for middle clouds and Figure 4.6 for cirrus cloud. For middle clouds c_1 and c_2 are equal to -18.53 and 3.007, respectively, with the correlation coefficient of 0.984, while c_3 and c_4 equal 19.19 and -4.089 with a correlation coefficient of 0.960. For the cirrus case the values of c_1, c_2, c_3, and c_4 are -21.40, 5.75, 21.19, and -6.526, respectively. The constants c_1 and c_2 and a correlation coefficient of 0.988 and c_3 and c_4 had a correlation of 0.983.

Upon substituting a_1 and a_2 in Eqs. (4.6) and (4.7) into Eq. (4.2), the thickness of any middle or high cloud is given by

$$\Delta z = \exp\left[(\overline{y} - \overline{R}c_1 - c_3)/(c_2\overline{R} + c_4)\right], \tag{4.11}$$

The cloud mass is then derived by multiplying the cloud thickness expressed in km by 28.3 gm m^{-2} for cirrus cloud and 1.5×10^2 gm m^{-2} km^{-1} for middle clouds.

4.4   Data Description and Selection

The method to determine cloud type and ice or water content developed in the previous section was applied to a selected set of Nimbus VI High Resolution Infrared Sounder (HIRS) data. The results of this application were compared to the Air Force Three Dimensional Nephanalysis (3DNEPH) and satellite cloud pictures since these were the only source of consistent cloud information available on a routine basis.

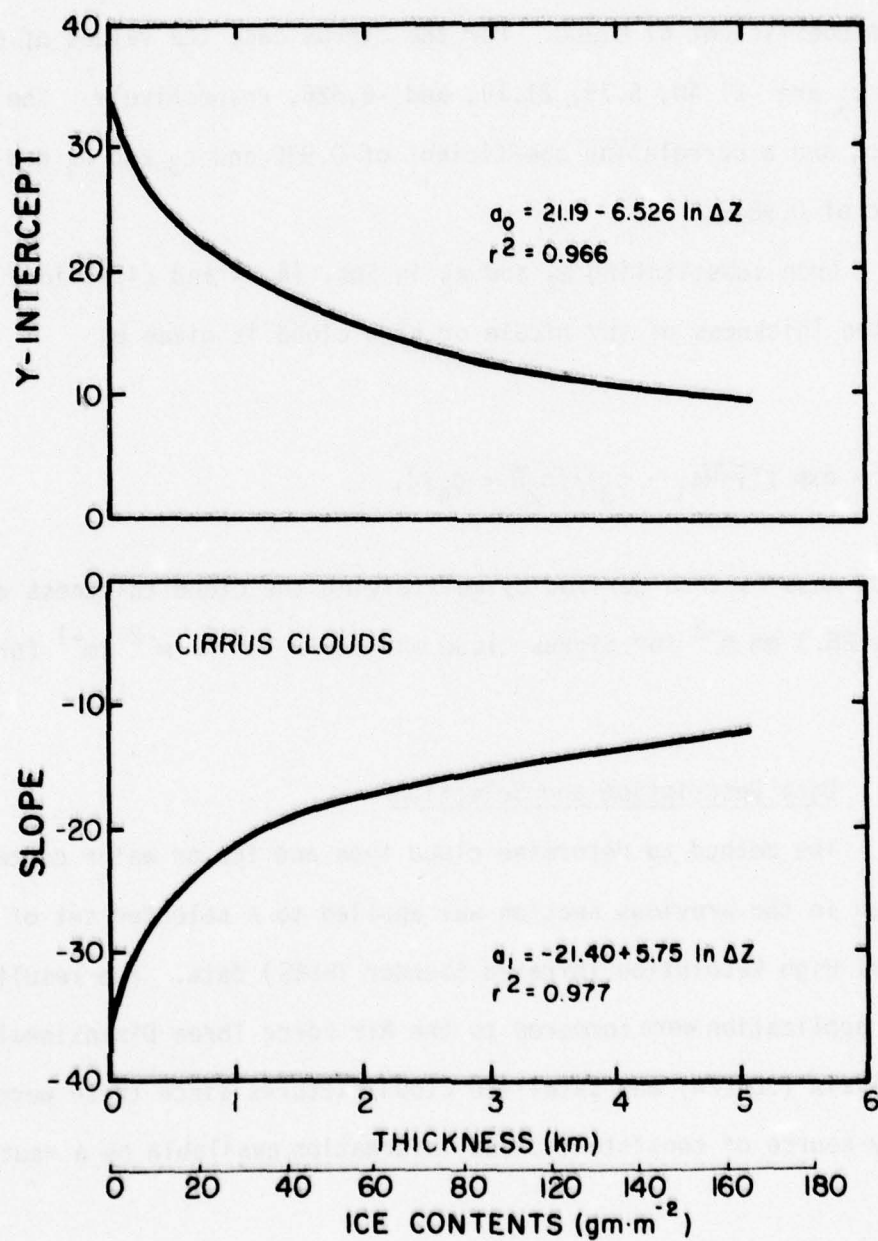### 4.4.1   The three-dimensional nephanalysis data. The Three-Dimensional

65

Figure 4.6   Best fit of y-intercept (top) and slope (bottom)
for four cirrus cloud thicknesses.

Nephanalysis (3DNEPH) program was developed at the Air Force Global
Weather Central (AFGWC) to incorporate the tremendous quantity of
satellite sensed cloud data and conventionally sensed meteorological
parameters into a three-dimensional cloud model of the atmosphere.
Basic to the design of the 3DNEPH is the assumption that satellite
information is available for its data base in a timely manner. However,
in the event that satellite data is not available, the 3DNEPH has the cap-
ability of extrapolating past analysis until such time as satellite data
does become available.

The 3DNEPH program is built as a series of input processors.
These processors include the surface data processor, radiosonde obser-
vation (RAOB) processor, aircraft data processor, manual data processor,
decision tree processor, satellite video data processor, satellite in-
frared data processor, final processor, forecast processor, verification
processor, and display processor. Because of the modular nature of the
3DNEPH program, processors can be added to or deleted from the system
with a minimum of programming problems. Descriptions and functions of
each of the processors can be found in the AFGWC Technical Memorandum
71-2 by Coburn (1971).

The horizontal resolution of the 3DNEPH program is limited by
the resolution, and mapping and gridding accuracy of the input satellite
data. The hemispheric grid chosen for the 3DNEPH, which was compatible
with the accuracy of its input satellite data, was a 512 x 512 array cen-
tered at the north (south) pole of a polar stereographic map and having
a distance between grid points of 40 km at 60° latitude. This 512 x 512

67

grid was further subdivided into 64 squares (boxes) so that the finest
mesh was 4096 grid points over each hemisphere. Once again, each grid
point contains information representative of a 40 km square centered at
the grid point when at 60° latitude. The vertical resolution of the
3DNEPH program divides the atmosphere into 15 layers. The first six lay-
ers are terrain following layers and the last nine layers are categorized
in feet above mean sea level (MSL). In addition to the information given
for cloud amounts in the layers, seven additional pieces of data are given
at each point. These data denote information about the cloud types,
maximum tops and minimum bases, the current weather and the total cloud
cover.

   The use of the 3DNEPH as a source of comparison to the technique
developed here has many shortcomings. These problems include timeliness,
layer resolution, dependence on subjective observations, and the horizon-
tal spreading of the data. The 3DNEPH was used as a comparison, however,
since no other known source containing the routine analysis of cloud
parameters is available.

   The ever-changing cloud scene at a point makes the timeliness of
the 3DNEPH and the HIRS data very important. The 3DNEPH is produced every
three hours, and if there is no new data for an update, the previous an-
alysis or a cloud forecast is used for the new analysis. This problem is
minimized since we are considering overcast cases in which the cloud scene
at a point will probably not change significantly over a short period of
time.

   A second problem area is the layer resolution of the 3DNEPH.

68

The resolution can be as poor as 4000 feet for middle cloud layers and as thick as 20,000 feet for high cloud layers. If a thin layer of cloud is reported to be in one of the layers, the model must automatically fill the entire layer with clouds. As noted earlier, an error of 4,000 ft (1.2 km) is one-half of the thickness of middle cloud that can be detected by the theoretical model. In the case of cirrus clouds, a 20,000 ft error is equivalent to 6.1 km, a greater thickness than the model can handle. This large error can be somewhat offset when the maximum cloud top parameter is considered. At middle and high cloud top levels, the coding for this parameter is accurate to 5,000 ft or 1.5 km. For lower middle cloud tops, this parameter is accurate to 1,000 ft or 0.3 km.

The use of subjective weather observations plays an important role in the accuracy of the 3DNEPH clouds. If there is no current satellite data, the cloud top cannot be determined and persistence prevails, and the cloud thickness is over or under-estimated. Another case would be when satellite data is available but no surface observation is present (over oceans). Here, the satellite can determine the cloud top height only, and no information about the cloud depth can be determined.

Another problem is that surface observations are spread horizontally. The 3DNEPH grid point represents a 40 km box at 60°N. If there is no current satellite data and the observation network is not at a 40 km resolution, some influence of the surface observation is spread to adjacent points in the 3DNEPH. This can be seen by examining an area of 3DNEPH data where the cloud thickness will be constant over a large area. Steps taken to minimize these problem areas will be discussed below.

69

4.4.2   High resolution infrared sounder data.   HIRS data is routinely

processed at NOAA/NESS and is available on nine-track, 1600 bpi tapes.

The data is packed in such a way that six or seven orbits are available

on each tape. These tapes contain located and calibrated radiance values

for all 17 channels. The Nimbus VI User's Guide gives a detailed explan-

ation of the calibration procedure used on the radiance measurements in

each channel. The resolution of the HIRS data decreases with increasing

scan angle. This decrease in resolution of a scan spot is from approxi-

mately 23 km at nadir to 31 km at a scan angle of 36.9^0.

The data set used in this analysis was for 20-30 August 1975,

a time when all channels of the HIRS instrument were operating properly.

Further, it was required to have data over North America since the com-

parison was being used with the 3DNEPH which depends heavily upon good

surface observations. We therefore requested data from 20^0-55^0 N and

80^0-150^0 W which includes both land and ocean areas. To further com-

plicate the data selection, examination of satellite photographs indi-

cated a general lack of middle and high clouds over this region for this

time period except in areas north of 40^0 N. As a result, all of the data

used in the analysis are along a storm track north of 40^0 N.

A total of 26 passes were provided in the data set of which

five were analyzed for cloud information at the two scan angles closest

to nadir. To check consistency of the data from channel to channel

within a pass, the five passes used in the analysis were displayed by

using an overprinting technique to simulate grey shading on the line

printer. All the passes used in subsequent analyses were overprinted

to verify the HIRS data by comparing the overprints with surface analysis

70

and NOAA satellite visible and infrared mosaic.

The basic criteria for the selection of 3DNEPH data for comparison with the HIRS data was the reliability of the 3DNEPH data. This criteria dictated that data be chosen where the 3DNEPH had good surface data as well as satellite data. Additionally, the areas of interest must be in the presence of synoptic scale weather so that continuous cloud decks would be insured. The use of HIRS data points at or near nadir would insure the least amount of error in applying the real data to the theoretical calculations, since the fitting of the theoretical upwelling radiances to different scan angles would be most accurate at nadir.

Based on these criteria, five passes on five consecutive days were chosen for this comparison. These days included August 21 through August 25, 1975. The pass on each day that included Western North America and was closest to a 3DNEPH analysis time was used. Nimbus VI has an approximate equator crossing at 1000 local time on its ascending pass and corresponds to an 1800Z (GMT) analysis time for the 3DNEPH. Box number 44 of the 3DNEPH covers this area and has the following latitudes and longitudes for the upper left, upper right, lower left and lower right, respectively, 52°N, 125°W, 62°N, 80°W, 31°N, 106°W, and 36°N, 80°W. Inspection of satellite pictures on these five days show that all the clouds are north of 40°N and a majority of them are north of 45°N. Hence, all the points used in the comparison are at these latitudes.

A clear column radiance representative of the pertinent area was chosen using the satellite pictures in conjunction with the HIRS

71

data for each day under investigation. These clear column radiances were used to reduce the cloudy radiances to ratios as was discussed in a previous section. Note that both theoretical calculations and the real data are for mid-latitude summer conditions.

The colocation of the HIRS data with the 3DNEPH was accomplished using the latitude and longitude from the HIRS data. These quantities were then converted to 3DNEPH grid location. Since this location is never an exact 3DNEPH point, the 3DNEPH point used for the comparison was that point closest to the calculated grid location.

4.5   Cloud Type and Mass Determination from HIRS Data

4.5.1   Cloud type. All of the HIRS data applied to the theoretically based empirical relationships are from the cloudy areas, north of 40°N. The slope and y-intercept of each case were calculated. The cases with the magnitude of the slope greater than the magnitude of the y-intercept were assumed to be cirrus clouds. The cases with the magnitude of the y-intercept greater than the magnitude of the slope were assumed to be middle or lower clouds. These cases were then examined in conjunction with the IR pictures. In all cases, the empirically derived relationships that were based on the theoretical model indicated the proper cloud type.

The theoretical empirical model indicated the presence of middle clouds in the vicinity of 52°N, 115°W to 43°N, 100°W on August 21. Examination of the IR picture not shown here verifies the presence of lower clouds in this area. For August 22, the model indicated a mixture of cirrus and lower clouds from 52°N, 104°W to 49°N, 102°W and then extensive lower clouds to 43°N, 99°W. This same pattern can be noted by examining Figure 4.7.

72

In the vicinity of 50^ON the IR picture shows an area of some cirrus clouds and some warmer lower clouds. South of 49^ON there are only lower clouds in the IR picture of Figure 4.7. It also indicates little cloud south of 43^ON. One of the clear points in this area was used for the clear column radiance in the ratioing for this day. The IR picture for August 23 (not shown here) indicates extensive cirrus on the subtrack of the satellite from 53^ON, 120^OW to 42^ON, 115^OW. The model shows all cirrus clouds in this area except for the indication of some middle clouds near 53^ON. Further examination of the IR picture on this day reveals some breaks in the cirrus cloud in this area. On August 24, cirrus was again indicated from 52^ON, 109^OW to 48^OW, 106^OW and middle clouds were present south of 47^ON. Examination of the satellite picture for that day not shown here verifies this analysis. The clear column radiance for this day was taken from an area just south of 47^ON along the subtrack of the satellite. The model analyzed middle clouds from 53^ON, 97.5^OW to 47^ON, 94.5^OW and cirrus clouds from 44^ON, 93^OW to 39^ON, 91.7^OW for August 25. This again is represented well on the IR picture of Figure 4.3. The clear column radiance for this day was from near 38^ON and 91^OW. The ice and liquid water content for this pass along with the pass for August 22 are mapped in a subsequent section.

4.2   Cloud mass. To determine the cloud mass the data described in the previous section was divided into middle and high clouds. The 3DNEPH points that correspond to these data cases were then selected from Box 44 of the 3DNEPH at 1800Z for the five days analyzed. In all cases the 3DNEPH indicated lower clouds below the cirrus or middle cloud. This indicates one of the basic problems discussed earlier about the 3DNEPH,
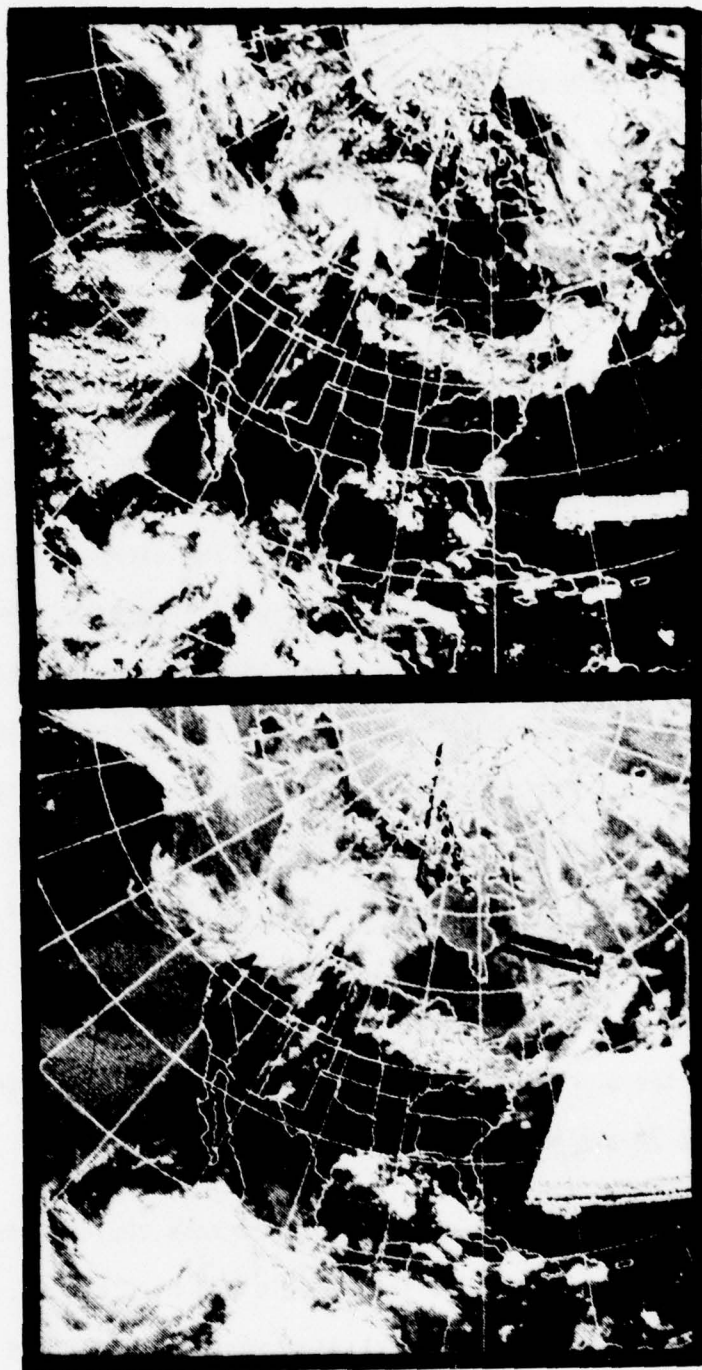
Figure 4.7 NOAA 4 mosaic for August 22, 1975 with the
visible channel on the top and the infrared
channel on the bottom.

74

that with only surface analysis the cloud top is over estimated and with
only satellite data the cloud base is lower than it should be, so that
the error can be greater than the thickness of the cloud. It is virtually
impossible to correct this problem without instrumentation that can see
through clouds. In addition, the spreading of an observation to many
3DNEPH points tends to smooth the area out so that cloud thicknesses are
constant over large areas. To minimize these problems, the 3DNEPH cloud
thickness data were used as either cirrus or middle cloud. As noted
earlier, this would not affect the ice and water content calculation
significantly because middle cloud in the presence of thin cirrus has
the same appearance as moderately thick cirrus. The effect of lower
clouds on middle cloud ratios remained virtually unchanged when comparing
the slopes and y-intercepts derived from the empirical-theoretical approach.

The 3DNEPH thicknesses were parameterized by assuming that the
actual base of the cloud corresponded to the theoretical base of the cloud.
This was 3.1 km for middle cloud and 6.7 km for cirrus clouds. The cloud
thickness in the middle cloud case was then obtained by adding the terrain
height to the middle cloud base and subtracting this from the layer top
or the maximum cloud top parameter. This was then multiplied by 1.5 x
10^2 gm m^{-2} km^{-1} to obtain the liquid water content. The cirrus cloud thick-
ness was obtained by subtracting 6.7 km from the height of the top of the
layer containing clouds or the maximum top parameter whichever was smaller.
This result was then multiplied by 28.3 gm m^{-2} km^{-1} to obtain the ice
content. This should minimize as much as possible the thickness grouping
in the 3DNEPH.

Figure 4.8 is a graph comparing the model ice and liquid water

75

contents with the 3DNEPH derived ice and water contents. Part a of the
graph is for middle cloud cases and part b is for cirrus cloud cases.
In both parts, both the 3DNEPH and the theoretical-empirical relation-
ships indicated middle or cirrus clouds. The ordinate is for the 3DNEPH
and is labeled in both thickness and equivalent ice or liquid water con-
tent based on the ice and liquid water contents used in the theoretical
calculations. The abscissa is for the empirical-theoretical calculations
and is also labeled in thickness and equivalent liquid water content for
part a and equivalent ice content for part b.

Comparison of the 3DNEPH derived water contents in Figure 4.8
with the empirically derived theoretical water contents is somewhat vari-
able. Although the linear relationship desired is not present some
correlation can be noted. The data points in the comparison primarily
occur at four 3DNEPH thicknessess while the model derived water contents
covered a wide range. This grouping is present since the 3DNEPH has
only four middle cloud layers in its data base. The further parameteriza-
tions done to the 3DNEPH in this analysis made it possible to increase
the number of water contents that could be obtained from the 3DNEPH. The
error range of the comparisons for part a of Figure 4.8 is up to 2.25 x
10^2 gm m^{-2}. Analysis of Figure 4.8 also indicates the grouping of the
3DNEPH data at basically three ice content values although the range
from the empirical-theoretical calculations vary widely over a given
3DNEPH value. The error range in Figure 4.8 is as much as 84.9 gm m^{-2}.
We note that there appears to be some agreement between the two independent
methods of computing cloud ice or liquid water content.

The above comparisons point out the simple fact that new methods
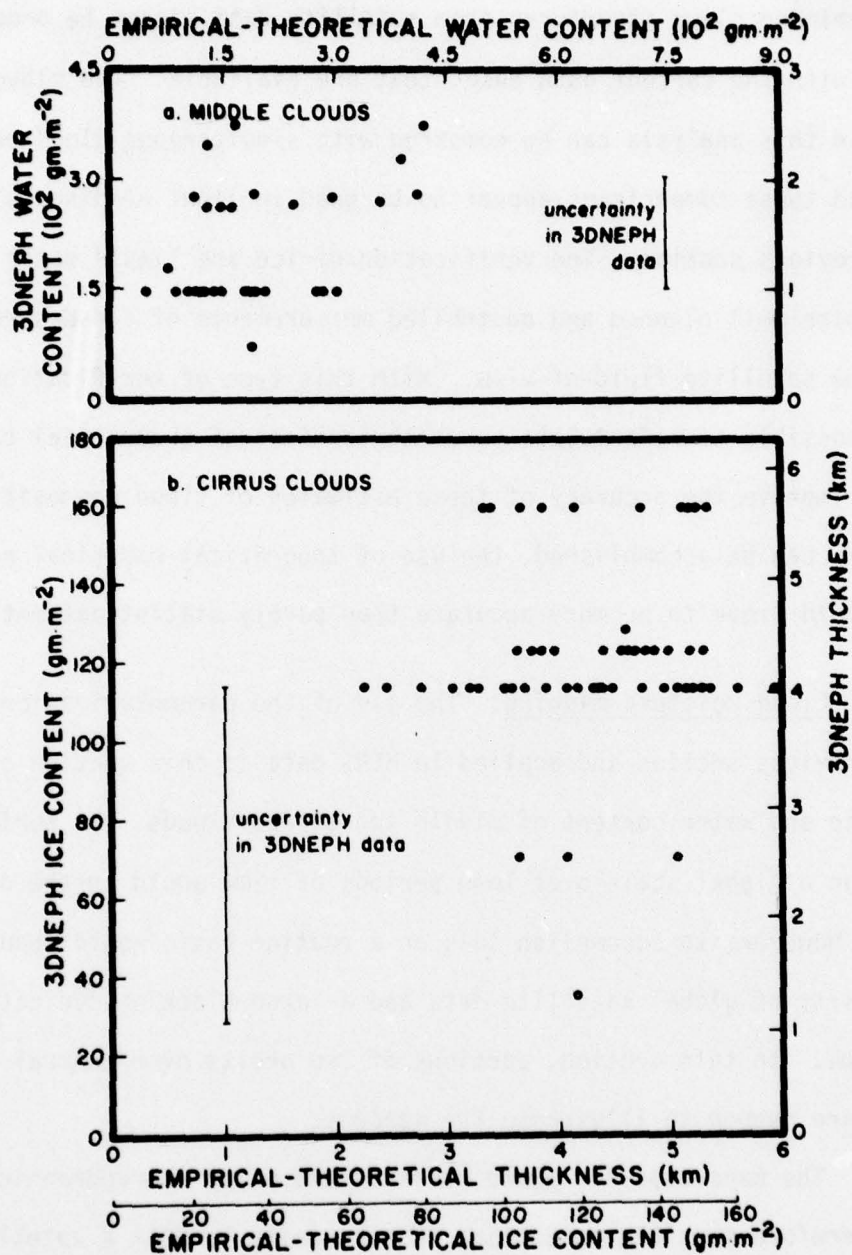
76

Figure 4.8 Comparison of 3DNEPH middle cloud water content with empirical-theoretical middle cloud water content from HIRS in Part a and comparison of 3DNEPH cirrus cloud ice content with empirical-theoretical cirrus ice content from HIRS in Part b.

for determining cloud structures from satellite data cannot be properly verified with the current data bases that are available. The cloud typing derived in this analysis can be compared with simultaneous cloud photographs and these comparisons appear to be good in light of discussions in the previous section. The verification of ice and liquid water content will require well planned and controlled measurements of cloud structures within the satellite field-of-view. With this type of verification, it will be possible to reformulate parameterizations of theoretical calculations to improve the accuracy of these estimates of cloud compositions. Until this can be accomplished, the use of theoretical-empirical relationships should prove to be more accurate than purely statistical methods.

4.5.3   Cloud moisture mapping. The use of the parameterizations described in the previous section and applied to HIRS data in this section can be used to map ice and water content of middle and cirrus clouds. To perform this mapping on a global scale over long periods of time would be the desired result. However, to accomplish this on a routine basis would require the availability of global satellite data and a large block of dedicated computer time. In this section, portions of two orbits over central North America are mapped to illustrate the concept.

The maps used for these projects are polar stereographic and it is therefore possible to compare rather easily to NOAA 4 satellite pictures. In each of the cases the clear column radiance at satellite nadir was used to perform the ratioing over ten scan spots on each side of nadir. Beyond these scan angles a clear column radiance representative of a large scan angle should be used to perform the ratioing to derive the amount of liquid water or ice content.

78

As noted earlier, the slope and y-intercept of the linear fit determine whether middle or high clouds are present. If the magnitude of the slope is greater than the y-intercept cirrus cloud is assumed. A further criterion established for mapping was to eliminate data points where the magnitude of the slope was greater than 25, or the correlation coefficient was less than 0.70. After comparing many cases of actual data with theoretical calculations, we found that cases that do not meet the above criterion were low cloud which were not addressed in this study.

For passes on August 22 and August 25, the latitudes and longitudes of the data points that met the above criterion were plotted on the polar projection and then analyzed. In both cases the cirrus and middle cloud are mapped on the same figure. The isolines are labeled with vertical ice or liquid water content based on the constants derived from parameterizations of the theoretical calculations. The solid lines are isolines of middle cloud, dashed lines are for cirrus cloud and the darker lines are separation of middle and high cloud analysis.

The analysis for August 22 shows two areas of overcast conditions under the satellite. The northern area is over southern Canada and extreme northern Montana and North Dakota and is characterized by both middle and high clouds. Since the data is cut off to the north, east and west, the analysis shows sharp break points in these directions. NOAA 4 pictures indicate that the southern cloud areas analyzed for this pass have little cirrus cloud present which is in agreement with the present analysis. The theoretical analysis also shows middle cloud less than 1 km thick both south of the northern area and north of the southern area of clouds.

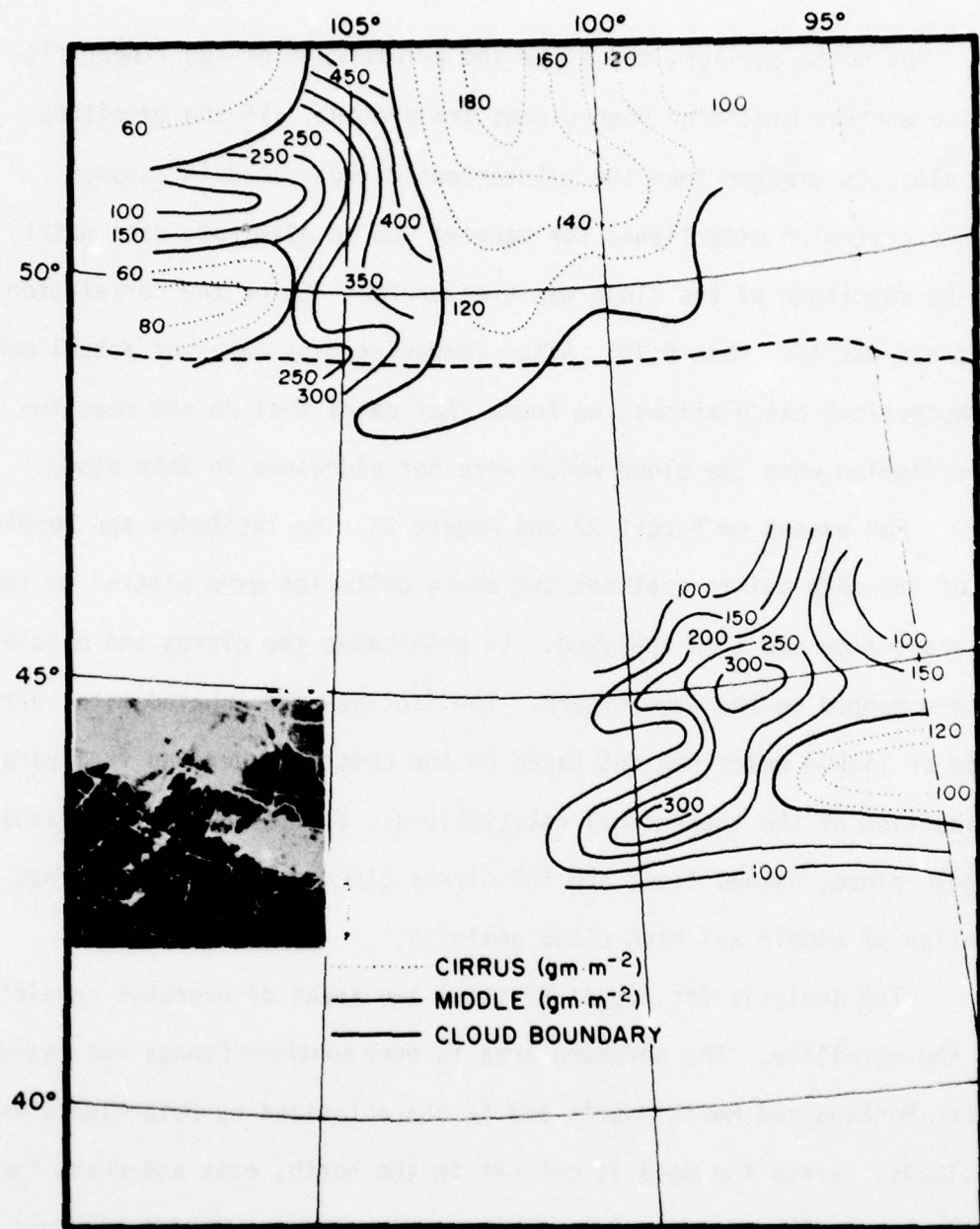Analysis of the figure for August 25 shows a similar set of two

79

Figure 4.9 Cloud ice and water content based on empirical-theoretical calculations for August 22, 1975. Dotted lines are for cirrus clouds (gm m⁻²) and solid lines are for middle clouds (gm m⁻²). The heavy line is the cloud boundaries.
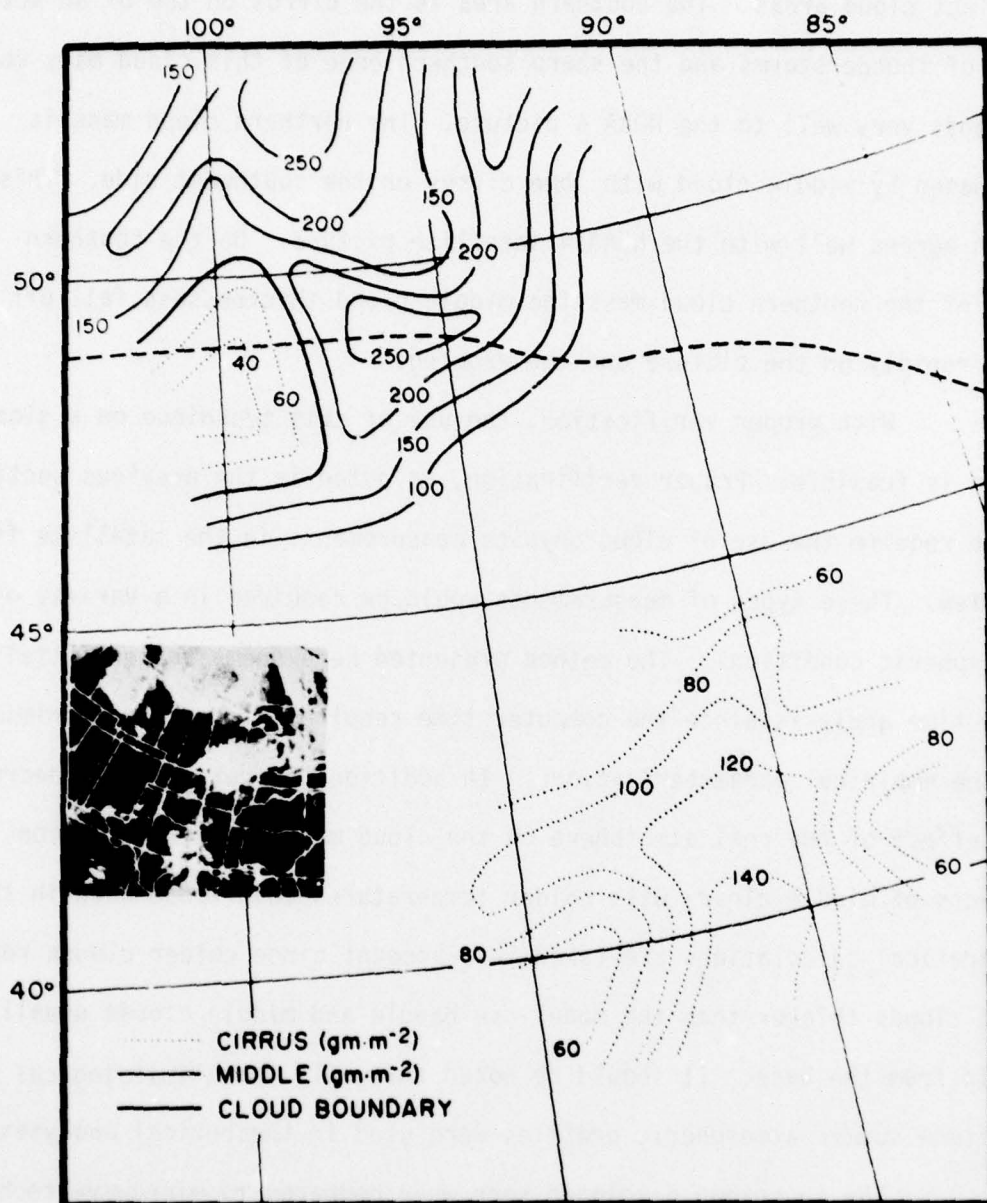
Figure 4.10 Cloud ice and water content based on empirical-theoretical calculations for August 25, 1975. Dotted lines are for cirrus clouds (gm m^{-2}) and solid lines are for middle clouds (gm m^{-2}). The heavy line is the cloud boundaries.

distinct cloud areas. The southern area is the cirrus on top of an active area of thunderstorms and the sharp southern edge of this cloud mass corresponds very well to the NOAA 4 picture. The northern cloud mass is dominated by middle cloud with some cirrus on the southwest side. This again agrees well with the NOAA 4 satellite picture. On the southern edge of the northern cloud mass the middle cloud thicknessess fall off very rapidly on the picture and the mapping.

With proper verification, the use of this technique on a global scale is feasible. Proper verification, as noted in the previous section, would require the use of cloud physics measurements in the satellite field-of-view. These types of measurements would be required in a variety of atmospheric conditions. The method presented here seems to lend itself to real time analysis since the computer time requirement has been minimized by the empirical parameterizations. In addition the ratioing has decreased the effect of the real atmosphere on the cloud moisture determination. The effects of middle clouds with colder temperatures than those used in the theoretical calculations are taken into account since colder clouds represent clouds thicker than the model can handle and middle clouds usually build from the base. It should be noted that only the climatological mid-latitude summer atmospheric profiles were used in theoretical analyses.

The technique developed here when compared to microwave techniques has both advantages and disadvantages. Two advantages are the higher resolution of the HIRS instrument when compared to the Nimbus VI SCAMS instrument and the detection of cirrus clouds that are transparent in the microwave portion of the spectrum. Another advantage of this technique is that it can be applied over both land and oceans, while

82

microwave interpretation of clouds is restricted to oceans because of the change of land emissivity. Disadvantages of this technique when compared to microwave include the opacity of water clouds in the infrared portion of the spectrum and the sensitivity of the technique to the water cloud temperature. By combining infrared and microwave measurements along with the proper cloud physics verification data, operationally significant recovery of cloud parameters from satellite data appears feasible.

4.6   Conclusions

A theoretical model that calculates transfer of spectral infrared radiation based on the discrete-ordinate method developed in Section 2 was modified to include cirrus and middle clouds and absorbing gases. This analysis used one model atmosphere and one middle and high cloud type for all calculations. The top of the cirrus cloud and the base of the middle cloud were held constant to minimize computer time. The layers in the transfer computations were assumed to have constant temperatures so that the effects of the change in cloud thickness on the upwelling radiance could be studied. Various thicknesses and combinations of middle and cirrus clouds were used in the analysis. This model was then applied to the HIRS channels of the Nimbus VI satellite. A case study using the actual HIRS radiance data shows that it is feasible to estimate the cirrus cloud thickness employing the combination of infrared channels with the assistance of IR and visible cloud pictures from the NOAA IV satellite.

The theoretical calculations of upwelling radiance were divided by their clear column radiances to give a ratio for each channel in

which the atmospheric temperature effect was minimized. These ratios were then fitted with a straight line for each theoretical cloud thickness for both cirrus and middle clouds. It was found that cases where the slope was greater than the magnitude of the y-intercept derived from transfer calculations corresponded to the cirrus clouds. The reverse of the slope and y-intercept relation corresponded to middle clouds or lower clouds. The resulting slopes and y-intercepts for different cloud thicknesses for the two cloud types were then fitted with a logarithmic function. This made it possible to infer ice and water content in the case of high and middle clouds, respectively, for a given thickness based on the theoretical calculations.

These theoretical parameterizations were applied to five days of HIRS data. The empirical parameterization method appears to be successful in identifying high and middle clouds. The resulting cloud ice and liquid water contents were compared to the 3DNEPH to indicate whether this technique could be applied in an operational mode. It was found that the comparisons with the 3DNEPH were marginal. This can be traced to the 3DNEPH and the methods used to determine cloud thicknesses as well as approximations in the theoretical calculations and the parameterization of these calculations. Two days of ice and water content for actual HIRS data were then mapped. These results were good when comparing the resulting maps with the corresponding NOAA IV infrared and visible satellite pictures.

The technique developed in this report is ideally suited to enhance the cloud parameterizations in the 3DNEPH. As noted earlier the 3DNEPH is a modular program that processes all kinds of meteorological

84

data. The only satellite data that is currently used is broad band visible and infrared channels of a NOAA 4 type scanning radiometer. The addition of this technique would use satellite data that is not in current use for cloud detection and it would give valuable input into the final results. Since the 3DNEPH is a routinely produced product, much of the software required to implement this procedure is already in existence and the operational development could be carried out independently of 3DNEPH production. As noted earlier the resolutions of the HIRS and the 3DNEPH are similar so that in an operational implementation the 3DNEPH could be used to further verify the technique.

Although an objective way of deriving cloud type information and cloud ice or water content has been illustrated in this analysis, a more reliable method of verification must be found. However, verification of satellite sensing techniques requires carefully designed field experiments in which highly reliable cloud parameters could be obtained under the satellite pass. With sufficient cases from which cloud parameters may be derived locally, intercomparisons with satellite derived values may be carried out to establish the statistical significance of this technique to parameterize satellite measurements.

85

REFERENCES

Asano, S., 1975: On the discrete ordinates method for the radiative trans-
  fer. J. Meteor. Soc. Japan, 53, 92-95.

Bignell, K.J., 1970: The water-vapor infrared continuum. Quart. J. Roy.
  Meteor. Soc., 96, 390-403.

Chandrasekhar, S., 1950: Radiative Transfer. New York, Dover Publ., 393 pp.

Coburn, A.R., 1971: Improved three-dimensional nephanalysis model. Air
  Force Global Weather Center Tech. Memo., AFGWCTM 71-2, 72 pp.

Drayson, S.R., 1971: Transmittances for use in remote soundings of the
  atmosphere. Space Res. XI, COSPAR, Proceedings Symposium on Remote
  Sounding of the Atmosphere, Leningrad, U.S.S.R. 585-592.

Feddes, R.G. and R.D. Smith, 1974: A synoptic scale model for simulating
  condensed atmospheric moisture. USAFETAC TN74-4, United States Air
  Force Environmental Technical Applications Center, Washington, D. C.,
  31 pp.

Hale, G.M. and M.R. Querry, 1973: Optical constants of water in the 200 nm
  to 200 μm wavelength region. Appl. Opt., 12, 555-563.

Heymsfield, A.J., and R.G. Knollenberg, 1972: Properties of cirrus gener-
  ating cells. J. Atmos. Sci., 29, 1358-1366.

Knollenberg, R.G., 1970: The optical array: An alternative to scattering
  or extinction for airborne particle size determination. J. Appl.
  Meteor., 9, 86-103.

Liou, K.N., 1972: Light scattering by ice clouds in the visible and
  infrared: A theoretical study. J. Atmos. Sci., 29, 524-536.

Liou, K.N., 1973: A numerical experiment on Chandrasekhar's discrete-ordinate method for radiative transfer: Applications to cloudy and hazy atmospheres. J. Atmos. Sci., 30, 1303-1326.

_____, 1974: On the radiative properties of cirrus in the window region and their influence on remote sensing of the atmosphere. J. Atmos. Sci., 31, 522-532.

_____, 1975: Applications of the discrete-ordinate method for radiative transfer to inhomogeneous aerosol atmospheres. J. Geophys. Res., 80, 3434-3440.

_____, 1977: Remote sensing of the thickness and composition of cirrus clouds from satellites. J. Appl. Meteor., 16, 91-99.

McClatchey, R.A., et al., 1971: Optical properties of the atmosphere. Environmental Res. Pap., 354, AFCRL.

McMillin, L.M., et al., 1973: Satellite infrared soundings from NOAA space-craft. NOAA Tech. Rept. NESS 65, 112 pp.

Panofsky, H.A. and G.W. Brier, 1968: Some Application of Statistics to Meteorology. University Park, Pa., Pa. St. Univ., 224 pp.

Shaaf, J.W., and D. Williams, 1973: Optical constants of ice in the infrared. J. Opt. Soc. Amer., 63, 726-732.

Smith, W.L., P.G. Abel, H.M. Woolf, A.W. McCullock and B.J. Johnson, 1975: The high resolution infrared radiation sounder (HIRS) experiment. Nimbus VI Users Guide, Goddard Space Flight Center, Greenbelt, Md., 227 pp.

Weickmann, H.K., 1949: Die Eispase in der atmosphäre. Ber. Deut. Wetterd., No. 6, 54 pp.

Weinreb, M.P., and A.C. Neuendorffer, 1973: Method to apply homogeneous path transmittance models to inhomogeneous atmosphere. J. Atmos. Sci., 30, 662-666.

Remote Sensing of the Thickness and Composition of Cirrus Clouds from Satellites

KUO-NAN LIOU

Department of Meteorology, University of Utah, Salt Lake City 84112

(Manuscript received 5 March 1976, in revised form 14 December 1976)

ABSTRACT

A retrieval technique is presented for the determination of the surface temperature, the thickness and transmissivity of cirrus clouds, and the fraction of the cirrus cloudiness by means of four observed upwelling radiances in the 10 μm window region. On the basis of radiative transfer calculations for mean wavenumbers of 900, 950, 1100 and 1150 cm^{-1}, assumptions are made in the theoretical retrieval analyses that water vapor effects above cirrus clouds are negligible and that ratios of the transmissivities are linear functions of the cloud thickness. Error analyses employing climatological data reveal that independent random errors in temperature and humidity profiles introduce insignificant errors in the four resulting parameters. The resulting errors caused by random errors in the expected upwelling radiances, however, depend upon their standard deviations. Once the thickness and the transmissivity at a given wavenumber of a cirrus cloud have been determined, we illustrate that the vertical ice content may be estimated assuming that ice particles are randomly oriented in a horizontal plane.

1. Introduction

Cirrus clouds have been noted to introduce serious difficulties in remote sensing of atmospheric temperature and humidity profiles and surface conditions, owing to their semi-transparent appearance in the visible as well as in the infrared region. It is extremely important, therefore, to derive the reliable and accurate radiation properties of cirrus clouds from an independent set of sounding frequencies in conjunction with the atmospheric parameter evaluation. Moreover, determination of the vertical ice content over the global atmosphere is equally important from the point of view of climatology studies and, perhaps, numerical weather prediction.

The paper by Houghton and Hunt (1971) apparently was the first one to explore the passive remote sensing possibility of ice clouds by means of two wavelengths in the far infrared. Liou (1974) discussed emission and transmission properties of cirrus clouds in the 10 μm window region in conjunction with the remote sensing potential from satellites. Bunting and Conover (1974) proposed a simple means for the estimation of the vertical ice content of cirrus clouds assuming the exponential attenuation of IR radiation.

With respect to the atmospheric parameter determination, Chahine (1974) presented a numerical method to derive vertical temperature profiles in cloudy atmospheres by means of radiances obtained from two partially overlapping fields of view. Taylor (1974) described an approach employing soundings at two different zenith angles for the determination of temperature profiles in the presence of clouds. Both of these two important studies concerning the remote sensing of cloudy atmospheres involved attempts to remove the cloud effect rather than to incorporate it into the radiative transfer equation.

Cirrus clouds consist of non-spherical ice crystals of various sizes, possibly randomly oriented in a horizontal plane. Other unknown variables include the ice-crystal concentration, the cloud thickness and the location of the cloud in the atmosphere. Moreover, for a given upwelling radiance at the satellite point of view, there will be additional unknown variables associated with the atmospheric temperature and gaseous profiles. In view of a large number of unknown variables, parameterization equations describing the radiation field of an atmosphere containing cirrus clouds have to be formulated. Retrieval of the unknown parameters, each of which may represent a combination of several variables, may be carried out from satellite radiance observations.

In this paper, I would like to present some hypothetical analyses and calculations concerning the determination of the structure and composition of cirrus clouds from a set of synthetic radiance observations in the window region.

2. Theoretical analyses

We assume that within the field of view of the satellite radiometer the atmosphere contains η portion of cloudiness. The monochromatic upwelling radiance measured by the satellite radiometer at the top of a
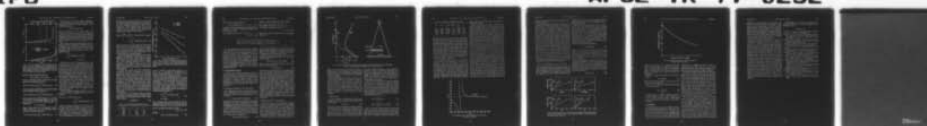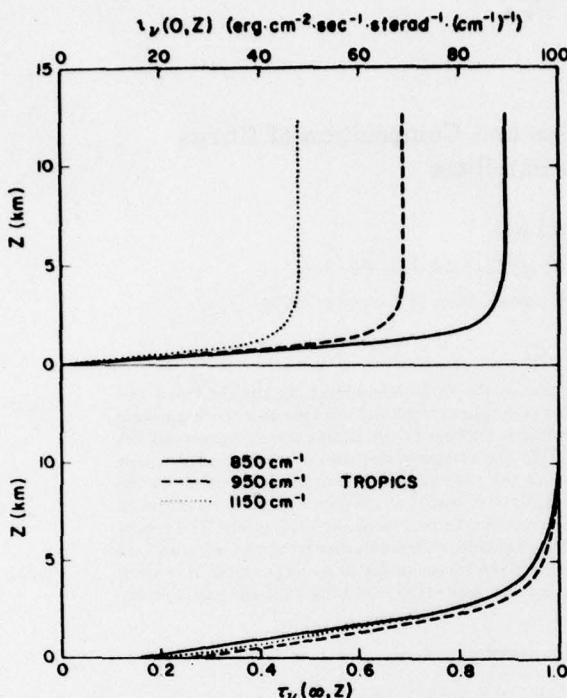
FIG. 1. Values of the integral term and transmission function shown in Eq. (2). The integral term is evaluated from the surface to the level z, while the transmission function of water vapor is calculated from the top of the atmosphere to the level z. The calculations are carried out for wavenumbers of 850, 950, 1150 cm^{-1} employing a tropical atmosphere.

partially cloudy atmosphere is given by

$$\bar{I}_\nu^{pc}(\infty) = \eta I_\nu^c(\infty) + (1-\eta) I_\nu^{nc}(\infty), \qquad (1)$$

where the upwelling radiance arising from the clear portion of the atmosphere is simply

$$I_\nu^{nc}(\infty) = B_\nu(T_s)\tau_\nu(\infty,0) + \int_{z=0}^{z=\infty} B_\nu[T(z)]d\tau_\nu(\infty,z). \qquad (2)$$

And the upwelling radiance due to the cloudy portion of the atmosphere may be expressed as

$$I_\nu^c(\infty) = \tau_\nu^c I_\nu(z_b)\tau_\nu(\infty,z_t) + \int_{z=z_t}^{z=\infty} B_\nu[T(z)]d\tau_\nu(\infty,z). \qquad (3)$$

In this equation the cloud transmissivity τ_ν^c is defined as the ratio of the upwelling radiance at the cloud top, i.e., $I_\nu(z_t)$, to that at the cloud base, and it can be written as

$$\tau_\nu^c = I_\nu(z_t)/I_\nu(z_b), \qquad (4)$$

where z_b and z_t denote the cloud-base and cloud-top heights, respectively, and the upwelling radiance reaching the cloud base is given by

$$I_\nu(z_b) = B_\nu(T_s)\tau_\nu(z_b,0) + \int_{z=0}^{z=z_b} B_\nu[T(z)]d\tau_\nu(z_b,z). \qquad (5)$$

In Eqs. (3)–(5), T_s is the surface temperature, τ_ν the transmission function of gases which will be discussed later, and the Planck function in the wavenumber domain is

$$B_\nu(T) = a\nu^3/(e^{b\nu/T}-1), \qquad (6)$$

with $a = 1.1272 \times 10^{-5}$ erg cm^2 s^{-1} and $b = 1.4389$ cm K. It should be noted that $I_\nu(z_t)$ in Eqs. (3) and (4) must be evaluated from the transfer equation including absorption, emission and scattering of gases and cloud particles subject to the radiation boundary conditions of the top and base of the cloud concerned (Liou, 1974).

Cirrus clouds are normally fairly high in the atmosphere with their top heights on the order of 10 km or higher. Thus, we may select spectral channels in the window region where the effect of water vapor absorption above the cirrus cloud layer can be neglected such that

$$\left. \begin{array}{c} \int_{z=z_t}^{z=\infty} B_\nu[T(z)]d\tau_\nu(\infty,z) \approx 0 \\ \\ \tau_\nu(\infty,z_t) \approx 1 \end{array} \right\}. \qquad (7)$$

Justification of Eq. (7) is illustrated in Fig. 1 (see also Section 3a for water vapor absorption). We have employed a tropical atmospheric profile (McClatchey et al., 1971) in the calculations. The upper diagram represents the results of the first equation in (7) for the integration limits from the surface to a level z. Three wavenumbers of 850, 950 and 1150 cm^{-1} were used. It is evident that the integral term in Eq. (2) has negligible contribution above a height of about 5 km, which is normally lower than the base heights of cirrus clouds. The lower diagram represents the transmission term in Eq. (2). Clearly, we see that above about 8 km, the transmission function τ_ν of water vapor for a moist atmosphere is very close to 1. Consequently, we would expect that our first assumptions can be applied to other atmospheric profiles without difficulties.

Thus the observed upwelling radiance at the top of a partially cloudy atmosphere denoted in Eq. (1) becomes

$$\bar{I}_\nu^{pc}(\infty) \approx (1-\eta+\eta\tau_\nu^c)\Big\{ B_\nu(T_s)\tau_\nu(z_b,0) + \int_{z=0}^{z=z_b} B_\nu[T(z)]d\tau_\nu(z_b,z) \Big\}, \qquad (8)$$

where the unknown parameters are the fraction of cloudiness, the surface temperature, the cloud transmissivity which is wavenumber dependent, and the temperature profile and the transmission function of water vapor. Eq. (8) expresses the upwelling radiance for a single wavenumber. However, a satellite instrument can distinguish only finite bandwidths $\Delta\nu(\nu_1,\nu_2)$

with the instrumental slit function $\phi(\nu_1,\nu_2)$, which we shall ignore in the following theoretical development. The finite bandwidth is normally so small that the variation of Planck function with respect to the wavenumber can be neglected. This is particularly evident in the 10 μm window region. Thus, the up-welling spectral radiance may be written as

$$I_{\Delta\nu}^{pc}(\infty) = \int_{\nu_1}^{\nu_2} I_\nu^{pc}(\infty)\frac{d\nu}{\Delta\nu} = (1-\eta+\eta\tau_{\Delta\nu}^c)\{B_{\Delta\nu}(T_s)\tau_{\Delta\nu}(z_b,0)$$

$$+ \int_{s=0}^{s=z_b} B_{\Delta\nu}[T(z)]d\tau_{\Delta\nu}(z_b,z)\}. \quad (9)$$

Here we also note that the variation of cloud transmissivity within a small spectral interval is relatively small in view of the slow varying refractive indices of ice in the window region. Consequently, it is physically reasonable to use a mean wavenumber to calculate the spectral cloud transmissivity.

If prior knowledge of the temperature and humidity profiles in the atmosphere were available, say from climatological data, then $\tau_{\Delta\nu}(z_b,0)$ and the integral term in Eq. (9) could be evaluated. With a measurement of the upwelling radiance from the satellite radiometer in the window channel, there are only three unknown parameters, η, $\tau_{\Delta\nu}^c$ and T_s. How many radiance measurements are required to determine all these variables?

We shall now examine the cloud transmissivity $\tau_{\Delta\nu}^c$ defined in Eq. (4). Calculations of the transmissivity as a function of the cirrus cloud thickness and ice content were carried out by Liou and Stoffel (1976). It was assumed that the cirrus cloud was composed of long circular cylinders randomly oriented in space with a base height of 8 km and an isothermal temperature of $-36°$C. Mean wavenumbers of 900, 950, 1100 and 1150 cm^{-1} were chosen in this investigation. Fig. 2 shows the ratios of the transmissivities of 950, 1100 and 1150 cm^{-1} to the transmissivity of 900 cm^{-1}. It is evident that to a good approximation, these curves are fairly close to a linear function of the thickness.

On the basis of the theoretical radiative transfer calculations, we postulate that the transmissivities of cirrus clouds for wavenumbers in the window region can be scaled as

$$\tau_i^c = (a_i\Delta z + b_i)\tau^c, \quad (10)$$

TABLE 1. Linear coefficients for cloud transmissivities.

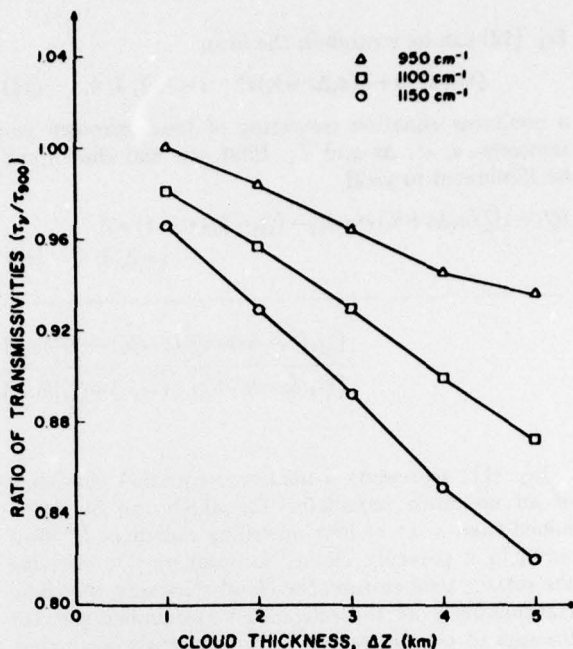| ν(cm^{-1})	i	a_i	b_i
900	1	0	1
950	2	−0.02	0.99
1100	3	−0.25	1.23
1150	4	−0.04	1.01

FIG. 2. Ratios of the cloud transmissivity of 950, 1100 and 1150 cm^{-1} to that of 900 cm^{-1}. The cloud transmissivities are computed from the radiative transfer program including scattering, absorption and emission of water vapor and cloud particles.

where we change the wavenumber index $\Delta\nu$ to i. In Eq. (10), τ^c represents the transmissivity at a reference wavenumber (900 cm^{-1} in Fig. 2), and a_i and b_i are certain constants given in Table 1.

In view of the linear approximation for the ratios of the transmissivities, the cloud fraction η, the surface temperature T_s, the cloud thickness Δz and the cloud transmissivity τ^c at the reference wavenumber may be determined from four radiance measurements in the window region provided that the atmospheric temperature and humidity profiles are given, for example, from climatological data. For the convenience of the following discussions, let

$$\left.\begin{array}{l} I_i^* = \int_{s=0}^{s=z_b} B_i[T(z)]d\tau_i(z_b,z) \\ \\ \tau_i^* = \tau_i(z_b,0) \end{array}\right\}, \quad (11)$$

with * denoting values to be evaluated from the climatological data. Thus from Eq. (9) we have the following expressions for the four upwelling radiances:

$$I_i^{pc} = [1-\eta+\eta(a_i\Delta z+b_i)\tau^c][B_i(T_s)\tau_i^*+I_i^*],$$
$$i = 1, 2, 3, 4. \quad (12)$$

Defining

$$Q_i(T_s) = I_i^{pc}/[B_i(T_s)\tau_i^*+I_i^*], \quad (13)$$

Eq. (12) can be written in the form

$$Q_i = 1 - \eta + \eta(a_i \Delta z + b_i)\tau^c, \quad i = 1, 2, 3, 4, \quad (14)$$

a nonlinear equation consisting of four unknown parameters, η, τ^c, Δz and T_s. First, we find that η can be eliminated to yield

$$(Q_1 - 1)[(a_i \Delta z + b_i)\tau^c - 1] - (Q_i - 1)(\tau^c - 1) = 0,$$
$$i = 2, 3, 4. \quad (15)$$

Second, τ^c can be omitted in Eq. (15) to obtain

$$\frac{(Q_1 - Q_2)[(Q_1 - 1)(a_i \Delta z + b_i) - (Q_i - 1)]}{(Q_1 - Q_i)[(Q_1 - 1)(a_2 \Delta z + b_2) - (Q_2 - 1)]} - 1 = 0,$$

$$i = 3, 4. \quad (16)$$

Finally, from the two equations in (16) we eliminate Δz to give

$$\frac{[Q_1(b_3 - b_2) + Q_2(1 - b_3) + Q_3(b_2 - 1)][Q_1(a_2 - a_4) + Q_2 a_4 - Q_4 a_2]}{[Q_1(b_4 - b_2) + Q_2(1 - b_4) + Q_4(b_2 - 1)][Q_1(a_2 - a_3) + Q_2 a_3 - Q_3 a_2]} - 1 = 0. \quad (17)$$

Eq. (17) represents a nonlinear equation consisting of an unknown parameter T_s, which can be determined from a set of four upwelling radiances $\bar{I}_i^{pc}$ measured in a partially cloudy atmosphere. On deriving the surface temperature, the cloud thickness, the cloud transmissivity at the reference wavenumber and the fraction of cloudiness can be subsequently evaluated. In the next section, we shall investigate the possible errors of the resulting parameters caused by the use of the climatological temperature and humidity profiles and the possible random errors in the expected upwelling radiances.

3. Computational analyses

In order to test the idea outlined in the previous section, computational analyses have been carried out. Water vapor absorption properties are first discussed in Section 3a. In 3b, a synthetic partially cloudy atmosphere is constructed. Error analyses are then presented in 3c. Some notes are finally given in 3d for the estimation of the vertical ice content of cirrus clouds.

a. Water vapor absorption in the 10 μm window

The transmission function for water vapor in the 10 μm window region is due to the selective absorption by weak lines and the continuous absorption, and can be written

$$\tau_v = \tau_v(\text{selective}) \times \tau_v(\text{continuum}). \quad (18)$$

The selective absorption by weak lines is well understood (see, e.g., Goody, 1964). However, continuous absorption in the 10 μm window has been a subject of considerable speculation. In recent years, it seems to have been established that the water vapor continuum is caused by the broadening of foreign gases and the e-type (water dimmer) absorption (Bignell, 1970; Burch, 1970). Thus the absorption coefficient of the continuum may be expressed as

$$k(T, p, e) = k_1(T)p + k_2(T)e, \quad (19)$$

where p is the total pressure and e the partial vapor pressure. Based on Bignell's measurements, k_2 is much greater than k_1, although the temperature dependence of k_2 has not been investigated completely.

With these sources of absorption taken into consideration the transmission function for water vapor may be written as

$$\tau_v(u) = \exp[-\eta_v u^{\frac{1}{2}} - (k_1 p + k_2 e)u], \quad (20)$$

where u is the vertical path length of water vapor and the weak line parameter

$$\eta_v = (\pi \alpha \sigma)^{\frac{1}{2}}/\delta, \quad (21)$$

with σ the mean line intensity, δ the mean line spacing and α the mean line width. These weak line parameters have been given by Roach and Goody (1958) based on fitting the statistical band model from observed data. According to Bignell (1970) and Burch (1970), the e-type absorption continuum is dominant in the 10 μm window region. Furthermore, comparisons of synthetic IRIS (Infrared Interferometer Spectrometer) radiances computed from Bignell's water vapor continuum data with observed radiances gave good agreement (Kunde et al., 1974). In view of this evidence and in view of the fact that the absorption coefficient is continuous, we have computed water vapor transmissivities employing the mean wavenumbers of 900, 950, 1100 and 1150 cm^{-1} in conjunction with radiative transfer calculations reported in this paper.

b. Synthetic partially cloudy atmosphere

To test the accuracy of the procedures described in Section 2, a synthetic partially cloudy atmosphere has been constructed (Fig. 3). It is assumed that within the field of view of the satellite radiometer, there is 70% of cirrus cloudiness whose thickness is 2 km, and the base of the cirrus cloud is located at 8 km in the atmosphere. Based on radiative transfer calculations, we obtain a transmissivity of 0.675 for a 2 km cirrus cloud at a wavenumber of 900 cm^{-1}.
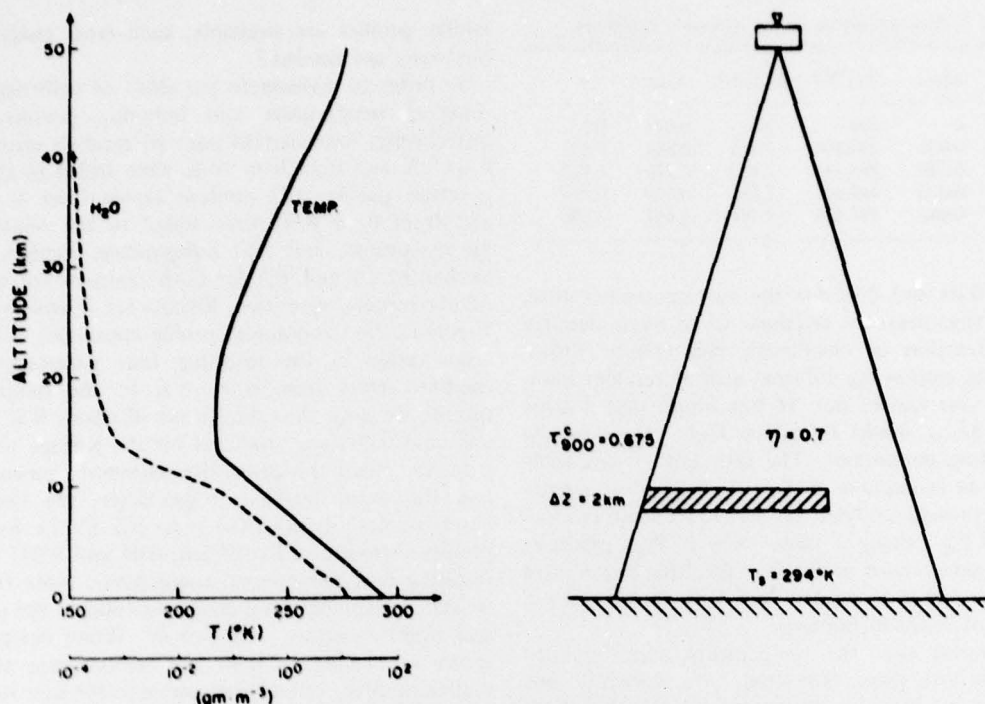
FIG. 3. A diagram for the synthetic partially cloudy atmosphere. The climatological temperature and humidity profiles for a mid-latitude summer atmosphere are used in the analyses.

Moreover, a surface temperature of 294 K is employed. With respect to the atmospheric temperature and humidity profiles, we use the tabulated climatological data by McClatchey *et al.* (1971) for the mid-latitude summer atmosphere.

With the transmissivity at 900 cm^{-1} given, the rest of the transmissivities can be evaluated according to Eq. (10). Hence, we can theoretically calculate the expected upwelling radiances in the partially cloudy atmosphere for four wavenumbers by means of Eqs. (1)–(3). Once the upwelling radiances have been obtained, we proceed to Eqs. (14)–(17) to retrieve the surface temperature, the cloud thickness, the transmissivity at 900 cm^{-1} and the fraction of cirrus cloudiness.

c. Error analyses

Eq. (17) represents a complicated nonlinear equation which contains the unknown surface temperature. We may write

$$F(T_s) = 0. \qquad (22)$$

Since the function is a high-order nonlinear equation, we would expect that it consists of a number of roots for T_s in the $(0, \infty)$ domain. However, there will be only one root that is our desired solution. Fig. 4 illustrates the behavior of Eq. (22) for the conditions given in Section 3b with the realistic range of T_s

from 240 to 340 K. In addition to the desired root of 294 K, we find that 263 K also satisfies Eq. (22). Hence, care should be taken in the error analysis to disregard the undesirable roots. Fortunately, from a number of error analyses exercises, we found that the correct value always lies at the zero intersection of the right-hand curve in Fig. 4.

The first error analyses were done for the upwelling radiance. Random numbers were arbitrarily selected and added to the upwelling radiances calculated exactly from the synthetic atmosphere. The retrieval procedures using the upwelling radiances with random errors were carried out for the surface temperature, and subsequently for the cloud thickness, the reference cloud transmissivity and the cloud fraction. We define the following statistical terms:

$$\Delta I_m = \frac{1}{N} \sum_{i=1}^{N} \Delta I_i / I_i, \qquad (23)$$

$$\Delta I_{rms} = \left[\sum_{i=1}^{N} (\Delta I_i / I_i - \Delta I_m)^2 \right]^{\frac{1}{2}}. \qquad (24)$$

Table 2 lists the resulting parameters in terms of these two variables. The second line of this table shows that 1.2% random error produces almost negligible errors in the four resulting parameters. A random error of 11.2% introduces deviations of about 3.6 K,

TABLE 2. Random errors in the measured radiances.

ΔI_m	ΔI_{rms}	T_S(°K)	ΔZ(km)	τ^c_{900}	η
0	0	294	2	0.675	0.7
0.012	0.002	294.346	1.924	0.684	0.702
0.056	0.010	295.745	1.655	0.719	0.710
0.112	0.020	297.549	1.385	0.760	0.719
0.002	0.003	297.486	2.187	0.644	0.690

0.61 km, 0.08 and 0.02 for the surface temperature, the cloud thickness, the reference cloud transmissivity and the fraction of cloudiness, respectively. Other experiments employing different sets of random numbers were also carried out. It was found that a large value of ΔI_{rms} would introduce large errors in the four resulting parameters. The fifth line of this table illustrates an example as to how the root mean square affects the present analysis. We see that a small random error of 0.2% having a larger rms (0.3%) produces about the same errors in the four resulting parameters as the case when a random error of 11.2% with a small rms of 2% is introduced.

It is known that the temperature and humidity profiles derived from radiosonde are normally not available in ocean areas, particularly in the Southern Hemisphere. The best guesses of the temperature and humidity profiles in cloudy conditions, perhaps, may be obtained from climatology. Deviations of the climatological values from the true profiles are likely to occur. Thus, it is of importance to examine how the errors in the temperature and humidity profiles affect the resulting recovered parameters developed previously. (Note that if true temperature and hu-

midity profiles are available, such error analyses are obviously not needed.)

In order to investigate the effect of utilizing climatological temperature and humidity profiles, three experiments were carried out: (i) random errors from 0 to 5 K and from 0 to 10 K were added to the temperature profile, (ii) random errors from 0 to 5% and from 0 to 10% were added to the relative humidity profile, and (iii) independent random errors similar to (i) and (ii) for both temperature and humidity profiles were used. Results are shown in Fig. 5. Errors in the temperature profile apparently introduce large errors in the resulting four parameters. For random errors from 0 to 5 K in the temperature profile, we note that deviations of about 9 K, 1 km, 0.07 and 0.006 are produced for the surface temperature, the cloud thickness, the reference transmissivity and the cloud fraction, respectively. On the other hand, random errors from 0 to 5% in the humidity profiles introduce 5 K, 0.5 km, 0.04 and 0.003 for the resulting four parameters, respectively. Note that the + and − signs in these diagrams indicate the positive and negative errors, respectively. When independent errors are added to both the temperature and humidity profiles, we find that errors in the four resulting parameters are greatly reduced. The reason for this may be caused by the compensating effect of opposite errors for the temperature and humidity profiles as evident from Fig. 5. It should be noted that simultaneous deviations of the true temperature and humidity profiles from the climatological means are to be expected in the atmosphere. Hence we would anticipate that the use of climatological data in the
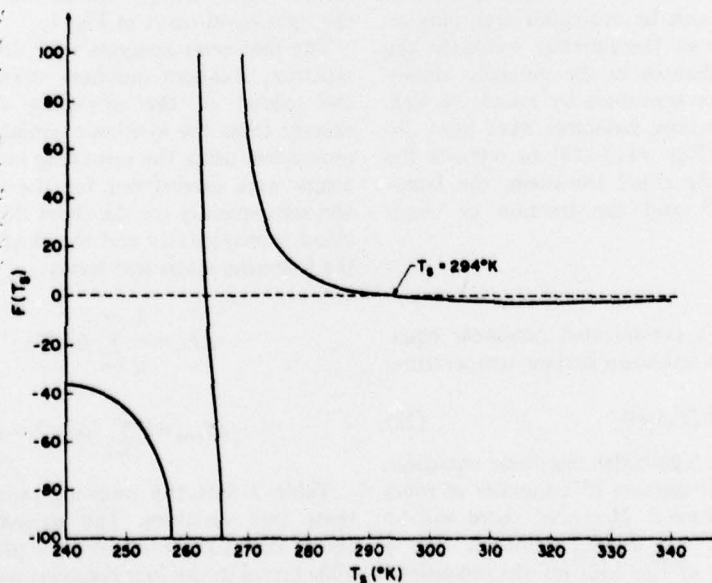

FIG. 4. Behavior of the nonlinear equation (17) as a function of the surface temperature.

present retrieval analysis introduces insignificant errors in cloud parameters.

In the development of the retrieval technique, the assumption has been made that the cloud is high in the atmosphere so that radiative effects of water vapor above the cloud can be neglected. Hence the method should be applied as such and cases when low cumulus and/or stratus are present are to be disregarded. Since visible and IR cloud pictures are routinely available from operational satellites, discrimination between low and high clouds appears possible. There are cases when high and low clouds occur simultaneously in the atmosphere. In these situations, low clouds, which are generally optically thick, may be considered as surfaces and to a good approximation the theoretical approach reported here may also be applicable. Note that we have employed 900, 950, 1100 and 1150 cm^{-1} in the theoretical analysis to demonstrate that information associated with cirrus may be derived from satellite radiance observations. Of course, other spectral bands within the window region ought to be explored to ensure the optimum bands, which could be proposed for future satellite experiments concerning the detection of cirrus cloud compositions and structure in the atmosphere.

d. Note on the determination of cirrus ice content

In the preceding analyses, we have shown that the surface temperature, the cloud thickness, the reference cloud transmissivity and the fraction of cloudiness may be inferred from four radiance measurements in the window region. Once a reliable reference cloud

transmissivity has been derived, it seems possible to *estimate* the vertical ice content following the procedures described below.

Based on the theoretical radiative transfer calculations, we may construct a diagram (Fig. 6) consisting of the transmissivity at a given wavenumber and the optical depth at that given wavenumber. We note that the transmissivity is nothing but an attenuation parameter. (For a cirrus cloud whose optical depth is less than about 0.5 it appears that an exponential attenuation may be applied.) By means of this curve constructed prior to the retrieval experiment, a transmissivity derived from the previous analysis should correspond to an optical depth.

We now express the optical depth as

$$\tau(\bar{\nu}) = \Delta z \beta_{ext}(\bar{\nu}), \qquad (25)$$

where $\beta_{ext}(\bar{\nu})$ denotes the volume extinction cross section for a given mean wavenumber $\bar{\nu}$. Now with the information of the cloud thickness which has been determined simultaneously with the cloud transmissivity, the important volume extinction cross section may be estimated.

Since cirrus clouds are composed ice particles on the order of 100–1000 μm (see, e.g., Heymsfield and Knollenberg, 1972), an extinction parameter (usually denoted as Q_{ext}) of about 2 may be adopted. Consequently, the extinction cross section is mainly a function of the size and concentration of ice particles and may be written as

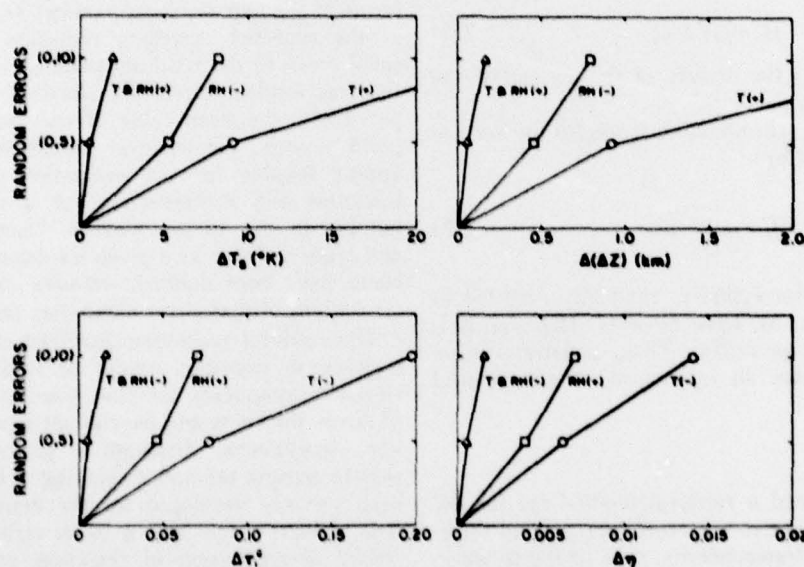$$\beta_{ext} \approx Q_{ext} \bar{A} N, \qquad (26)$$

FIG. 5. Error analyses for the use of the climatological temperature and humidity profiles. The abscissa and ordinate represent random errors and deviations of the four parameters from the true values, respectively.
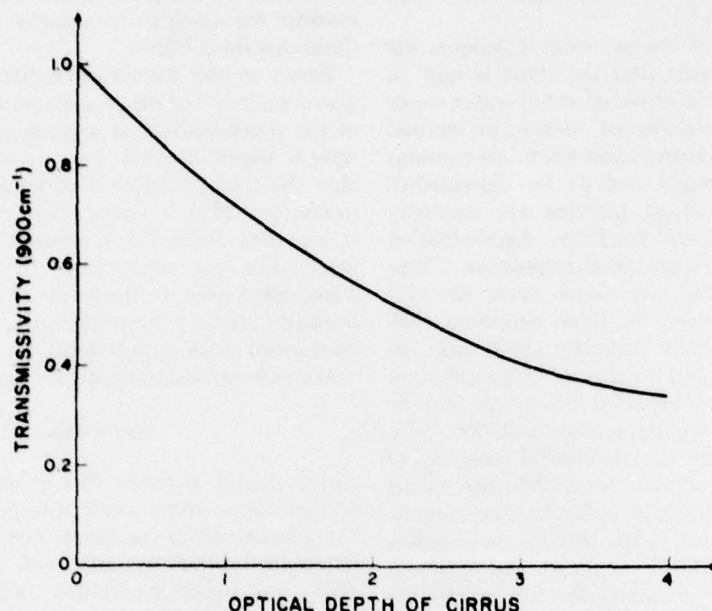
FIG. 6. Transmissivity as a function of optical depth based on
radiative transfer calculations.

where N and $\bar{A}$ denote the concentration and the mean cross-section area of ice particles, respectively. For ice crystals randomly oriented in a horizontal plane, we should have $\bar{A} \approx l\bar{d}$, with l and $\bar{d}$ representing the mean length in the major and minor axes, respectively.

Finally, the vertical ice content can be written in the form

$$IC = \rho_I \bar{V} N \Delta z, \qquad (27)$$

where ρ_I represents the density of the ice and $\bar{V}$ the mean volume of ice particles.

If we let $\xi = \bar{V}/\bar{A}$, the above equation for the vertical ice content is given by

$$IC \approx \rho_I \frac{\beta_{ext}}{Q_{ext}} \xi \Delta z. \qquad (28)$$

For long circular ice cylinders randomly oriented in a horizontal plane, we have $\xi = \pi \bar{d}/4$. Here, ρ_I, Q_{ext} and ξ are known quantities. Thus, a determination of β_{ext} and Δz gives an estimation on the vertical ice content.

4. Conclusion

We have presented a retrieval method for the determination of surface temperature, cirrus cloud thickness, cirrus cloud transmissivity at a reference wavenumber and the fraction of cirrus cloudiness within the field of view from four expected upwelling radiance observations in the 10 μm window region. Theoretical analyses assume that water vapor effects above the

cirrus cloud are negligible and that the ratios of transmissivities are linear functions of the cloud thickness. Justifications of these two assumptions are given on the basis of radiative transfer calculations.

Computational analyses employing the climatological means show that random errors in both the temperature and humidity profiles produce insignificant errors in the four resulting parameters. Random errors in the expected upwelling radiances also introduce small errors in the resulting parameters provided that the rms random errors are relatively small as compared with the mean value. Hence, from a theoretical point of view, the retrieval procedures demonstrated appear feasible for the evaluation of cirrus cloud thickness and transmissivity at a reference wavenumber in the 10 μm window. Once the thickness and transmissivity at a given wavenumber of a cirrus cloud have been derived, we note that the vertical ice content of that cirrus cloud may be estimated.

The retrieval technique described in the preceding sections, in principle, should be applicable to cirrus cloudy atmospheres for the quantitative estimation of cirrus thickness and ice content from passive satellite observations. Although a ground-based active remote sensing method employing a laser source has been recently developed for the detection of cirrus, it is of local nature and is to be verified for the successful determination of thickness and ice content. However, cirrus clouds cover a large portion of the planet. It is therefore vitally important to explore passive remote sensing techniques from which cirrus cloud composition and structure may be derived from

satellites on a routine basis over the global scale. There has been hardly any investigation on the recovery of cloud properties from passive satellite sensing owing to the complexity of the cloud interaction with the radiation field of the atmosphere. This is particularly apparent for the high, semi-transparent cirrus clouds. This paper represents an approach based on which the thickness and ice content of cirrus may be evaluated by utilizing four pieces of radiance information in the 10 μm window region.

Any satellite sensing technique for the recovery of atmospheric composition and structure is subject to verification by utilizing real data. The data source that may be of use in connection with the present theoretical analysis would be the IRIS experiment on board Nimbus 4 as reported by Kunde *et al.* (1974). IRIS measured the thermal emission of the earth's atmosphere and surface from 400–1600 cm^{-1} with an apodized spectral resolution of 2.8 cm^{-1}. It seems possible to select a set of four spectral intervals in the 750–1250 cm^{-1} region to carry out the analyses described in this paper provided that the synoptic and cloud information of a cirrus cloudy atmosphere is available. Unfortunately, satellite cloud experiments require *in situ* information of the cloud thickness and composition, which are normally not available under the satellite pass. Perhaps the major thrust of the present paper is to illustrate that certain cirrus cloud parameters could be evaluated from a set of radiance observations in the 10 μm window region. Such a theoretical demonstration seems to warrant a possibility of pre-satellite experiments for the quantitative determination of cirrus cloud composition and thickness.

REFERENCES

Bignell, K. J., 1970: The water-vapor infrared continuum. *Quart. J. Roy. Meteor. Soc.*, **96**, 390–403.

Bunting, J. T., and J. H. Conover, 1974: Progress on derivation of cloud water content from satellites. *Preprints Sixth Conf. Aerospace and Aeronautical Meteorology*, El Paso, Amer. Meteor. Soc., 205–207.

Burch, D. E., 1970: Investigation of the absorption of infrared radiation by atmospheric gases. Air Force Cambridge Research Laboratories, Publ. U-4784.

Chahine, M. T., 1974: Remote sounding of cloudy atmospheres. I. The single cloud layer. *J. Atmos. Sci.*, **31**, 233–243.

Goody, R. M., 1964: *Atmospheric Radiation*. Clarendon Press, 436 pp.

Heymsfield, A. J., and R. G. Knollenberg, 1972: Properties of cirrus generating cells. *J. Atmos. Sci.*, **29**, 1358–1366.

Houghton, J. T., and G. E. Hunt, 1971: The detection of ice clouds from remote measurements of their emission in the far infra-red. *Quart. J. Roy. Meteor. Soc.*, **97**, 1–17.

Kunde, V. G., B. J. Conrath, R. A. Hanel and C. Prabhakara, 1974: Nimbus 4 IRIS spectra in the 750–1250 cm^{-1} atmospheric window region. *J. Atmos. Sci.*, **31**, 600–603.

Liou, K. N., 1974: On the radiative properties of cirrus in the window region and their influence on remote sensing of the atmosphere. *J. Atmos. Sci.*, **31**, 522–532.

——, and T. Stoffel, 1976: Remote sensing of cirrus cloud compositions. Sci. Rep. No. 1, AFGL-TR-76-0027, Air Force Geophysics Laboratory, 81 pp.

McClatchey, R. A., *et al.*, 1971: Optical properties of the atmosphere. Environ. Res. Pap. 354, AFCRL.

Roach, W. T., and R. M. Goody, 1958: Absorption and emission in the atmospheric window from 770 to 1250 cm^{-1}. *Quart. J. Roy. Meteor. Soc.*, **84**, 319–333.

Taylor, F. W., 1974: Remote temperature sounding in the presence of cloud by zenith scanning. *Appl. Opt.*, **13**, 1559–1566.